(NASA-CR-152027) FLEXIBLE CRYOGENIC HEAT PIPE DEVELOPMENT PROGRAM Final Report (Rockwell International Corp., Downey, Calif.) 147 p HC A07/MF A01 CSCL 20D

N77-29451

Unclas
G3/34 44012

FLEXIBLE CRYOGENIC HEAT PIPE DEVELOPMENT PROGRAM

Final Report

NASA CR 152027

July 1976

SD 77-AP-0088

CONTRACT NAS2-8830

Rockwell International
Space Division

NASA CR 152027

FLEXIBLE CRYOGENIC HEAT PIPE DEVELOPMENT PROGRAM

By J. P. Wright

Rockwell International
Space Division
12214 Lakewood Blvd.
Downey, CA 90241

July 1977

Final Report

Contract No. NAS2-8830

Prepared For

Ames Research Center

National Aeronautics and Space Administration

Moffett Field, California 94035

SD 77-AP-0088

FOREWORD

This report is submitted by the Space Division of Rockwell International Corporation to the National Aeronautics and Space Administration, Ames Research Center in accordance with the requirements of Contract NAS2-8830. The work was administered by the Project Technology Branch of the Space Projects Division, with Dr. Craig McCreight as Technical Monitor,

The program was performed under the direction of J. P. Wright, Program Manager. Technical and Laboratory assistance was provided by G. W. Gurr, Jr., C. D. Rosen, D. E. Wilson, A. M. Lehtinen, and T. T. Cafferty.

CONTENTS

CONTENTS (CONTINUED)

LIST OF ILLUSTRATIONS

LIST OF ILLUSTRATIONS (CONTINUED)

TABLES

1.0 SUMMARY AND BACKGROUND

SUMMARY

This report summarizes the results of Contract NAS2-8830, "Development of a Flexible Cryogenic Heat Pipe Program." The program was initiated in July 1975 and was completed in July 1977. The program was an analytical and experimental technology development effort to develop the technology and experience necessary for successful application of high performance flexible cryogenic heat pipes. Two pipes were designed and fabricated for testing and evaluation. One was designed for operation in the 100-200 K temperature range with maximum heat transport as a primary design goal; the other was designed for operation in the 15 - 100 K temperature range with maximum flexibility as a design goal.

Parametric performance and design trade-off studies were performed to determine the optimum geometry and materials for the container and wicking systems. The 100 - 200 K pipe was designed for operation with methane and ethane, and was optimized for methane in the range 110 - 140K. The 15 - 100 K pipe was designed for operation with nitrogen and oxygen, and was optimized for oxygen in the range 75 - 90 K.

The selected wick design was a multi-wrap composite, consisting of a spirally-wrapped coarse mesh screen encapsulated by a fine mesh outer wrap. Screw thread type V-grooves were machined into the evaporator and condenser walls for circumferential liquid distribution. A braided flexible stainless steel bellows assembly was used for the flexible section. The container was designed for a pressure safety factor greater than four, with an ultimate design burst pressure of 10.3×10^7 Pa.

The high power (100 - 200 K) heat pipe was tested with methane at 100 - 140K, and test data indicated only partial priming with a performance limit of less than 50 percent of theoretical. A series of tests were conducted with ammonia at ~280 K to determine the performance under varying fluid charge and test conditions. The low temperature heat pipe was tested with oxygen at 85 - 95°K and with methanol at 295 - 315°K. Performance of the

low temperature heat pipe was above the specification (6 - 8w vs. 4.5w) but was below theoretical predictions. Results of the completed testing are presented and possible performance limitation mechanisms are discussed in sections 5.0 and 6.0. The lower-than-expected performance was felt to be due to small traces of non-condensible gases which prevented the composite wick from priming. Additional investigation and parametric testing is recommended since all cryogenic composite wicks are subject to the same potential degradation.

BACKGROUND

As performance and lifetime requirements for future spacecraft systems and experiments become more stringent, the need and demand for reliable and efficient passive thermal control systems becomes more critical. This has been evidenced by the increasing number of spacecraft systems utilizing ambient temperature heat pipes over the past five years. More recently, the advantages of heat pipes for thermal control have been realized on systems operating at cryogenic temperatures. The RM-20B radiator (Reference 1) was the first application of cryogenic heat pipes into a space qualified thermal control system.

Preliminary design studies of future DOD and NASA programs and experiments indicate increasing applications of cryogenic heat pipes. In many cases, flexibility is required because of co-planar ground test requirements or to facilitate on-orbit deployment, orientation or scanning. Although the technology of rigid cryogenic heat pipes is reasonably well established down to 80°K, flexible cryogenic heat pipe development to date has been limited. A flexible cryogenic heat pipe with methane as the working fluid was tested at 110°K during 1974 (Reference 2). Although test data indicated that the concept was feasible, a highly flexible cryogenic heat pipe has yet to be developed and qualified. Below 80°K, little or no data exists although there appear to be applications with requirements as low as 20°K or lower.

In addition to providing a flexible heat transfer link for deployable or moving spacecraft systems, flexible heat pipes offer several advantages over rigid heat pipes in many applications. A flexible heat pipe:

(1) Facilitates fabrication by eliminating the need for accurate bends and alignment tolerances. Flexibility also facilitates installation and allows more accurate alignment of the heat pipe at critical interfaces.

(2) Minimizes or eliminates stresses in a system due to differential thermal contraction between the heat pipe and the system as the system is cooled to operating temperature levels. This feature is critical in applications where heat pipes interface with optical or infrared sensors which require extremely accurate alignment tolerances.

(3) Allows meaningful ground testing of heat pipes which require multiple plane bends in the installed configuration.

Potential NASA applications include the Shuttle Infrared Telescope facility, the NASA/JPL Gamma Ray Spectrometer, and the NASA/JSC Superconducting Magnetic Spectrometer. The use of flexible heat pipes to thermally link a detector or sensor with a cryostat or radiator provides needed flexibility of detector location, whereas in many conventional systems, the cryostat or radiator location is constrained by pointing requirements for the detector. This flexibility of location could result in reduced space and weight, lower dynamic loads, and lower environmental heat loads. Cryostats could also be better located to minimize center-of-gravity changes as the cryogen evaporates.

The two flexible pipes reported here were each chosen to be representative of a particular class of applications. The 100 - 200 K high power heat pipe is of the type useful for deployable radiators, where large distances or heat loads and a small number of flexures are generally required. The low temperature, maximized-flexibility pipe is applicable to cooling of moveable cryogenically-cooled detectors.

2.0 SPECIFICATIONS AND REQUIREMENTS

The high power heat pipe was to be designed for a specific operating temperature in the range of 100-200°K, with the heat transport capability as great as possible. The low temperature heat pipe was to be designed for a specific operating temperature in the range of 15-100°K. The heat pipes should meet or exceed the heat transport and static height values shown in Table 2-1 for various fluids. As discussed in Reference 3, the specified heat transport and static height values for neon may not be achievable with a single design for all of the fluids because of its poor surface tension.

The high power heat pipe was designed and optimized for operation with methane at 100 to 140°K. The low temperature heat pipe was designed and optimized for operation with oxygen at 77 to 90°K. The heat transport and static height corresponding to these temperature ranges for the high power and low temperature heat pipe are shown in Table 2-3.

In addition to the above specifications, the primary wick must be capable of self-priming against an adverse elevation (0.2 cm was selected for design purposes). The heat pipe must also be designed to withstand a burst pressure of four times the internal pressure of a fully charged pipe at the maximum service temperature (315°K). A schematic of a flexible heat pipe is shown in Figure 2-1 for reference.

Table 2-1 Specified Heat Transport and Static Height

High Power Heat Pipe

Working Fluid	Approximate Operating Temperature °K	Horizontal Plane Heat Transport Capability, W	Static Height, cm
CH_4	110	40	1.7
C_2H_6	140	35	1.7
Freon 13	180	20	0.6
NH_3	200	100	3.0

Low Temperature Heat Pipe

Working Fluid	Approximate Operating Temperature °K	Horizontal Plane Heat Transport Capability, W	Static Height, cm
H_2	20	4.0	1.4
Ne	30	0.5	0.2
N_2	77	2.5	0.6
O_2	90	4.5	0.6
CH_4	100	20.0	2.0

Table 2-2 Specifications for Flexible Cryogenic Heat Pipes

High Power Heat Pipe

Dimensions:

Overall Length	95 cm
Evaporator Length	15 cm
Transport Length	65 cm
Condenser Length	15 cm
Evaporator and Condenser Diameter	TBD
Flexible Section Diameter	As small as possible
Weight	As low as possible
Operating Temperature	100 - 200°K
Heat Transport and Static Height	See Table 2-1
Allowable Temperature Differential	4°K

Flexibility Requirements:

Minimum Bend Radius	20 cm
Bend Angle (Primary Plane	0 - 180°
Bend Angle (All other Planes)	0 - 90°
Lifetime	> 1000 Cycles before failure at Oper. Temperature
Elongation from Cryogenic to Ambient Temperature	As small as possible

Low Temperature Heat Pipe

Dimensions:

Overall Length	95 cm
Evaporator Length	15 cm
Transport Length	65 cm
Condenser Length	15 cm
Evaporator and Condenser Diameter	TBD
Flexible Section Diameter	As small as possible
Weight	As low as possible
Operating Temperature	15 - 100°K
Heat Transport and Static Height	See Table 2-1
Allowable Temperature Differential	3°K

Flexibility Requirements:

Minimum Bend Radius	14 cm
Bend Angle (Primary Plane)	0 - 180°
Bend Angle (All other Planes	0 - 90°
Bend Force at Operating Temperature	≤ 13.3 Nt
Lifetime	> 1000 Cycles before failure at Oper. Temperature
Elongation from Cryogenic to Ambient Temperature	As small as possible

Table 2-3 Heat Transport and Static Height for Design Temperature Ranges

	Operating Temperature (°K)	Horizontal Heat Load (W)	Static Height (cm)
High Power Pipe			
	100	20	2.0
	110	40	1.7
	140	35	1.7
Low Temperature Pipe			
	77	2.5	0.6
	90	4.5	0.6

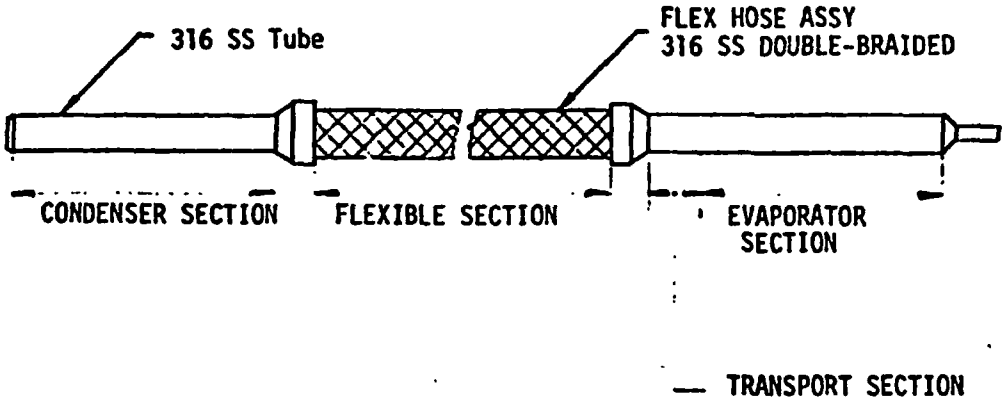

Figure 2-1 Flexible Heat Pipe Layout

3.0 DESIGN PARAMETERS AND TRADEOFFS

Although design procedures vary with application, the heat pipe design methodology generally consists of selecting a working fluid on the basis of its physical and thermodynamic properties in the required operating temperature range, and designing an envelope which will meet the specified performance and pressure containment requirements. Optimization generally involves either maximizing the transport capability within a fixed physical envelope, or minimizing the size and/or weight for a specified transport and conductance requirement.

The requirement for flexibility, particularly with cryogenic heat pipes, imposes a number of additional design considerations on the wick and container. The following paragraphs discuss the various factors as they relate to the optimization of a flexible cryogenic heat pipe.

WORKING FLUID

In general, the best working fluid is one which is compatible with applicable container materials and whose liquid transport factor $\left(N_\ell\right)$, wicking height factor (H), and thermal conductivity (k) are the highest. In addition, it is desirable to have the fluid's normal boiling point below the operating range in order to avoid excessive vapor losses. Furthermore, maximum flexibility and minimum container strength and weight are realized if the fluid has a low critical pressure and a high critical temperature. Pertinent fluid properties for the specified heat pipe fluids are shown as a function of temperature in Figures 3-1 through 3-4.

In the cryogenic regime, especially at the low end, there are a limited number of suitable fluids, and each has a relatively narrow operating range. For example, helium, hydrogen, and neon are probably the only fluids suited for operation in the 0 to 40°K range. Meaningful thermal tests with helium in the 0 to 8°K range are questionable. Hydrogen has adequate transport properties in the 15 to 30°K range but poses safety requirements. Neon has a relatively high liquid density and a very low surface tension which result

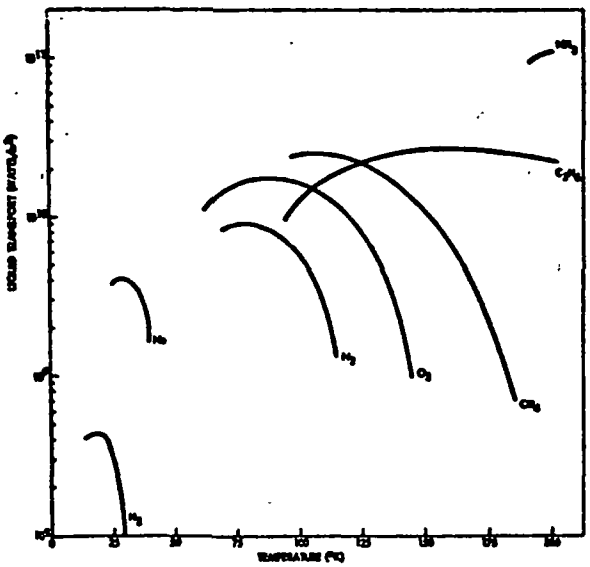

Figure 3-1. Liquid Transport Factor Vs. Temperature

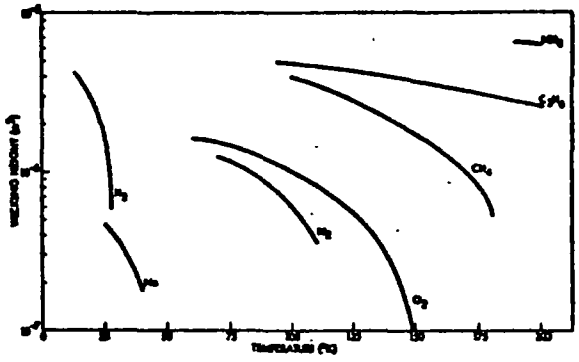

Figure 3-2. Wicking Height Factor Vs. Temperature

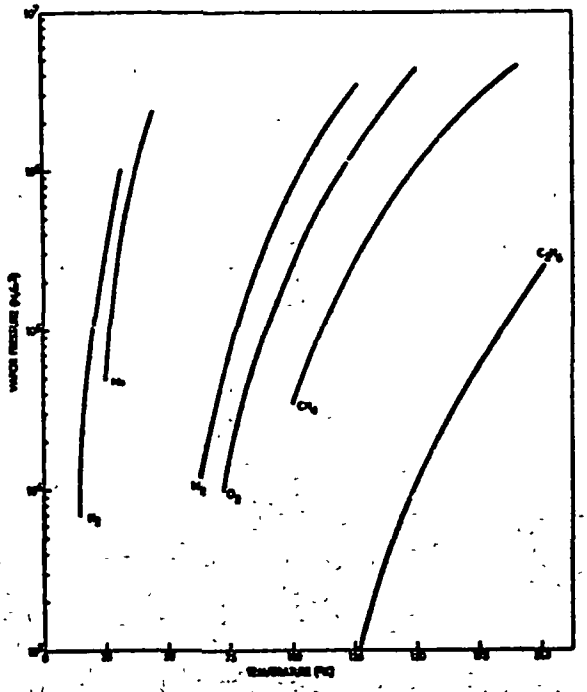

Figure 3-3. Vapor Pressure Vs. Temperature

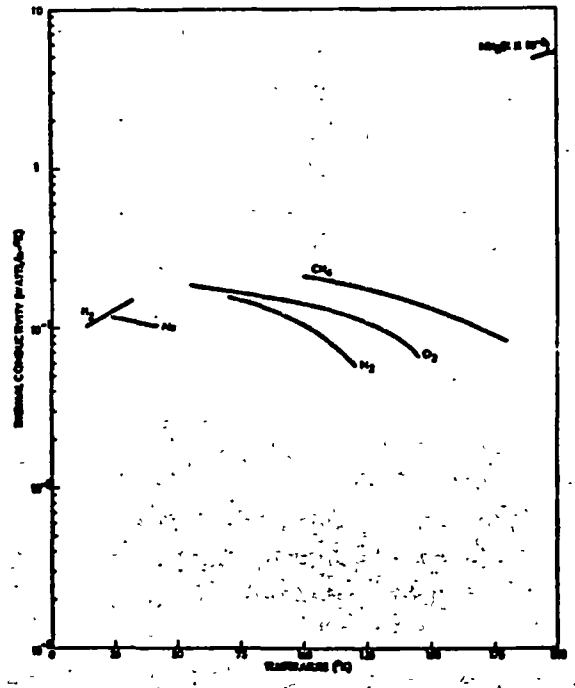

Figure 3-4. Thermal Conductivity Vs. Temperature

in an extremely low wicking height factor in the 3° to 40°K range. As a result, 1-g testing with this fluid is extremely difficult even with optimized wick designs. It should also be pointed out that between the critical temperature of neon (44.5°K) and the triple point of fluorine (54°K) no two-phase fluids exist. The 40-60°K range is therefore impractical for heat pipe operation.

Oxygen and nitrogen are the most suitable for the low temperature pipe. Fluorine was discounted on the basis of safety and handling; argon, on the other hand, has comparable transport properties, but its melting point is higher than either oxygen or nitrogen (84.2°K). Oxygen was selected as the working fluid for the low temperature pipe.

In the 100 to 200°K range, fluids have a broader operating range and their perofrmance is generally better. Methane and ethane have the highest heat transport and wicking height factors (with the exception of ammonia whose melting point is slightly below 200°K). Several of the Freons (e.g. F-13, F-14, and F-21) are also useable but their wicking height factors are approximately 1/2 that of either methane or ethane in the respective operating ranges. Consequently, less permeable wicks are required to satisfy the self-priming criterion and this in turn results in substantially lower transport. Methane was selected as the wicking fluid for the high power heat pipe.

CONTAINER DESIGN

Design considerations for the container include flexibility at operating temperatures, pressure containment at the maximum service temperature, flexural fatigue after repeated cycling, elongation, compatibility with the working fluid, and machinability and weldability. The thermal conductivity of the container wall is an important consideration in the evaporator and condenser. The material properties corresponding to pressure containment, elongation and flexibility are yield strength, thermal coefficient of expansion, and ductility, respectively. Various materials and designs for the flexible container were evaluated. The selected design is a 316 stainless steel braided flexible bellows assembly with a 316 stainless steel tube brazed at either end for the evaporator and condenser sections. In addition to satisfying requirements for flexibility, compatibility, containment, etc.,

this type of flexible hose is readily available as an "off the shelf" item.

The inside diameter (ID) of the container is determined by flexibility, thermal conductance, containment and transport requirements. Nominal 0.953 cm (3/8 in) and 0.635 cm (1/4 in) flexible hose sizes were selected for the high power and low temperature pipes, respectively, on the basis of a preliminary transport analysis and flexiblity requirements.

Evaporator and condenser I.D.'s must also be consistent with thermal conductance requirements. Available literature was reviewed to establish film coefficients for the methane and oxygen pipes (References 2, 4, 5 and 6). There are limited data for both fluids and in fact oxygen has been tested only in an axial grooved heat pipe (Ref. 4). Since axial groove film coefficients are generally lower than those for screw thread secondary wicks, the axial groove values were used to predict conservative conductances for the flexible pipe. A summary of film coefficients available in the literature for methane and oxygen is presented in Table 3-1.

Table 3-1 Film Coefficients for Oxygen and Methane

Fluid	Temperature °K	Wick Design	Evaporator		Condenser	
			(W/m^2-°C)	(BTU/hr-ft^2-°F)	(W/m^2-°C)	(BTU/hr-ft^2-°F)
Oxygen	100	Axial groove	2900	500	4900	865
Methane	100-130	Axial groove	1730	300	6100	1070
	100-120	Axial groove	2300	400	3300	570
	125	Spiral artery/ screw thread grooves	1700	300	-	-
	120	Multiple artery/ screw thread grooves	Average 3060 W/m^2-C (530 BTU/hr-ft^2-°F)			

The relatively low heat loads specified for the low temperature pipe allow the 3°C design goal to be satisfied with a tube ID less than 0.635 cm (1/4 in), and the specified 15-cm evaporator and condenser lengths. A 0.98 cm ID was selected for the evaporator and condenser sections to accommodate the oxygen pressure without using a reservoir.

It was necessary to increase the evaporator length of the high power pipe to 20.3 cm in order to limit its temperature drop to 3°C. Evaporator and condenser IDs could have been increased but these sections would become unnecessarily bulky and would impact the self-priming ability of the wick.

WICK DESIGN

The various factors that affect the wick design include self-priming and transport requirements, flexibility, and materials compatibility. Screen is readily available in 316 stainless which is also the container metal. Optimum flexibility in a screen wick is obtained by orienting the crossmembers or fibers on a bias relative to the longitudinal axis of the wick to avoid normal compression of the fibers in bending. With the square mesh screens that are commonly used to fabricate conventional wicks, bias angles between 30 and 60 degrees provide the greatest flexibility. In addition this also provides the axial pliability needed for expansion and contraction. Maximum flexure in all directions requires a wick which has a circular or annular cross-section and is concentric with the container. The cross-section should be as small as possible, consistent with transport and wicking height requirements.

Examination of the transport and static height specifications indicates that composite wick designs are required. Axially graded wicks are a possible alternative but they were not sufficiently developed to be considered for this application. A variety of composite wick designs have been tested. These include the pedestal artery, multiple central artery, spiral and tunnel artery, and multi-layer slab. The slab used in the feedback controlled heat pipe for the ATFE (Ref. 7) has demonstrated reliable zero-g start-up with a non-condensible gas present. Since some amount of gas generation must be expected over the life of a heat pipe, a multiwrap design with a circular cross-section was selected as the baseline. This wick consists of a circular core of coarse screen which is encapsulated by fine mesh screen at the inner and outer surfaces and at the ends. The coarse mesh provides high permeability for liquid flow while the outer mesh gives high capillary pumping. Spiral artery designs which utilize annular flow passages established by spacer wires between layers of fine mesh screen were considered

in the analysis as an alternate. Each design includes a centrally-located tunnel with both evaporator and condenser ends sealed with the fine mesh screen. This was done to permit operation with a Clapeyron-primed tunnel artery. No attempt was made to optimize with regard to the tunnel diameter.

Cross-sections of the two wick types are shown in Fig. 3-5. Four equally spaced interconnecting screen bridges are used in the evaporator and condenser sections to interface the centrally located primary wick with the circumferential screw thread grooves on the container wall. The bridges consist of two wraps of the fine mesh screen used in the primary wick.

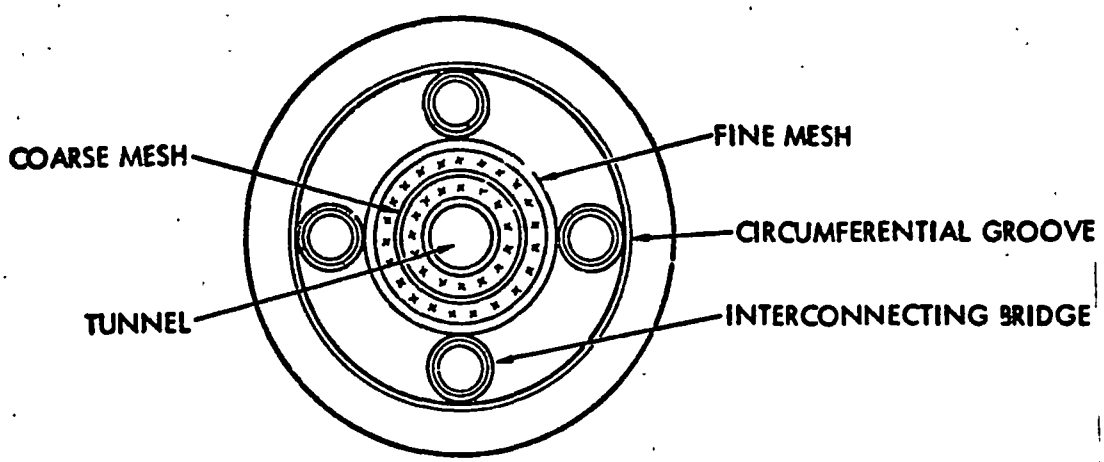

a) Multiwrap Wick Configuration

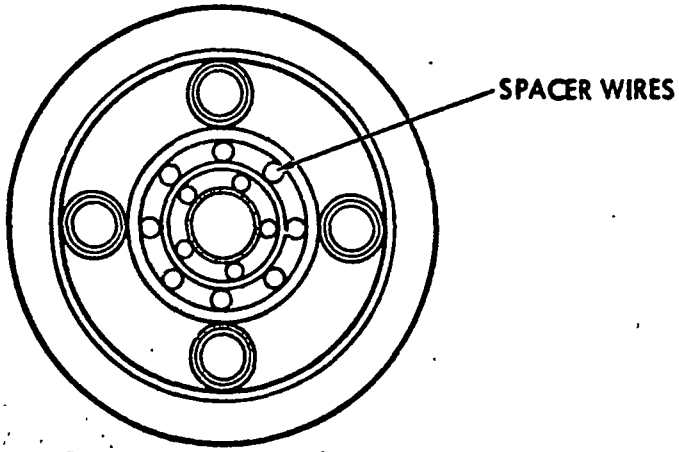

b) Spiral Artery Wick Configuration

Figure 3-5 Flexible Composite Wick Designs

4.0 ANALYSIS AND DESIGN

PARAMETRIC ANALYSIS

A parametric analysis was conducted to establish wick properties and cross-sections which yield optimized transport capability consistent with the previously specified design and performance criteria.

SELF-PRIMING

Once a container ID has been chosen, it is necessary to establish the wick parameters which satisfy the "1-g" self-priming requirement. The hydrostatic priming head $\left(H_{SP}\right)$ associated with priming a concentric wick of diameter D_W which is supported by bridges of diameter D_B and has an adverse elevation of 0.20-cm is given by

$$H_{SP} = D_W + D_B + 0.20 \text{ (cm)} \tag{4-1}$$

The corresponding pumping radius r_{SP} required for self-priming is

$$r_{SP} = \frac{2\sigma}{\rho_\ell g_o H_{SP}} \text{ (cm)} \tag{4-2}$$

where σ is the surface tension, ρ_ℓ the liquid density and g_o the gravitational constant. The self-priming radius was determined at 100°K and 140°K for oxygen and methane, respectively, since this will guarantee priming over the temperature range specified for each of these fluids. Also, in order to initiate the analysis it was necessary to estimate the diameters of the wick and bridges. This was done by assuming that the liquid and vapor flow areas are equal. Hence for a given container ID, values for D_W and D_B are readily determined. In general this assumption proved slightly conservative. Since transport requirements were easily satisfied, no iteration between self-priming and transport capability was performed.

In the case of the multi-wrap design, the corresponding mesh size of the coarse screen can be determined as (Reference 8)

$$M = \frac{2.54}{2\, r_{sp}} \qquad \left(\text{in}^{-1}\right) \tag{4-3}$$

Once the mesh size has been established, the coarse screen can be completely specified by defining its wire diameter d_w. This consists of maximizing the permeability within fabrication limits. The permeability of screens is determined from the Kozeny Equation (Reference 8).

$$K = \frac{1}{122} \frac{\epsilon^2}{(1-\epsilon)^2} d_w^2 \quad (cm^2) \tag{4-4}$$

where d_w is the wire diameter and

$$\epsilon = 1 - \frac{\pi}{4} (1.05) \frac{M d_w}{2.54} \tag{4-5}$$

Althout it is not explicit in the preceeding equations, for a given mesh size, the porosity and correspondingly the permeability increase as the wire diameter is decreased. However, experience gained in fabricating development samples of the wick for the low temperature pipe indicated that screens with wire diameters less than 0.17-mm are very sensitive to compression and tend to deform readily.

Flow permeability tests were rund on short spirally wrapped wick samples with various mesh sizes and wire diameters. The test set up is shown in Figure 4-1. Water was allowed to flow across the test specimen from a constant pressure head reservoir. The differential pressure across the specimen was measured with an open V-tube manometer. The mass flow rate was measured by collecting the efflux in a container and weighing it after a measured time interval. Test results for several wick samples are shown in Table 4-1.

Wire diameters of 0.33 and 0.14-mm were selected for the high power and low temperature heat pipes, respectively, on the basis of adequate permeability, and availability. For the spiral artery, the self-priming requirement dictates

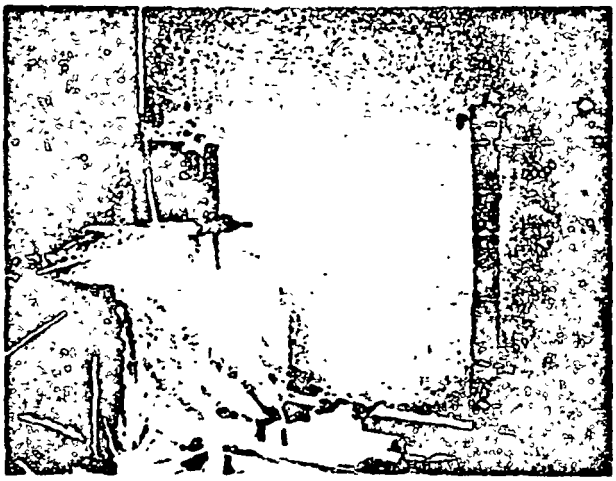

Figure 4-1 Wick Permeability Test Set-Up

Table 4-1 Permeability Test Results

Run	Specimen/ Description	Test Condition	Test Date	Diam (cm)	Length (cm)	$\dot{m}/\Delta h$ g/cm-sec	K $m^2 \times 10^{10}$
1	Ø1 - 200/36 composite	Tape wrapped (uncompressed)	9/15	.80	7.62	.099	18.8
2	"	Shrink Fit tubing (uncompressed)		.74	8.26	.047	11.4
3	Ø2 - 200/30 composite	Tape wrapped	9/15	.81	11.04	.066	17.6
4	"	"	9/23	"	"	.0656	17.5
5	"	Shrink Fit tubing (compressed)	9/23	.81	11.35	.092	25.2

the diameter of the spacer wires which in turn determines the wick's permeability.

TRANSPORT CAPABILITY

A computer program was written to determine the heat transport capability of the wicking system. The program models the secondary wick standoffs (bridges) and the circumferential screw threads as well as the primary axial wick. The program, called WICKPER, is described in Appendix A. Sample results are presented in Appendix B.

Once the wick parameters have been determined, the WICKPER program is used to establish the optimum wick area which gives the maximum transport capability at a specified temperature. The program calculates transport capability considering laminar liquid losses through the primary wick, the evaporator and condenser bridges, and the evaporator's screw thread grooves. Laminar or turbulent vapor flows are also taken into account. In order to avoid excessive vapor losses, which are less predictable than the laminar liquid flow, acceptable wick areas were limited to those which resulted in values of the friction parameter (F) being larger than 0.70, where

$$F = \frac{\Delta P_{\ell}}{\Delta P_{v} + \Delta P_{\ell}} \qquad (4\text{-}6)$$

This criterion was only applied in the wick optimization with the tunnel unprimed. Once the wick had been determined its performance with a primed tunnel was then predicted and generally the corresponding values of F were less then 0.70. The optimum wick area was determined at the low end of the specified temperature range (i.e., 75°K for oxygen, 100°K for methane), since the lower the temperature the more dominant the vapor losses.

HEAT PIPE DESIGN SUMMARY

A summary of the geometry, materials, and wick properties for the selected designs is shown in Table 4-2 for the high power heat pipe and in Table 4-3 for the low temperature heat pipe. These values were used for the parametric performance analysis described in the following section.

The methane pipe utilizes 200-mesh screen for the composite pumping and

Table 4-2 High Power Heat Pipe Design Summary

CONTAINER GEOMETRY	**LENGTH (CM)**	**I.D. (CM)**
EVAPORATOR	20.3	1.23
FLEXIBLE SECTION*	64.5	0.965
CONDENSER	15.0	1.23
WICK GEOMETRY		
PRIMARY WICK	MULTI-WRAP CIRCULAR CROSS-SECTION FORMED FROM 30-MESH COARSE SCREEN CORE WITH 200-MESH PERIPHERY	
O.D. (CM)	0.74	
TUNNEL DIAMETER (CM)	0.24	
INTERCONNECTING BRIDGES	TWO WRAPS OF 200-MESH SCREEN	
NUMBER	4	
I.D. (CM)	0.25	
CIRCUMFERENTIAL GROOVES	SCREW THREADS, 60° ANGLE	
NUMBER (GROOVES/CM)	72	
WICK PROPERTIES		
30-MESH WIRE DIAMETER (CM)		0.043
PERMEABILITY, THEORETICAL (CM^2)		2.70×10^{-5}
FLOW CONDUCTANCE (KA), THEORETICAL (CM^4)		0.82×10^{-5}
FLOW CONDUCTANCE (KA), MEASURED (CM^4)		2.54×10^{-5}
200-MESH PUMPING RADIUS (CM)		6.35×10^{-3}
MATERIAL	316 STAINLESS STEEL	
WORKING FLUID	METHANE	
OPERATING TEMPERATURE RANGE	100 - 140 K	

*NOMINAL 3/8 IN. FLEXIBLE HOSE

Table 4-3 Low Temperature Heat Pipe Design Summary

CONTAINER GEOMETRY		
	LENGTH (CM)	**I.D. (CM)**
EVAPORATOR (CM)	15.0	0.94
TRANSPORT (CM)	7.9	0.94
FLEXIBLE SECTION (CM)*	53.9	0.635
CONDENSER (CM)	15.0	0.94
WICK GEOMETRY		
PRIMARY WICK	MULTI-WRAP CIRCULAR CROSS-SECTION FORMED FROM 54-MESH COARSE SCREEN CORE WITH 250-MESH PERIPHERY	
O.D. (CM)	0.465	
TUNNEL DIAMETER (CM)	0.160	
INTERCONNECTING BRIDGES	TWO WRAPS OF 250-MESH SCREEN	
NUMBER	4	
I.D. (CM)	0.24	
CIRCUMFERENTIAL GROOVES	SCREW THREADS, 60° ANGLE	
NUMBER (GROOVES/CM)	72	
WICK PROPERTIES		
54-MESH WIRE DIAMETER (CM)		0.014
PERMEABILITY, THEORETICAL (CM^2)		1.148×10^{-5}
FLOW CONDUCTANCE (KA), THEORETICAL (CM^4)		0.126×10^{-5}
FLOW CONDUCTANCE (KA), MEASURED (CM^4)		0.386×10^{-5}
250-MESH PUMPING RADIUS (CM)		0.508×10^{-2}
MATERIAL	316 STAINLESS STEEL	
WORKING FLUID	OXYGEN	
OPERATING TEMPERATURE RANGE	70 - 110 K	

*NOMINAL 1/4 IN. FLEXIBLE HOSE

the bridges. This was selected since it is about the smallest mesh size that is compatible with the screw thread grooves. The oxygen pipe uses 250-mesh screen only to insure that equivalent 200-mesh pumping is attained even with degradation due to screen imperfections or as a result of fabrication. Theoretical and measured values are listed for the liquid flow conductance (KA). Theoretical values were used to define the wick geometry and verify that the heat pipe's performance satisfied the specified transport. After each wick had been fabricated, permeability tests were performed and the actual KA was measured (see Section 5.0). Transport capability was then recalculated using the measured values which are three times greater than theoretical for both wicks. The wick diameters which were determined from the analysis and subsequently fabricated are also listed in the Tables for completeness.

PARAMETRIC PERFORMANCE

The maximum zero-g transport capability that was determined for the multi-wrap design using theoretical wick properties is presented in Figure 4-2 as a function of temperature. These results are with the tunnel unprimed and were determined utilizing the wick area which gave the maximum transport at the low end of the specified temperature range for the oxygen and methane pipes. Performance with nitrogen and ethane is also indicated, as well as the effect of bellows size. The transport capability with oxygen or nitrogen is almost twice as great when the bellows size is 3/8-in. versus 1/4-in. Since the performance specified for the low temperature pipe was easily met with oxygen, the smaller diameter was selected to maximize flexibility. There is negligible improvement with a 1/2-in. bellows versus a 3/8-in. bellows with either methane or ethane. In this case, the area increase is not as pronounced and the gain is more than offset by the decrease in permeability which results from the higher self-priming requirement. However, sufficient performance margin is available with the 3/8-in. size.

The maximum heat transport capability is presented in Appendix B for each of the systems shown in Figure 4-2. Primed and unprimed tunnel performances are compared. The effect of the tunnel is to increase the liquid flow

LOW TEMPERATURE HEAT PIPE	HIGH POWER HEAT PIPE
(NITROGEN AND OXYGEN)	(METHANE AND ETHANE)
MULTI-WRAP WICK	MULTI-WRAP WICK
TUNNEL DIAMETER = 0.160-CM	TUNNEL DIAMETER = 0.241-CM
0.635-CM (1/4-IN.) BELLOWS	0.953-CM (3/8-IN.) BELLOWS
$(KA)_{THEOR} = 0.126 \times 10^{-13}$ M^4	$(KA)_{THEOR} = 0.816 \times 10^{-13}$ M^4
0.953-CM (3/8-IN.) BELLOWS	1.27-CM (1/2-IN.) BELLOWS
$(KA)_{THEOR} = 0.368 \times 10^{-13}$ M^4	$(KA)_{THEOR} = 0.740 \times 10^{-13}$ M^4

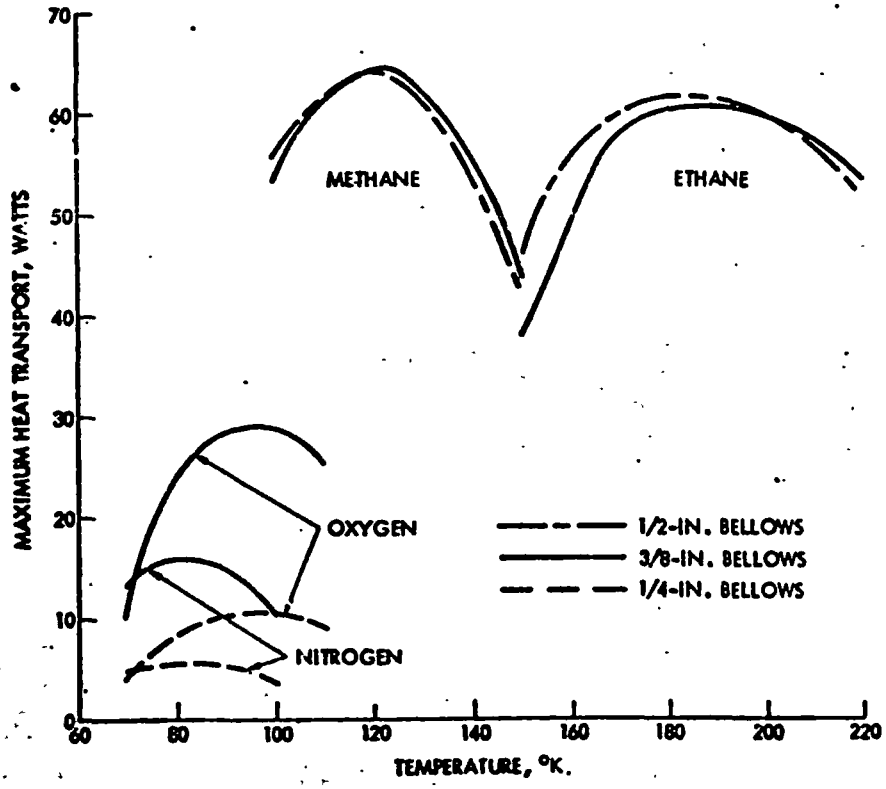

Figure 4-2 Heat Transport Summary based on Theoretical Wick Permeability

conductance (KA) where

$$KA = (KA)_{Wick} + (KA)_{Tunnel} \qquad (4\text{-}7)$$

Hence, the smaller the wick's conductance, the more dominant is the effect of the tunnel. As a result, improvements are most pronounced for nitrogen whose wick permeability is inhibited by the self-priming requirement and, correspondingly its relatively low wicking height factor (H). On the other hand, the higher the vapor losses (i.e., the smaller the values of F), the smaller the gain due to a primed tunnel.

Also included in Appendix B are the performance predictions for optimized spiral artery designs with methane and oxygen and 3/8 and 1/4-in. bellows, respectively. A comparison of Figures B-1 and B-3 shows approximately 20% higher performance for the spiral design with methane. In the case of oxygen, there is about a 2:1 increase (cf. Figures B-6 and B-8). The higher transport is derived from the higher flow conductance of the spiral wick. However, this wick is more difficult to fabricate than the multi-wrap design, particularly in smaller diameters. Furthermore, the realiability of the multi-layered system has been established with a non-condensible gas present. As a result, since its predicted performance margins are adequate, the multi-wrap was selected as the baseline design.

The maximum zero-g heat transport predicted for the as-built systems is presented in Figure 4-3 as a function of temperature for both a primed and unprimed tunnel. Performance with nitrogen in the low temperature pipe and ehtane in the high power pipe is also shown. A maximum of 27 W at 100°K can be attained with the baseline oxygen system. Its performance drops off to 5 W at 70°K due to high vapor losses. Performance with the tunnel primed is virtually identical at 70°K due to the predominance of the vapor loss. In the 90 - 110°K range, the primed tunnel offers approximately a factor of two (2) improvement. A maximum of 15 W at 82°K can be attained with nitrogen with the tunnel unprimed. Again the primed tunnel increases the maximum performance by about a factor of two (2). The results indicate that nitrogen, which has the same wicking height and therefore self-priming ability at 80°K as oxygen at 100°K, would be preferred at temperatures below 80°K.

LOW TEMPERATURE HEAT PIPE	HIGH POWER HEAT PIPE
(NITROGEN AND OXYGEN)	(METHANE AND ETHANE)
MULTI-WRAP WICK	MULTI-WRAP WICK
0.635-CM (1/4 IN.) BELLOWS	0.953-CM (3/8 IN.) BELLOWS
TUNNEL DIAMETER = 0.160 CM	TUNNEL DIAMETER = 0.241 CM
$(KA)_{MEAS} = 0.386 \times 10^{-5}$ CM^4	$(KA)_{MEAS} = 2.5 \times 10^{-5}$ CM^4

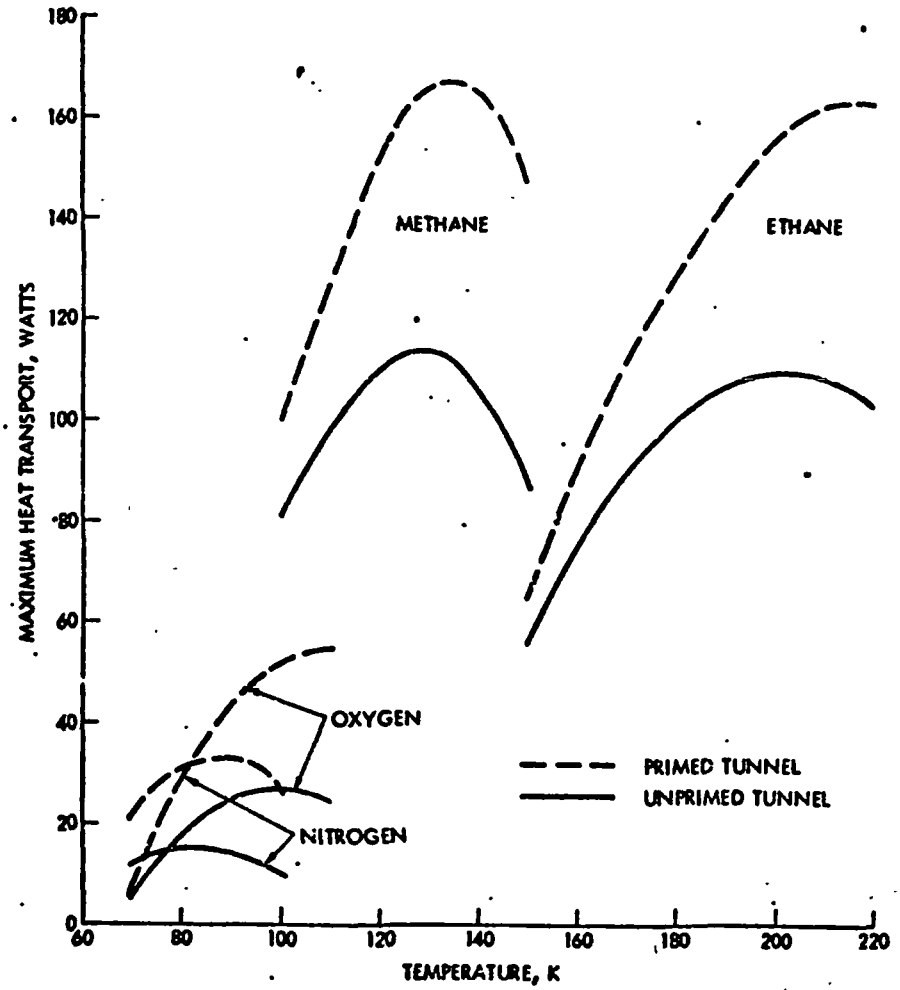

Figure 4-3 Heat Transport Summary Based on Measured Wick Permeability

Approximately 110 W can be transported with either methane or ethane at the midpoint of their respective operating ranges. The improvement afforded by the primed tunnel is only 50% in the high power pipe. This is due to the higher flow conductance (KA) of the multi-wrap wick in this system.

Although the measured (KA) of the fabricated wicks is approximately three times greater than the theoretical value, the overall heat pipe performance is generally only 2-2.5 times better. This is due to increased vapor losses and, as will be discussed shortly, the screw thread grooves are also limit the performance.

The zero-g transport with the wick performing as an open-artery (i.e. pumping derived from coarse mesh screen) is compared to the primed cases in Figures 4-4 through 4-7 for each of the fluids. In all cases, the performance is approximately 20% of that provided by the composite with the tunnel unprimed. Also shown in these figures are the friction parameter (F) and the pumping ratio (γ). As just discussed, the higher permeability obtained with the actual wicks leads to higher vapor losses and thus the values of F become less than 0.70 over a large fraction of the temperature range. As expected, the vapor losses are also more pronounced when the tunnel is primed. Turbulent vapor flow $\left(R_e > 2200\right)$ will exist in both pipes if the tunnel is primed. The vapor is turbulent with and without the tunnel primed for both methane and ethane.

The pumping ratio (γ) is defined as the ratio of the actual pumping developed by the primary wick to the maximum that can be obtained with the fine mesh screen. When this parameter is less than one (1), it indicates that the secondary wick in the evaporator (i.e., screw thread grooves) is limiting the heat pipe's performance. The vapor losses tend to be higher in the oxygen pipe and as a result the secondary wick, which represents a liquid loss, is limiting only when the tunnel is primed with oxygen. The screw thread grooves limit the performance of all other fluids in either tunnel condition. These results point up the need for improving circumferential liquid distribution in the heat pipe evaporator sections. An increase in the groove area covered by the bridges would tend to alleviate this situation.

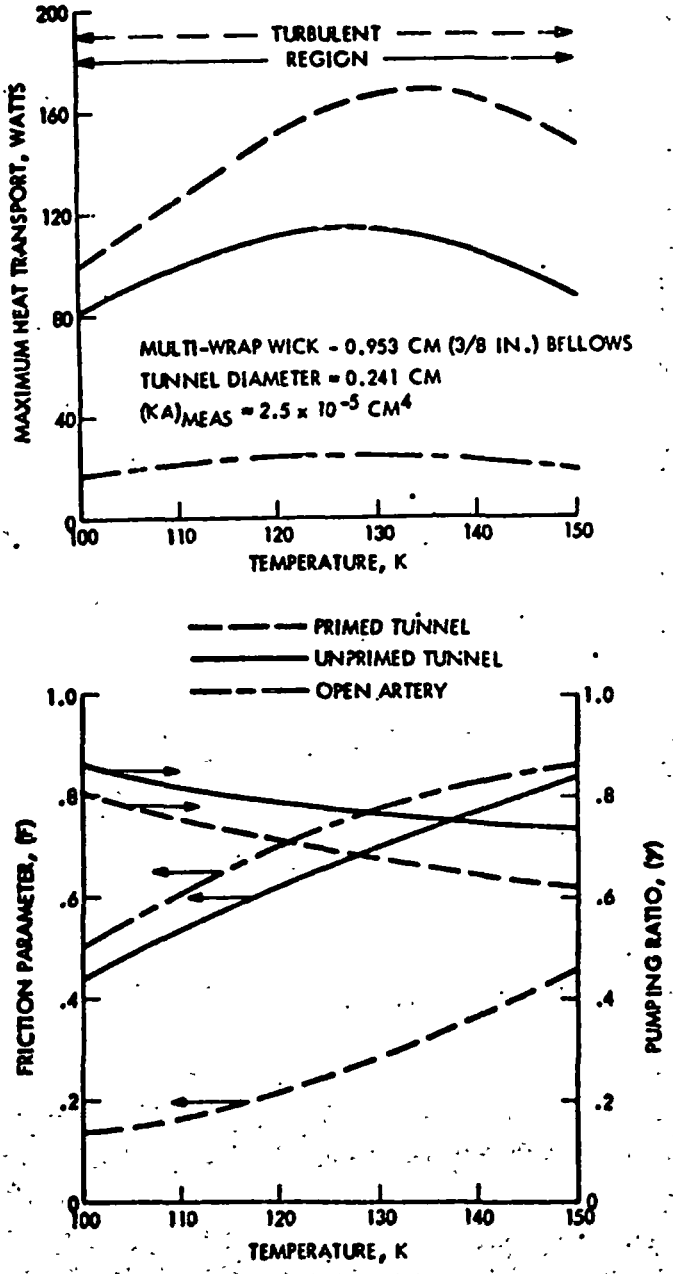

Figure 4-4 Theoretical Performance of High Power Flexible Heat Pipe in "0-g" (Methane)

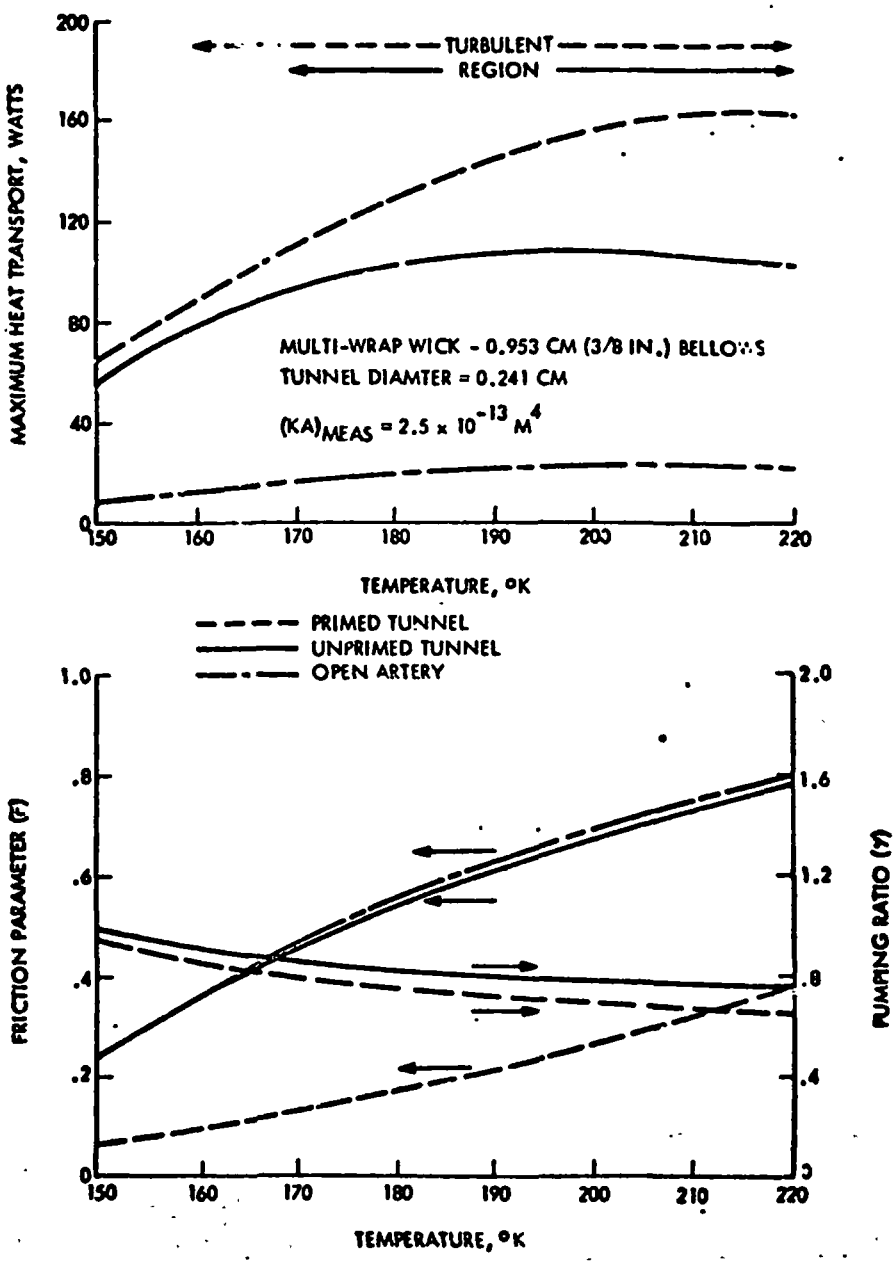

Figure 4-5 Theoretical Performance of High Power Flexible Heat Pipe in "0-g" (Ethane)

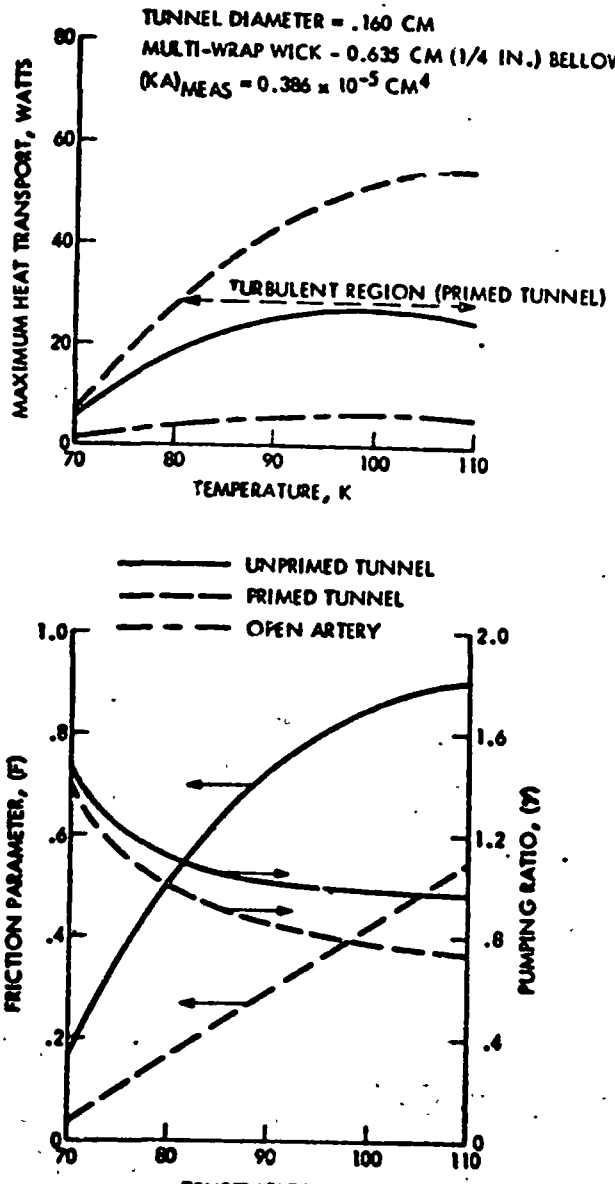

Figure 4-6 Theoretical Performance of Low Temperature Flexible Heat Pipe in "0-g" (Oxygen)

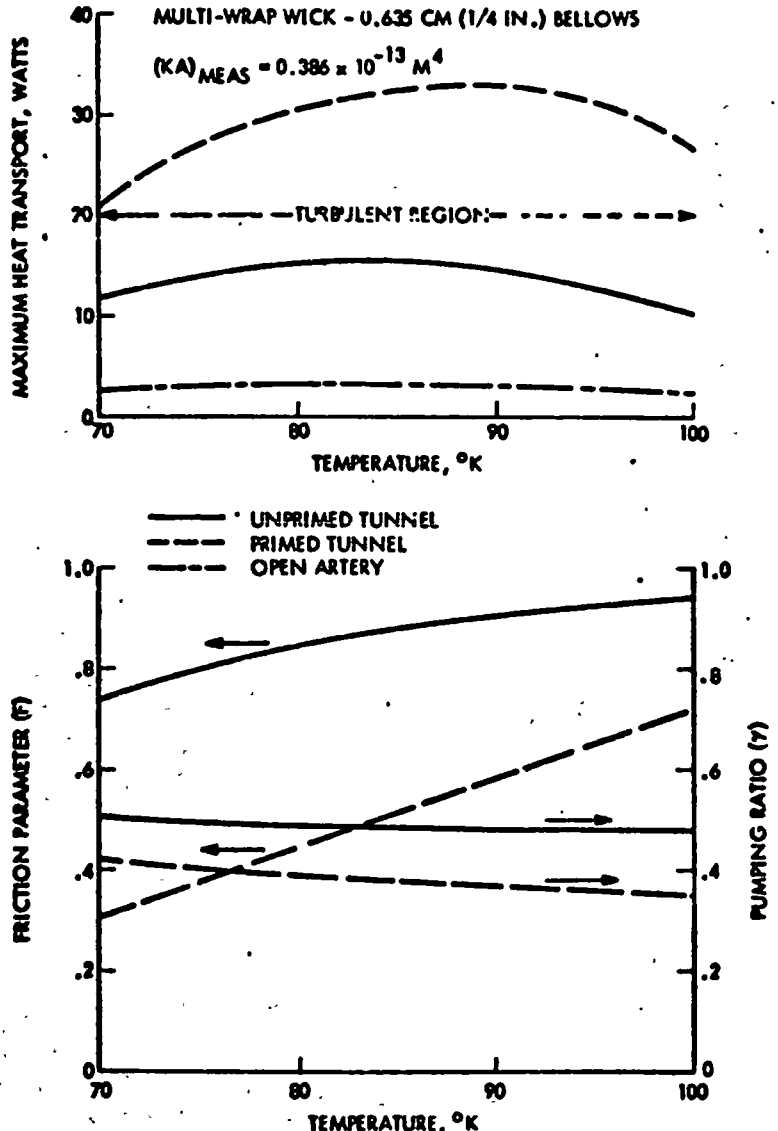

Figure 4-7 Theoretical Performance of Low Temperature Flexible Heat Pipe in "0-g" (Nitrogen)

The "1-g" transport capability of both heat pipes at various temperatures with the tunnel unprimed is shown in Figures 4-8 through 4-11 for each of the fluids. The change in slope exhibited by several of the curves is associated with the secondary wick limiting the system's performance at the higher heat flows. As the elevation is increased and the heat flow decreases, the ratio (γ) increases to a value of one (1). At this point the screw threads are no longer limiting and the curve changes slope.

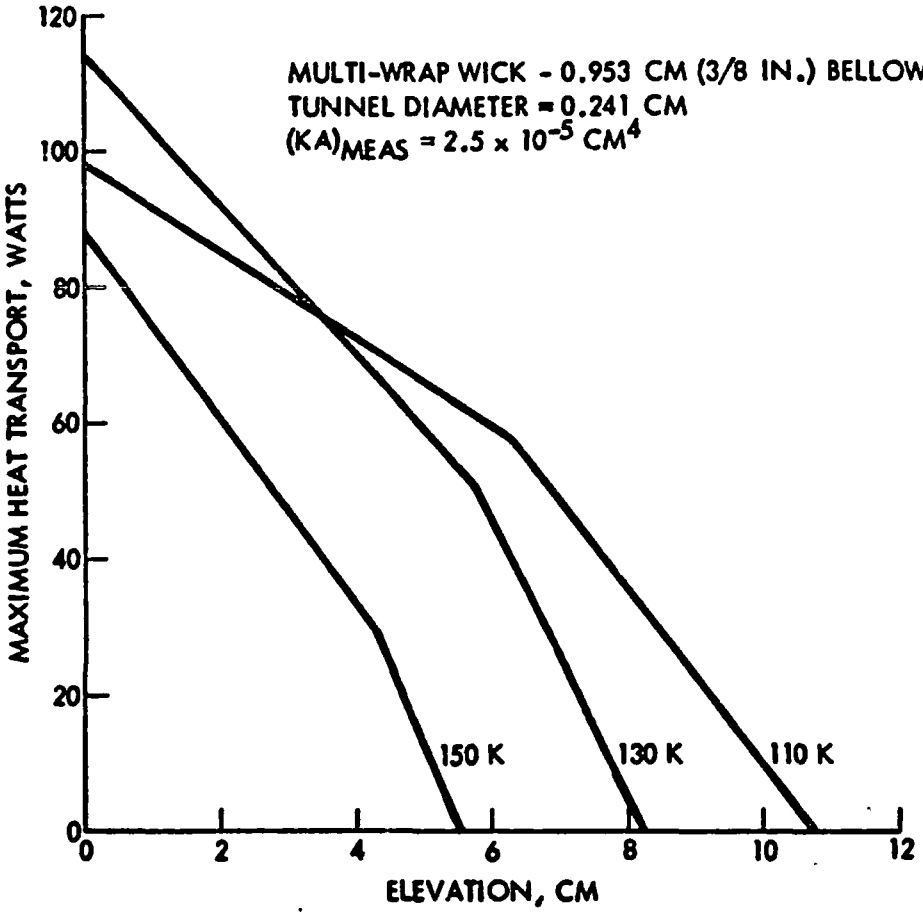

Figure 4-8 Heat Transport Capability of High Power Flexible Heat Pipe vs. Elevation (Methane)

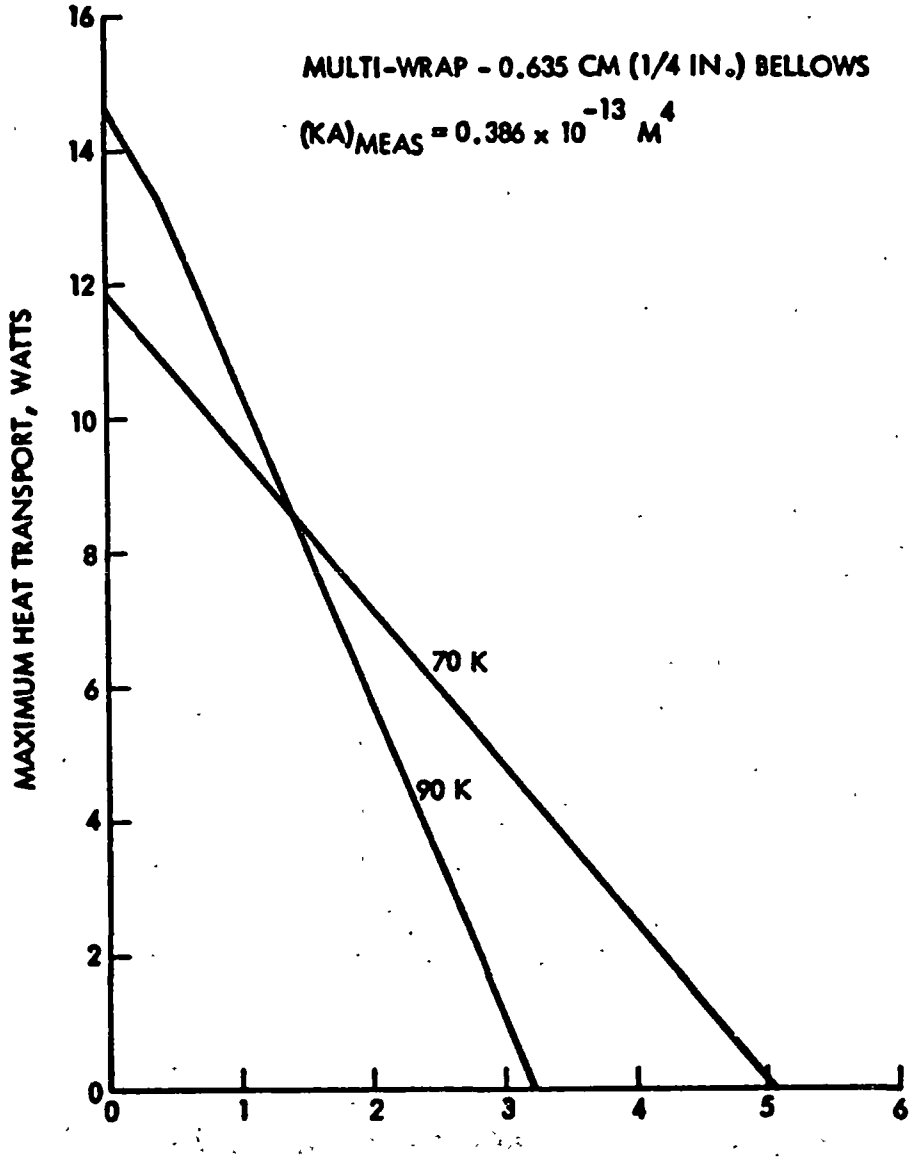

Figure 4-9 Heat Transport Capability of High Power Flexible Heat Pipe vs. Elevation (Ethane)

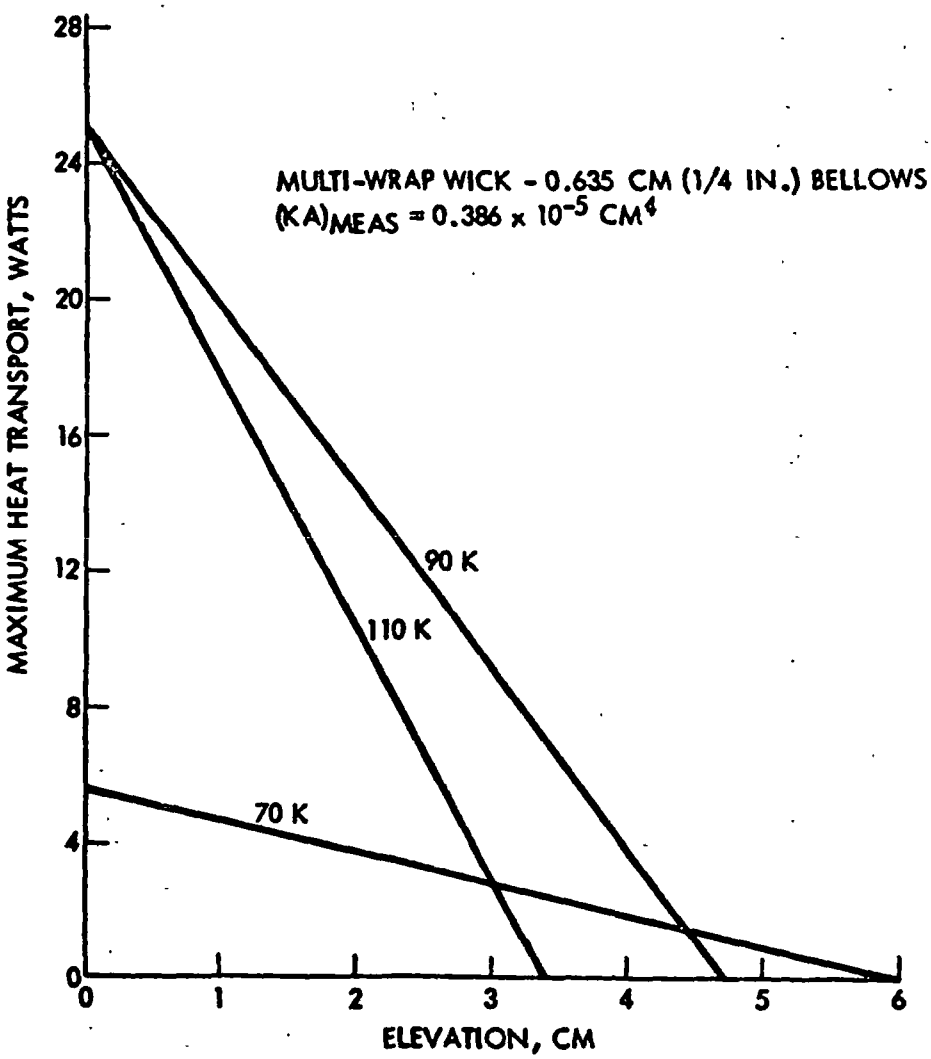

Figure 4-10 Heat Transport Capability of Low Temperature Flexible Heat Pipe vs. Elevation (Oxygen)

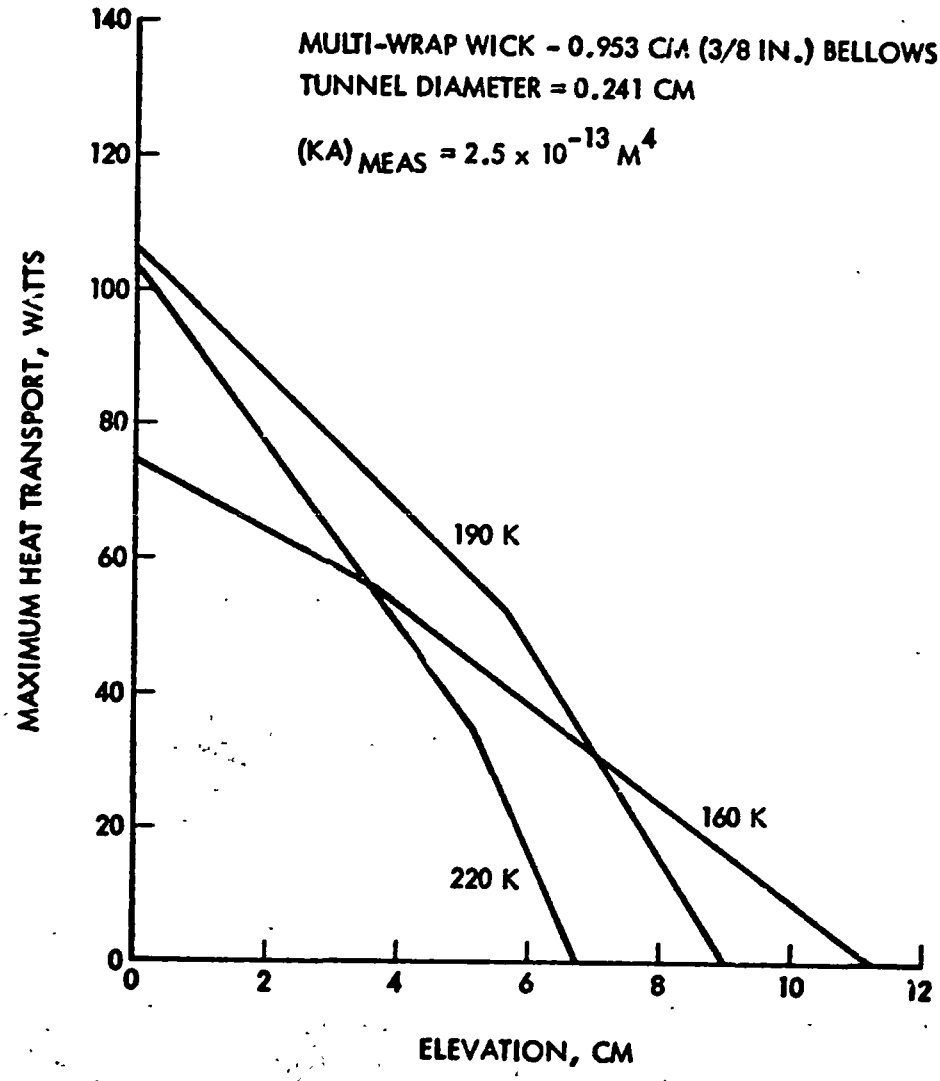

Figure 4-11 Heat Transport Capability of Low Temperature Flexible Heat Pipe vs. Elevation (Nitrogen)

5.0 HIGH POWER HEAT PIPE FABRICATION AND TEST

This section summarizes the results of the fabrication and test program for the high power heat pipe which was the first to be fabricated. Since this was a technology development program, both the fabrication and test efforts necessarily involved some degree of trial and error. The discussion below highlights some of the problems encountered and describes the method of solution. The test program involved several thermal performance tests with methane and with ammonia as well as investigative tests to help explain the behavior of the pipe. Preliminary test results were presented at the 11th AIAA Thermophysics Conference in 1976 (Reference 9).

HEAT PIPE FABRICATION

The high power heat pipe was fabricated in accordance with the assembly drawing, Figure 5-1. The container consists of a 0.95 cm (3/8 in) flexible metal bellows assembly with a length of schedule 80 tubing welded to each end (Figure 5-2). The bellows is covered with a double braided wire sheath to provide a design burst pressure of 1.03×10^8 Pa (15000 psi). The ends are machined and internally threaded with 72 threads /cm to provide circumferential wicking. The primary wick, as discussed in Section 4.0, is a spiral multiwrap of 30 mesh screen encapsulated by a 200 mesh outer wrap. The screen is cut on a 45° bias to provide flexibility. Four screen bridges are used at the evaporator and condenser ends provide radial liquid distribution (Figure 5-1) and are also 200 mesh screen.

The fabrication and testing sequence for the high power heat pipe is shown in Figure 5-2. A summary of the detailed fabrication and assembly is described below.

Flexible Container

The flexible container was purchased as an integral unit with a length of schedule 80 316 SS tubing welded at either end. The flexible container geometry is shown in Figure 5-3 in the as-purchased configuration. Dimensions are shown for both the high power and the low temperature heat pipe con-

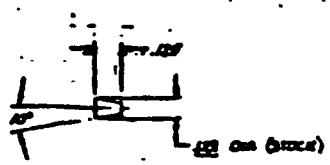

DETAIL -013
SCALE 4/1

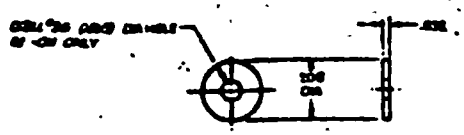

DETAIL -011 & -012
SCALE 4/1

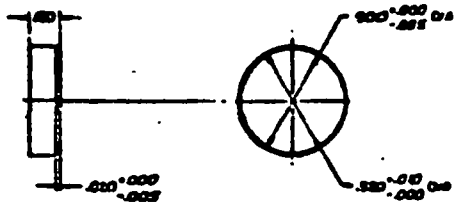

DETAIL -005
SCALE 4/1

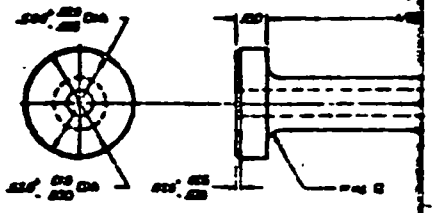

DETAIL -006
SCALE 4/1

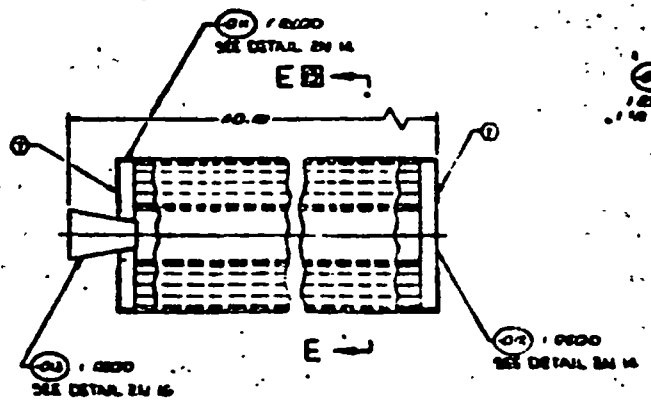

-003 ASSY
HEAT-REMP COMPOSITE WICK
SCALE 1/1

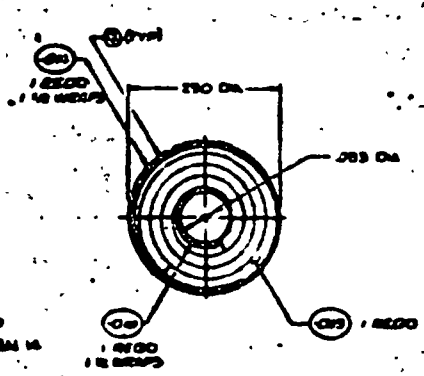

SECT E-E
SCALE 1/1

FOLDOUT FRAME

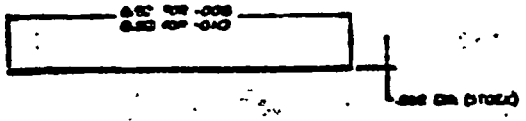

DETAIL -008 & -010 [5]
SCALE 1/1

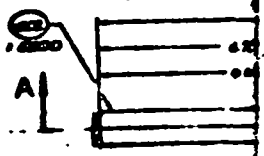

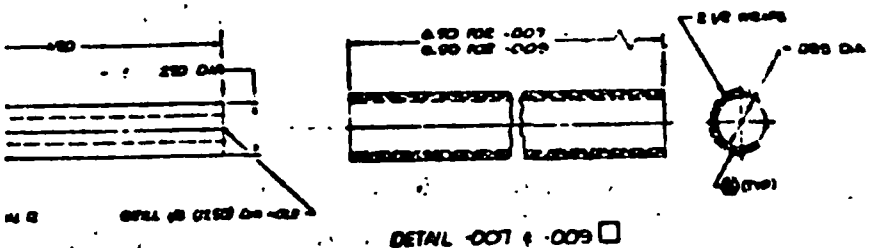

DETAIL -007 & -009 [6]
SCALE 10/1

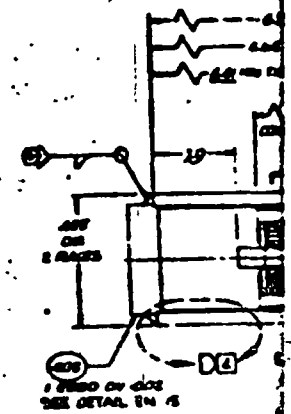

ORIGINAL PAGE IS
OF POOR QUALITY

FOLDOUT FRAME 2

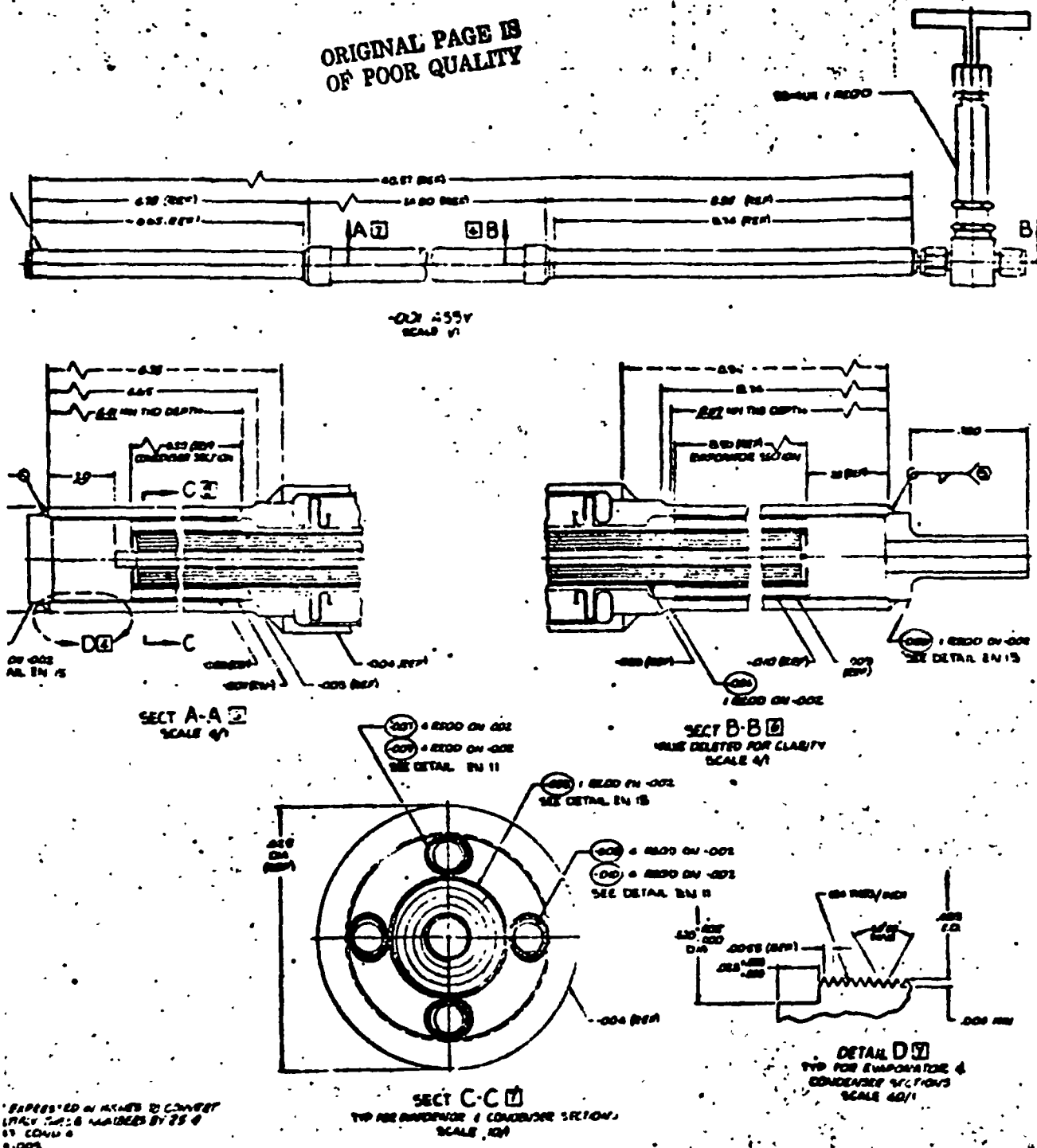

FOLDOUT FRAME 3

Figure 5-1 High Power Heat Pipe Design Details

FOLDOUT FRAME 4

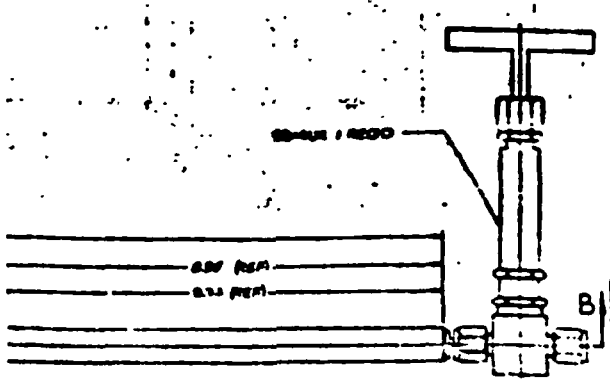

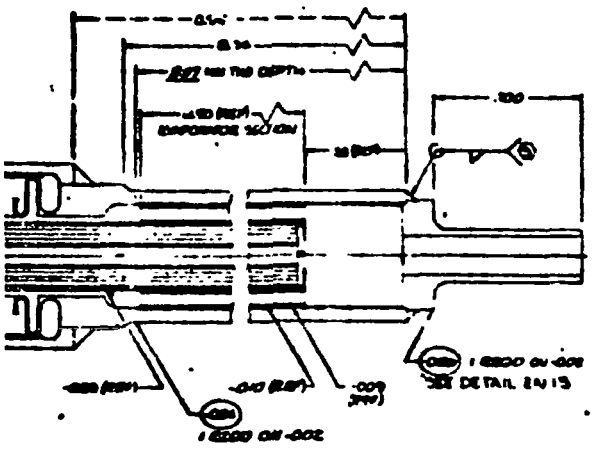

SECT B-B
VALUE DELETED FOR CLARITY
SCALE 4/1

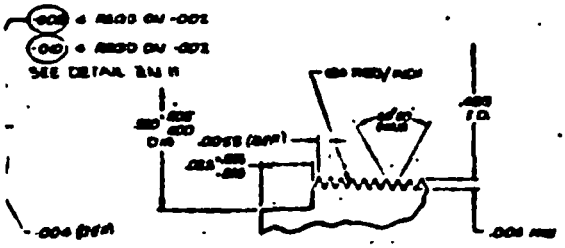

DETAIL D
TYP FOR EVAPORATOR &
CONDENSER SECTIONS
SCALE 40/1

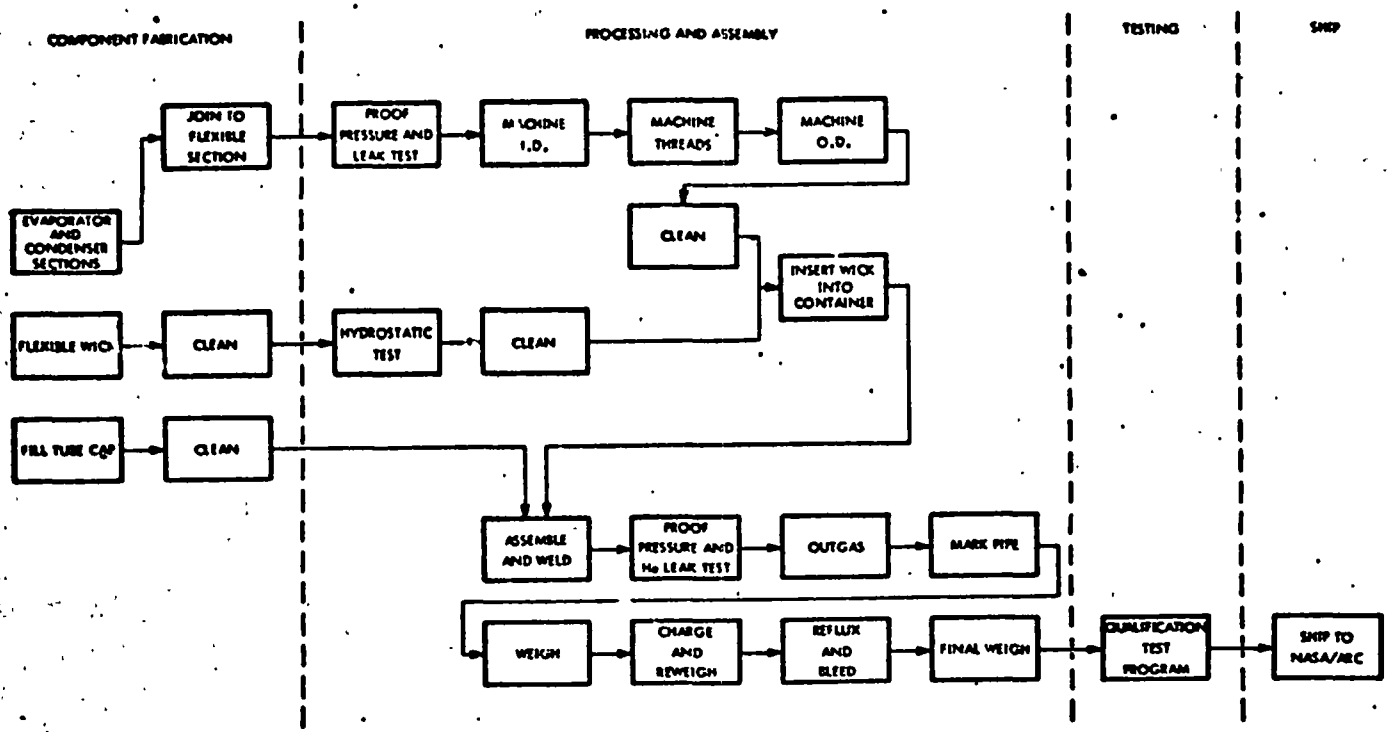

Figure 5-2 Heat Pipe Fabrication Sequence

figurations.

Upon receipt from the outside supplier, the assemblies were successfully subjected to a proof pressure test of 2.4×10^7 Pa (3500 psig) and a helium leak at 2.1×10^7 pa (3000 psig). One of the hose assemblies, identified as H8, was then hydrostatically burst tested. Failure occurred at 77.9MPa (11,300 psig) in the longitudinal weld of the bellows section (Figure 5-4).

The evaporator and condenser ends were subsequently drilled and reamed to an internal diameter of 1.23 cm (0.485 in). The inside walls were then internally threaded with 72 grooves /cm as indicated in Figure 5-1. Threading was accomplished with a "blind" boring bar developed by Rockwell under a previous IR&D program (Reference 10). The guide bar was modified for this program to match the I.D. of the tube. Problems were encountered during initial threading attempts due to galling between the guide bar and the tube which were both stainless steel. The problem was remedied by honing the inside diameter of the tubes and switching to an aluminum bronze guide bar. After threading, the ends were cut to length and the O.D. was turned down to a final diameter of 1.59 cm (.625 in). The final dimensions are shown in Figure 5-5.

Primary Wick Fabrication and Testing

The primary heat pipe wick consists of two types of annealed 316 stainless steel screen wrapped, on a 45 degree bias, in multilayers. The inner layer was 200 x 200 mesh .0058 cm (0.0023 inch) diameter screem with a tunnel .24 cm (0.093 in). After continuous resistance welding of the longitudinal overlap seam, the tunnel was static pressure tested to determine the minimum bubble pressure of the wick assembly. The test set-up, shown in Figure 5-6, consists of a methanol bath in which the wick is inversed, a regulated GN_2 supply and a micrometer needle value, and an open U-tube manometer. The wick is held level just below the surface of the methanol. Pressure is gradually increased and read out on the manometer. When the first leak (bubble) occurs, the pressure is reduced slightly and recorded. The pressure is then increased and the number and location of the first leaks is recorded.

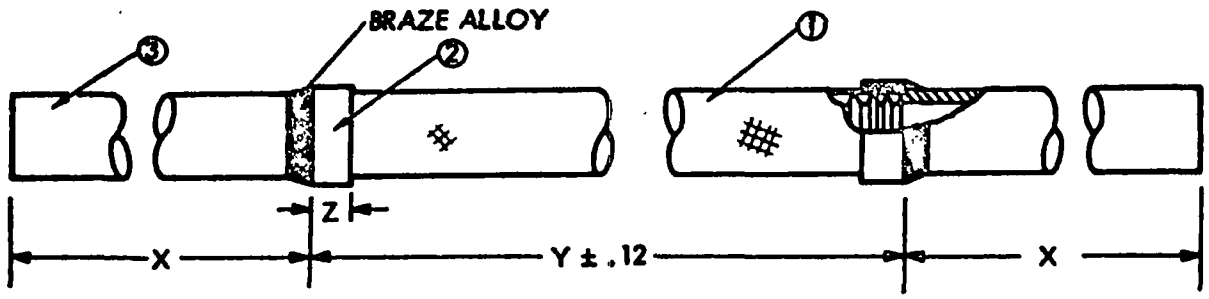

	ITEM NO.	DESCRIPTION	PART NO. - COAST METAL CRAFT	LENGTH (IN.)
LOW POWER HEAT PIPE	1	FLEX TUBE - .25 ID - BRAIDED, 2 LAYERS	1/4" BW 16 - 2H	Y = 19.90
	2	BRAID RETAINER	90890-020	Z = 11/32
	3	1/4" SCH 80S IPS (.540" OD/.302" ID)	90890-111	X = 12.00
HIGH POWER HEAT PIPE	1	FLEX TUBE - .38 ID - BRAIDED, 2 LAYERS	3/8" BW 16 - 2H	Y = 24.80
	2	BRAID RETAINER	S - 050	Z = 13/32
	3	3/8" SCH 80S IPS (.675" OD/.423" ID)	90888-111	X = 10.00

NOTE: ALL MATERIAL IS 316 STAINLESS STEEL, EXCEPT BRAID WIRE IS 321 STAINLESS STEEL AND RETAINER BRAZE ALLOY IS AMS4770 FILLER METAL

Figure 5-3 As-Received Flexible Bellows Assemblies

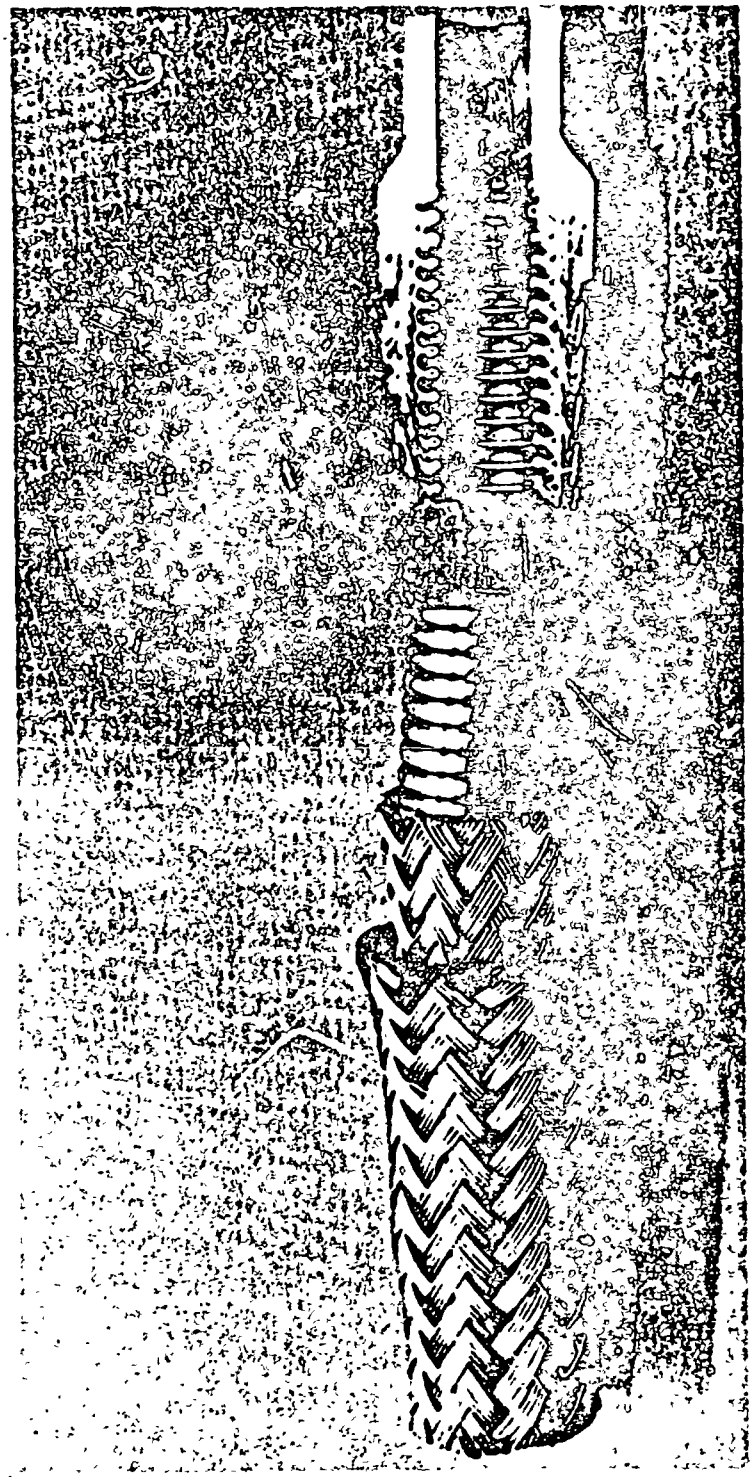

Figure 5-4 High Power Heat Pipe Bellows Failure

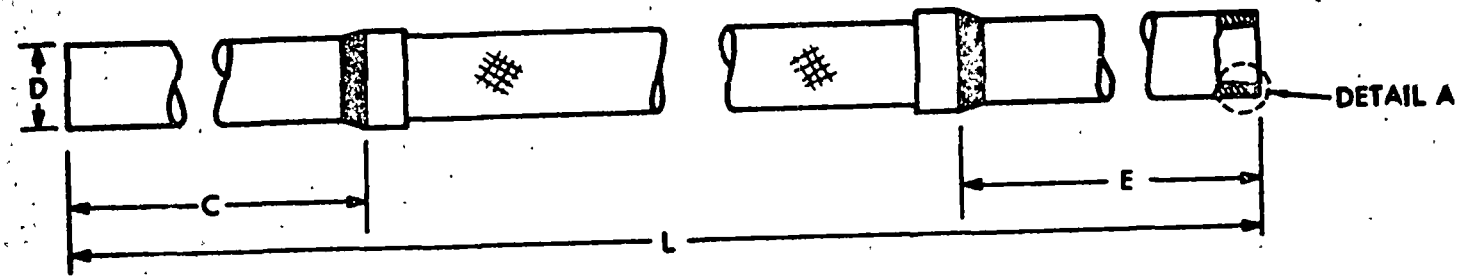

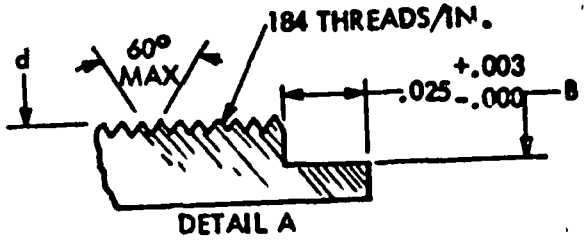

	HIGH POWER HEAT PIPE	LOW POWER HEAT PIPE
CONDENSER LENGTH (C)	6.78 IN.	6.70 IN.
EVAPORATOR LENGTH (E)	8.94 IN.	9.92 IN.
OVERALL LENGTH (L)	40.57 IN.	36.42 IN.
OUTSIDE DIAMETER (D)	0.625 IN.	0.500 IN.
C/BORE DIAMETER (B)	0.500 IN.	0.400 IN.
ID BEFORE THREADING (d)	0.485 IN.	0.368 IN.

Figure 5-5 Flexible Bellows Assemblies After Machining

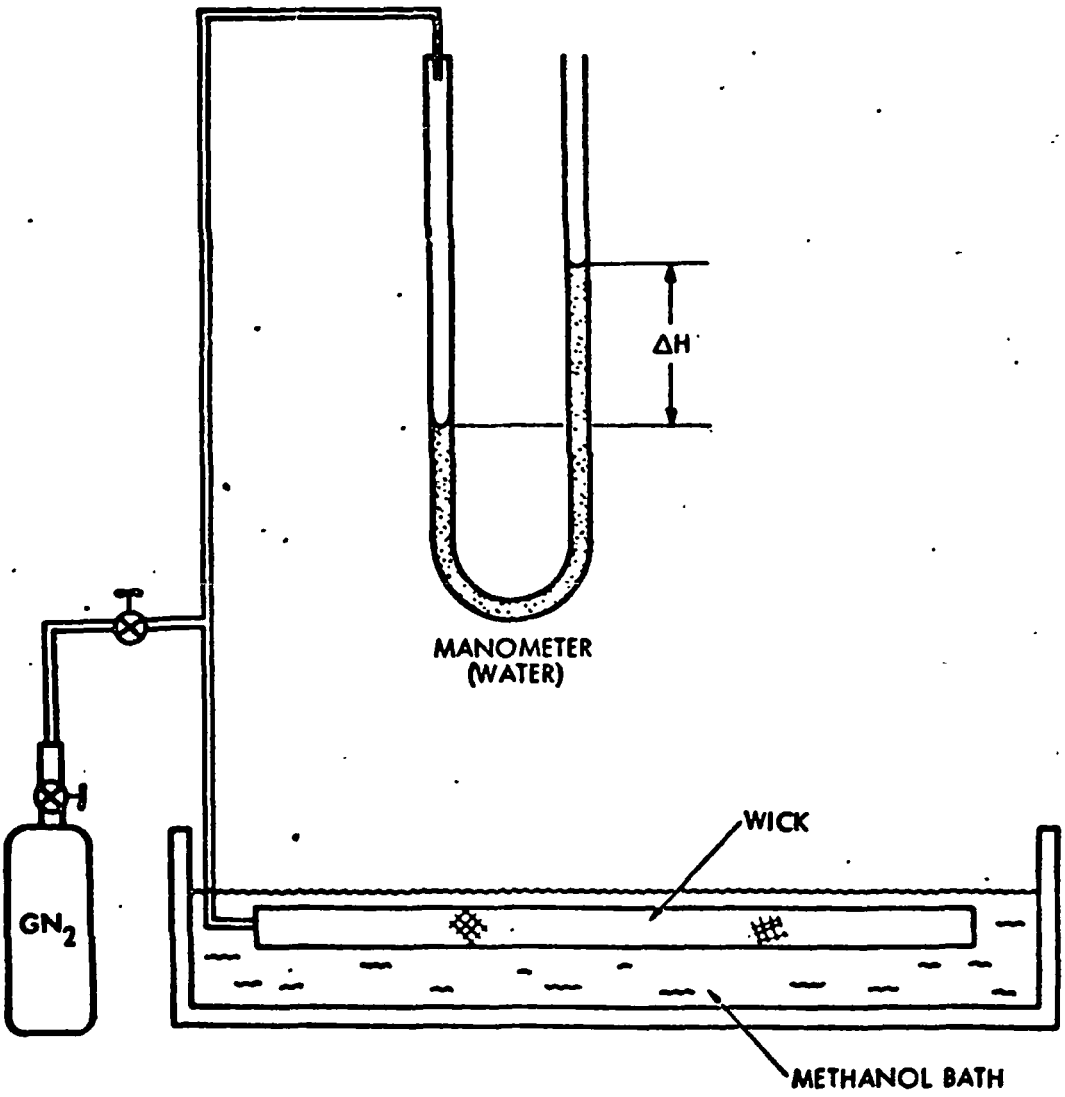

Figure 5-6 Heat Pipe Wick Static Pressure Test Set-Up

An acceptance level of 90 percent of 200 mesh pumping was established for the high power heat pipe wick. For a methanol bath and a water manometer, the required Δ H is given by

$$\Delta H = \frac{0.8\ M\ \sigma_T}{\rho_m\ g} \qquad (5\text{-}1)$$

where M is the mesh size, σ_T is the surface tension of the test fluid (methanol) at the measured test temperature, and ρ_m is the density of the fluid in the manometer at ambient temperature. For a methanol bath and a water manometer at 20°C, the minimum acceptance level is 5.84 cm. On the first try, the wick had a single leak at 5.6 cm. The leak was found to be due to an enlarged pore caused by movement of the screen wires during tack welding. The wires were repositioned and a 5.85 cm head pressure was achieved.

The wick assembly was then tested for flow permeability in the set-up described in Section 4.0 (Figure 4-1). The wick was tightly sealed with plastic and tape, leveled, and water at a fixed head pressure allowed to flow through the wick. The pressure drop across the wick was measured by pressure taps at either end leading to an open ended manometer. Flow rate samples were collected at 5 pressure settings in the range of 2.54cm to 15.24cm (1 to 6 in) of water. Results of the test are shown in Figure 5-7. The test was repeated without the mandrel to determine the flow permeability of the system with the tunnel primed. These results are also shown in Figure 5-7. The permeability x area (KA) product was determined from the expression

$$KA = \frac{\dot{m}\ L\ \mu}{\Delta P\ \rho} \qquad (5\text{-}2)$$

where

$\dot{m}$ is the flow rate (kg/sec)
L is the overall length (m)
μ is the viscosity N-s/m^2
ρ is the fluid density (kg/m^3)
K is the permeability (m^2) and

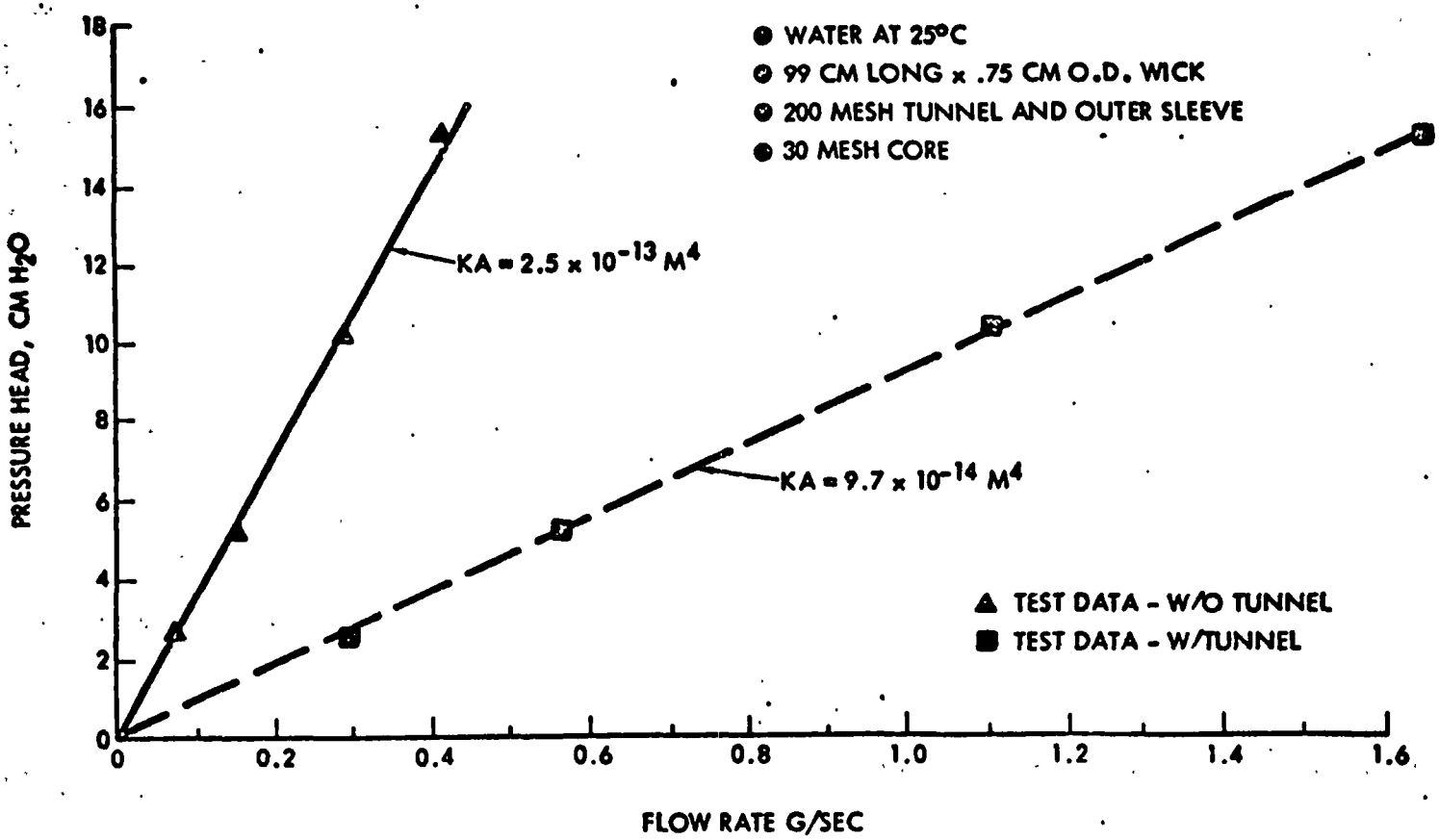

Figure 5-7 Flow Permeability Test Results with High Power Heat Pipe Wick

A is the flow area (m^2)

For the unprimed tunnel, KA was calculated to be 2.5×10^{-13} m^4. The theoretical value for 30 mesh screen with a .74 cm OD assembly is 0.86×10^{-13} m^4, or a little over one-third of the value calculated from test data. The difference in permeability was hypothesized to be due to gaps between the layers of 30 mesh screen. An analysis was performed to determine what size and geometry of gap could reconcile both the permeability data and the total volume of the wick. The coarse area of the wick was formed from a 4.45cm length of 30 mesh screen with a thickness of .061cm, for a total area of .271cm^2. The available area between the inner and outer wraps of 200 mesh screen is 0.346cm^2; thus the area of the gap is .075cm^2. The gap was assumed to be a rectangular channel of thickness t with width w, where the permeability is defined as $t^2/12$. The KA of the gap was assumed to be the difference between the measured KA of the system and the theoretical KA of the 30 mesh screen, or 1.8×10^{-13} m^4. The gap thickness was solved from the relationship

$$\frac{t^2}{12} A_g = 1.8 \times 10^{-13} \qquad (5\text{-}3)$$

where A_g is the area of the gap = 7.5×10^{-6} m^2.

Solving for t and w yields t = .0537cm, and w = 1.4cm. The calculated gap size was felt to be conservative since the additional flow area of the inner and outer screen was not accounted for, and because the gap would be expected to be uniformly distributed over the length of the 30-mesh spiral wrap. For the worst case, however, the question arose would such a gap, if it exists, be able to prime? Using property data for methane at the upper end of the 100 to 140°K range where the surface tension is lowest, the predicted priming height is ~ .85cm which is just equal to the maximum elevation of the top of the wick from the bottom of the inside of the pipe. The gap would therefore be expected to prime.

After the permeability test was completed, the wick assembly was cleaned and the end close-out caps (Figure 5-1) were installed. The wick close-off caps and the wick were cleaned as follows:

(a) Hot flushed with trichlorethylene for 5 minutes
(b) Flushed with MacDermid S487 at 160F for 10 minutes
(c) Rinsed with tap water - followed by a DI water rinse
(d) Immersed in 20% HNO_3 at 170F for 10 minutes
(e) Rinsed with DI water
(f) Dried at 300F for 1 hour

One wick close-off cap with a hole and one without a hole were butted up against each end of the 30 mesh center layers and the overlap of the outer 200 mesh screen was resistance welded to the circumference of the close-off caps. A final static pressure test was acceptable - the first "leak" occurring at 6.3 cm Δ H. A solid tapered stainless steel plug, approximately 0.25 cm long, was pressed into the hole of the one end cap.

Wick Standoffs (Bridges)

Eight pieces, 2.0 cm wide by 25 cm long, of the 200 mesh screen were wrapped around .24 cm diameter mandrel and resistance welded intermittently along the 25 cm length. Four were cut to 21.6 cm and four were cut to 16.5 cm long to become the standoff wicks for the evaporator and condenser sections respectively.

Eight 347 stainless steel rods - 0.16 cm diameter were cut to the same lengths as the standoff wicks. These rods, when inserted into the standoff wicks, keep the primary wick centered in the evaporator and condenser sections and insure continuity between the primary wick and the internal walls of the heat pipe.

Fill Tube and End Cap

A fill tube and end cap were machined from 316 ss per the dimensions in Figure 5-1. The I.D. of both ends was counterbored 0.064 cm deep by 1.27 cm diameter to match the step in the fill tube and end cap.

Final Assembly

All the parts for a complete high power heat pipe assembly as shown in Figure 5-8 were cleaned with the same procedure described above. After the wick was inserted into the flexible hose assembly and the standoff wicks

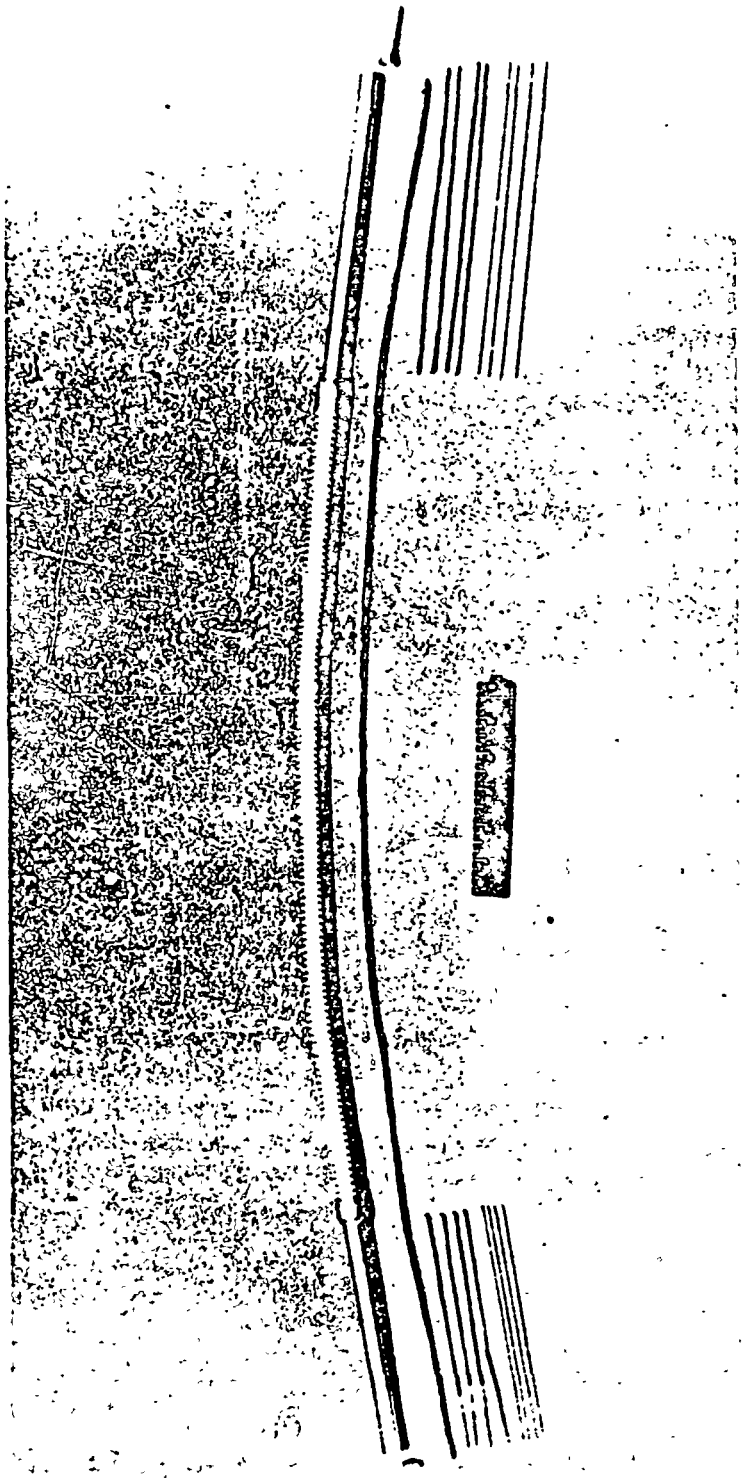

Figure 5-8 High Power Heat Pipe Components

and rods were installed, the end cap and fill tube were gas tungsten arc (GTA) welded to the condenser and evaporator sections respectively, using 316 stainless steel filler alloy.

The unit was successfully proof pressure tested at 2.4×10^7 Pa (3500 psig) and helium leak tested at 2.1×10^7 Pa (3000 psig).

BAKEOUT AND FILLING

For the bakeout and filling operations, a high pressure high vacuum valve was attached to the fill tube end of the pipe. Initially, a Whitey model 3NBS4 valve was used, but problems with leakage through the stem packing were encountered. The valve was subsequently changed to a Nupro model S4UK which is a high vacuum cryogenic valve with a bellows sealed stem. The Nupro valve worked exceptionally well during all filling and testing phases.

Bakeout

The heat pipe assembly was inserted into a bakeout shroud and hooked up to a high vacuum system. The pipe was baked out under vacuum at 121°C (250F) for 16 hours. The vacuum was maintained below 10^{-6} micron after the initial decay.

Filling

The theoretical fill determination was calculated based on the measured weight and dimensions of the primary wick, the standoff bridges, and the container. The theoretical 100 percent fill charge is 13.8g based on operation with methane at the minimum test temperature of 100°K. The pipe was charged with 14.8g (7 percent excess) and was weighed to verify the charge.

TEST PROGRAM

The high power heat pipe was subjected to a series of thermal tests to determine its performance under various conditions of temperature, tilt, and fluid charge. Initial tests were conducted with methane at 100 to 140°K. Initial test results indicated that the wick was not achieving full pumping. A series of parametric tests were run using ammonia at 280°K to try and determine what was causing the lower-than-expected performance. Mass spectrometerand gas chromatography tests were also run on the methane to see

if their were excess impurties that might have caused bubbles to form in the wick. Results of the overall test program are discussed in the following paragraphs.

Methane Tests

Test heaters and thermocouples were installed on the heat pipe as indicated in Figure 5-9. Thirty copper-constantan thermocouples were spot welded to the heat pipe. Each leg of the pair was separately attached so that the heat pipe wall becomes part of the electrical circuit. This ensures that the temperature indicated will be a true reading and permits continuity checking between the wires and the wall as well as between the two wires. A single roll of calibrated 28 gage thermocouple wire was used for all hookups. Figure 5-10 shows the heat pipe after installation of the heaters and thermocouples. The heat pipe was then installed in the test fixture and leveled. The test fixture, shown schematically in Figure 5-11, consists of a level test platform which is supported off a mounting plate by low conductance standoffs. Cooling is provided by an aluminum LN_2 reservoir which has a heater block between it and the heat pipe for temperature control. The heat pipe, mounting tray and LN_2 reservoir are shown prior to final installation in Figure 5-12.

The pipe was thermally tested in a straight configuration in the range of 100 to 140°K. Figure 5-13 shows burnout data at 140°K as a function of tilt compared to theoretical predictions. The 67 watt burnout at 0.5 cm indicates that the wick was primed. Detailed temperature profiles for 62w, 72w, 77w and 82w are shown in Figure 5-14. At 62 watts, the pipe was nearly isothermal with an average evaporator-to-condenser temperature drop of about 2°C (at 40 watts, the pipe was isothermal within 1°C). The profile for the 72w case seems to indicate a secondary wicking system burnout since thermocouple numbers 1-5 are still near the vapor temperature.

As shown in Figure 5-13, the burnout values at higher tilts were all significantly below theoretical, and all indications were that the wick was not primed. In fact, the 62 watt burnout point at 0.5 cm tilt could not be duplicated in subsequent tests. A summary of the burnout points for the entire test matrix is shown in Table 5-1.

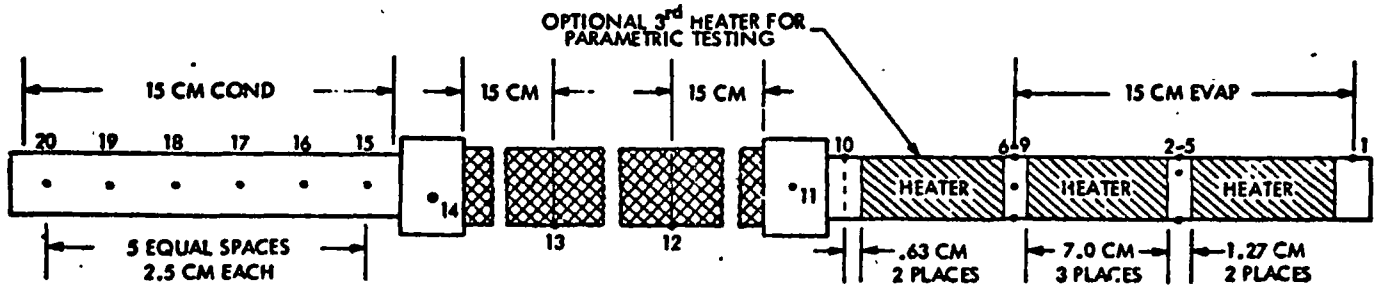

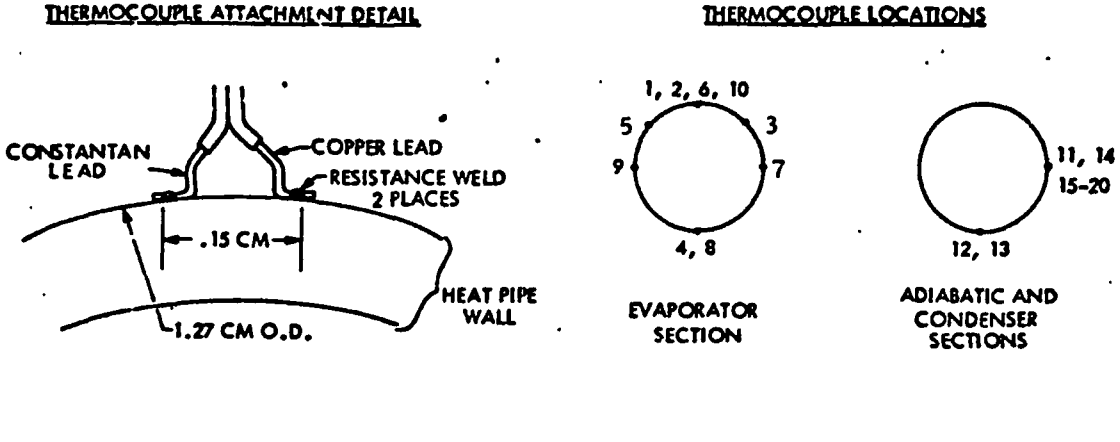

Figure 5-9 High Power Heat Pipe Heater and Thermocouple Locations

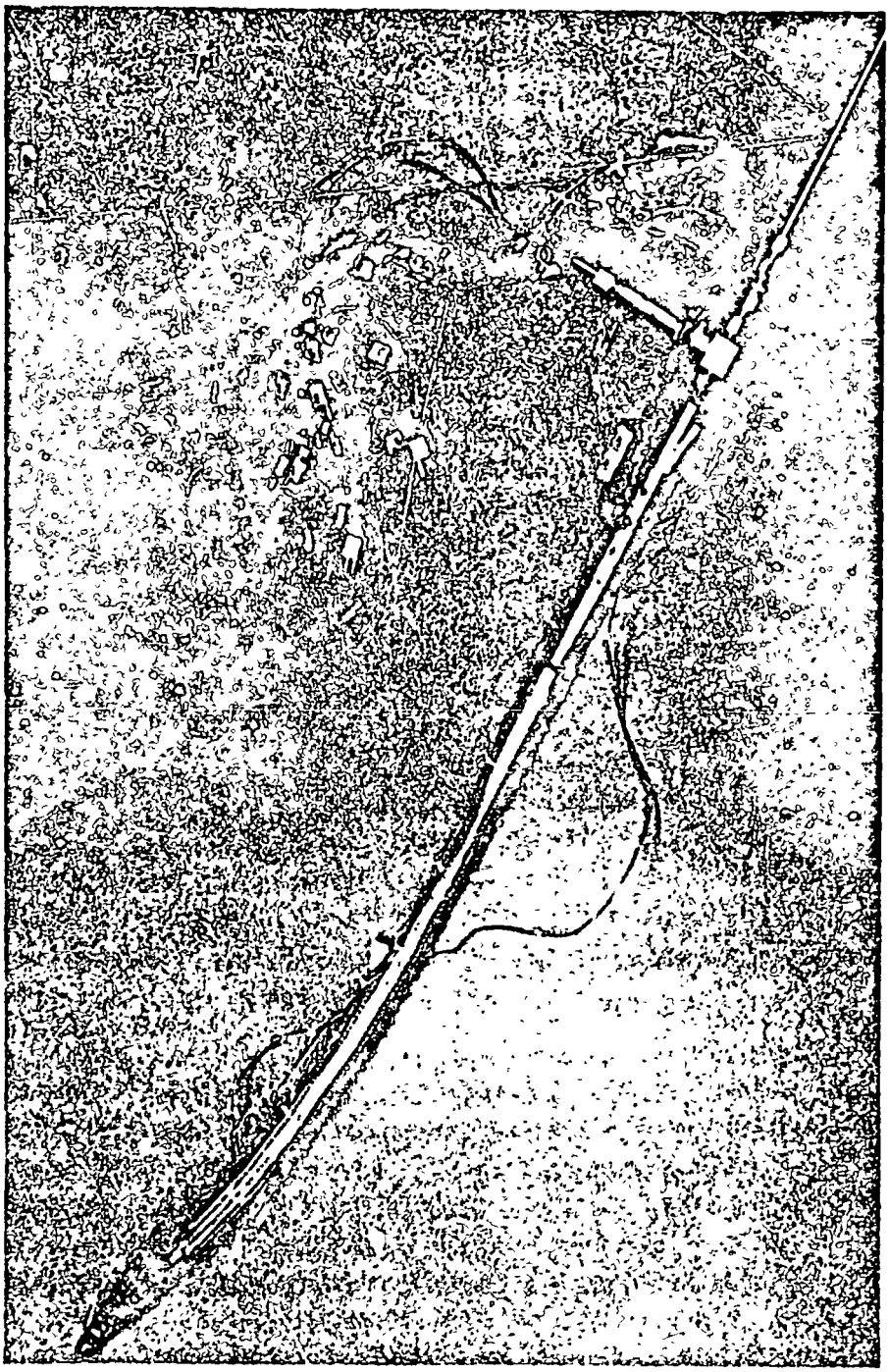

Figure 5-10 Instrumented High Power Heat Pipe

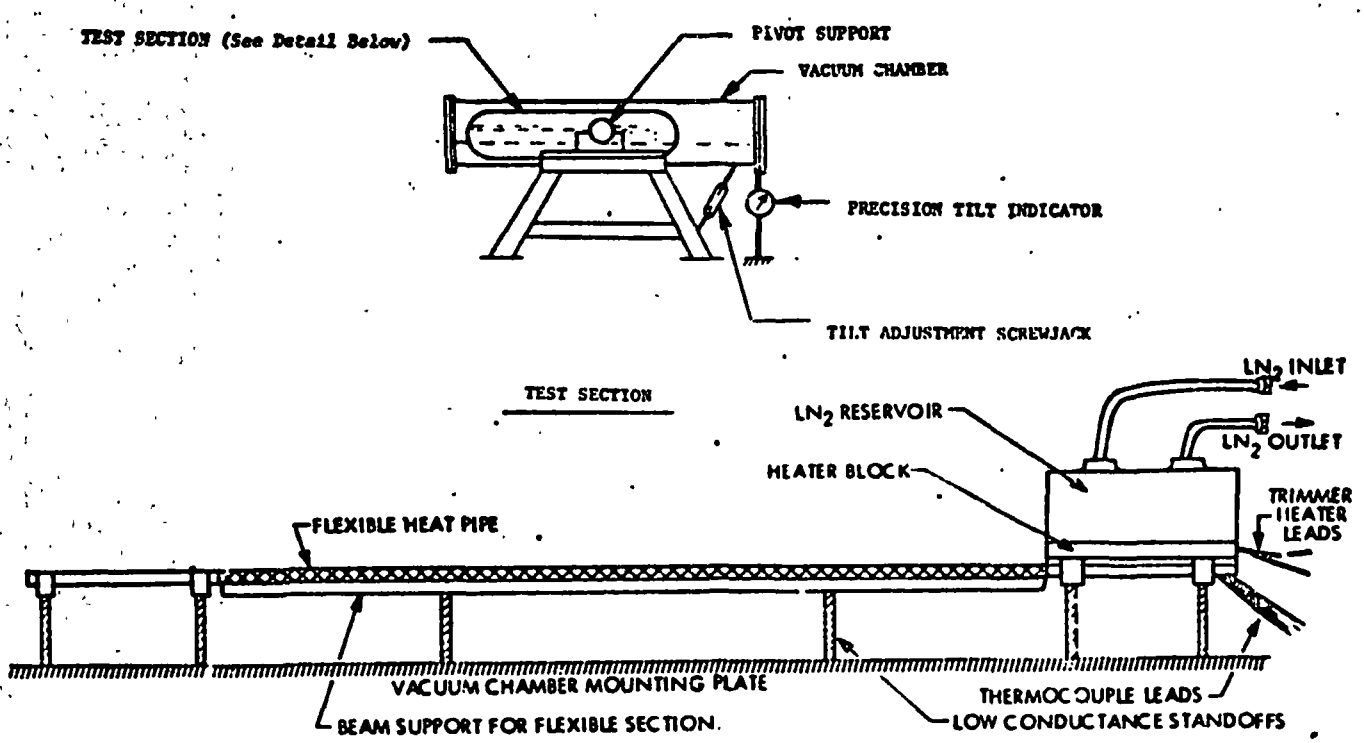

Figure 5-11 Test Set-Up Schematic

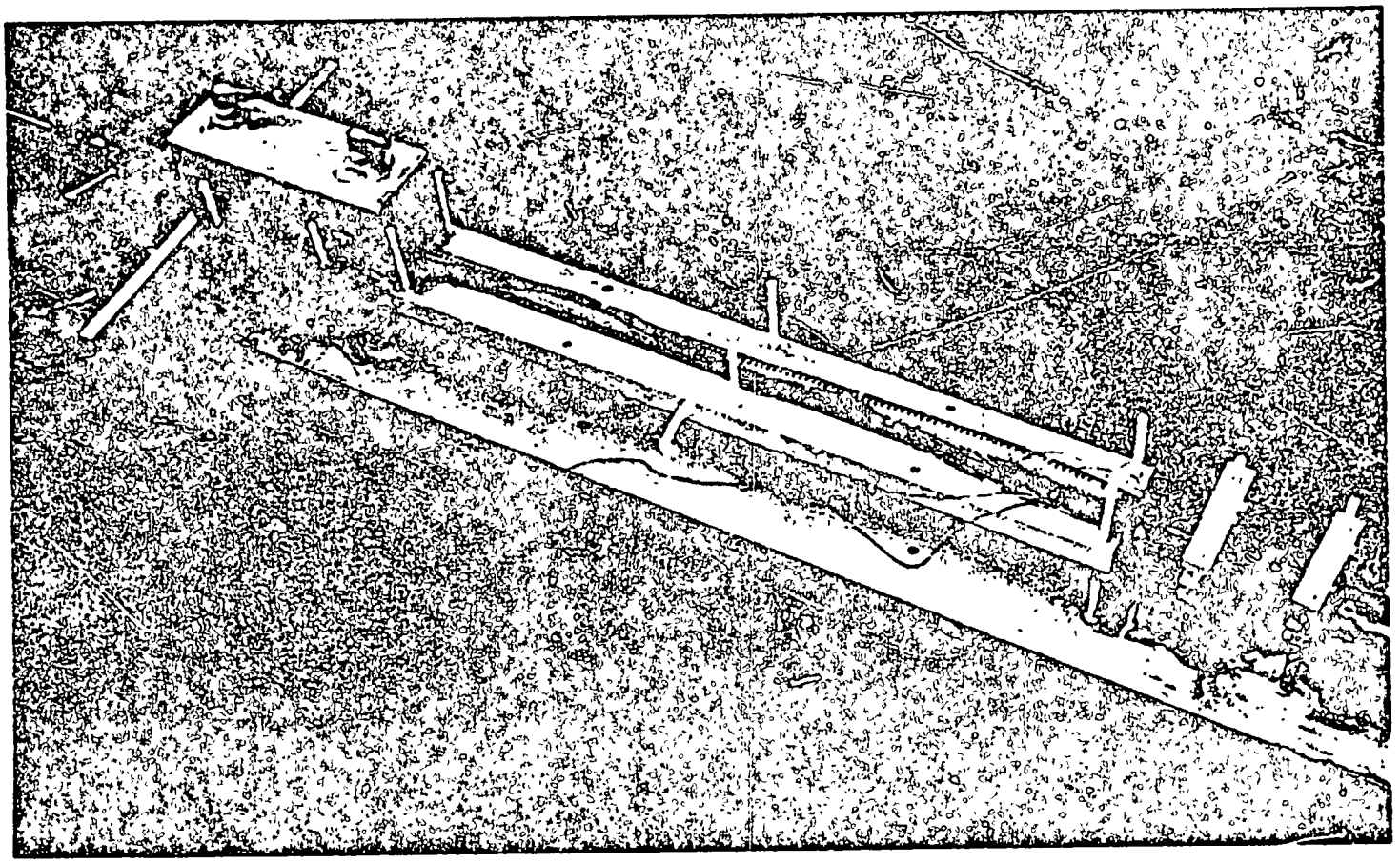

Figure 5-12 Heat Pipe, Test Fixture and Cooling Block

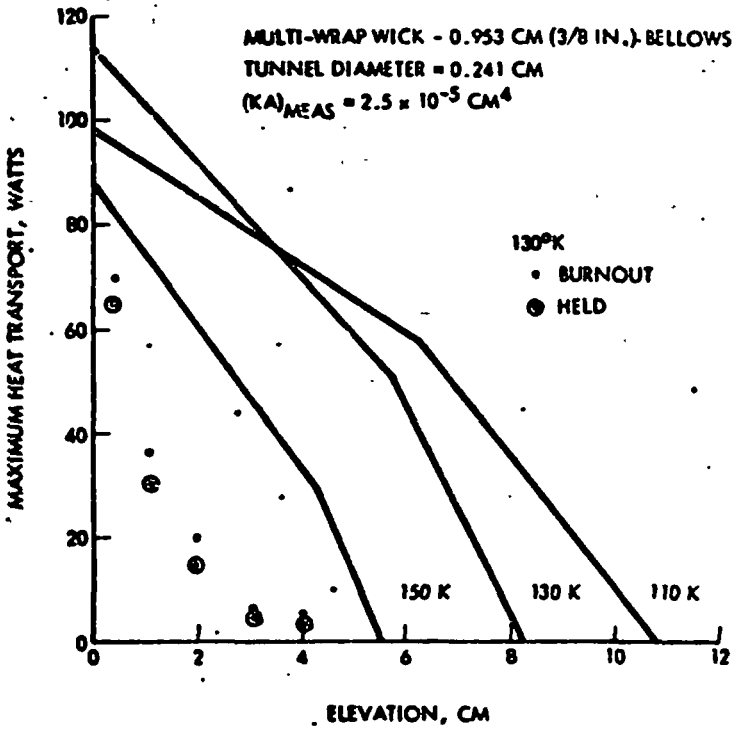

Figure 5-13 Methane Test Data

Table 5-1 High Power Heat Pipe Burnout Data

	Test Temperature (± 5°K)			
Tilt	110°K	120°K	130°K	140°K
0	15w	-	-	-
0.5 cm	8w	-	-	67w
1.0 cm	11w	-	34w	35w
2.0 cm	8w	-	715w	18w
3.0 cm	6w	-	5w	6w
4.0 cm	6w	3w	-	5w

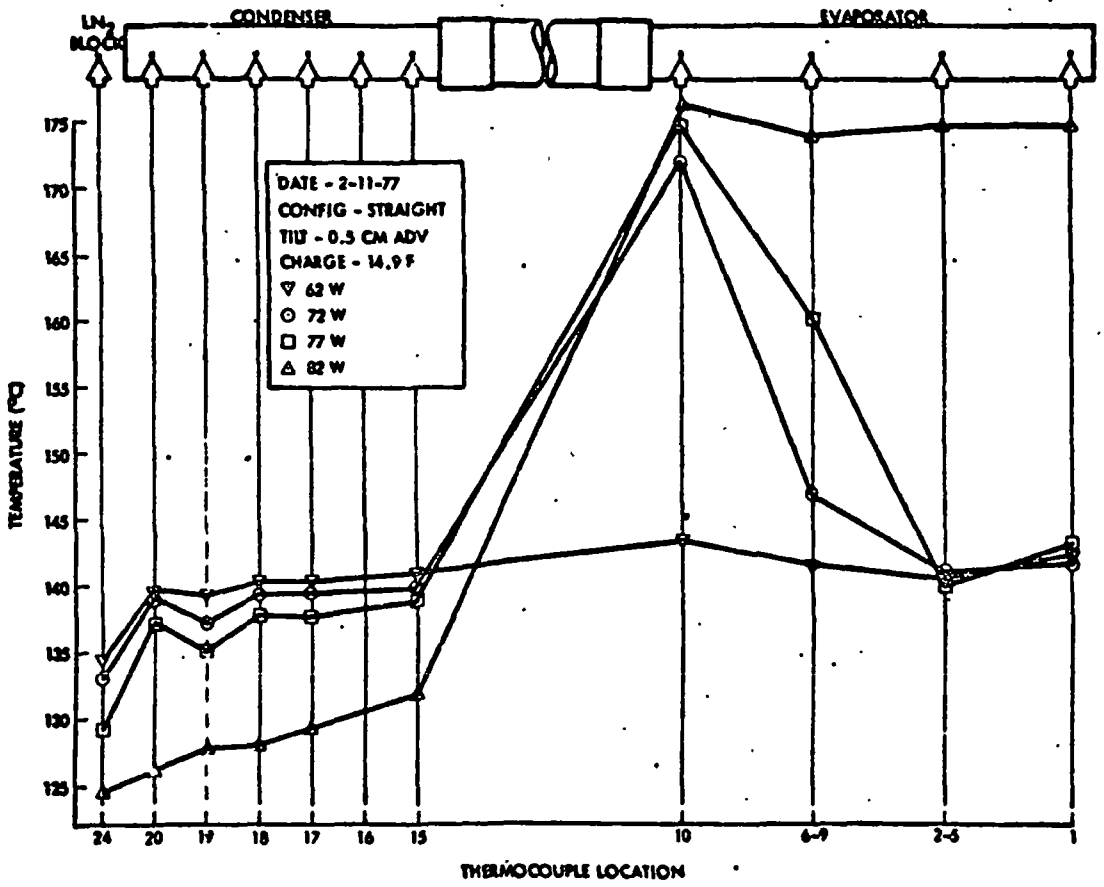

TABULAR DATA

POWER \ TC NO.	TEMPERATURE (°K) 24	20	19	18	17	15	10	6	2	1
62 W	134.9	140.6	139.2	140.8	140.8	141.2	143.9	142.0	141.8	142.2
67 W	133.2	139.7	137.7	139.9	140.0	140.6	156.5	141.9	141.5	141.9
72 W	133.4	139.8	137.7	139.9	139.8	140.3	171.5	145.8	141.4	142.2
77 W	129.8	137.3	135.3	138.3	138.1	139.2	185.0	159.5	141.7	143.4
82 W	125.2	127.1	129.8	129.0	130.0	132.5	186.7	192.7	161.6	173.6

Figure 5-14 Methane Test Temperature Profiles

The pipe was evacuated and recharged with methane. The pipe was refluxed for 4-6 hours and vented several times to purify the fluid. It was hypothesized that the low burnout levels were caused by non-condensible gas impurities which caused the pipe not to prime. In all subsequent tests, the burnout power levels did not improve, and the 67 watt burnout point at 0.5 cm tilt or at any other tilt including a 0.5 cm reflux could not be duplicated.

At that point, the test results were reviewed in detail with the NASA Technical Monitor. It was decided to forego other tests in various bend configurations in order to further investigate the problem. Three possible causes were postulated: (1) depriming or bubble formation due to trace contaminants or gas generations; (2) a secondary wicking system limitation; and (3) a hole or open seam in the composite wick assembly.

In order to ascertain which of these might be the cause, a trouble-shooting plan was formulated. The troubleshooting plan, shown in Figure 5-15, consisted of a series of tests and evaluation to systematically narrow down the possible causes of failures to a single alternative. The plan called for gas analysis of the methane, testing with ammonia; and reversing the evaporator and condenser of the heat pipe and testing with either methane or ammonia.

Gas Analysis Tests

Gas samples were taken from the heat pipe, the methane supply bottle (ultra high purity grade) and from a newly purchased supply bottle of research purity methane. Samples from the heat pipe and supply bottle were initially tested at Rockwell on a gas chromatograph. Results of the analysis are shown in Table 5-2. Matheson purity specifications (typical analysis) are also shown for comparison.

Several conclusions are evident from Table 5-2. First, the impurities in both the heat pipe and the supply bottle are considerably higher than quoted by Matheson. This had been suspected based on previous experience cited by the Technical Monitor. Second, the impurities in the heat pipe and supply bottle are of roughly the same order. Therefore, evidence of corrosion or internal gas generation is not apparent. The slightly higher

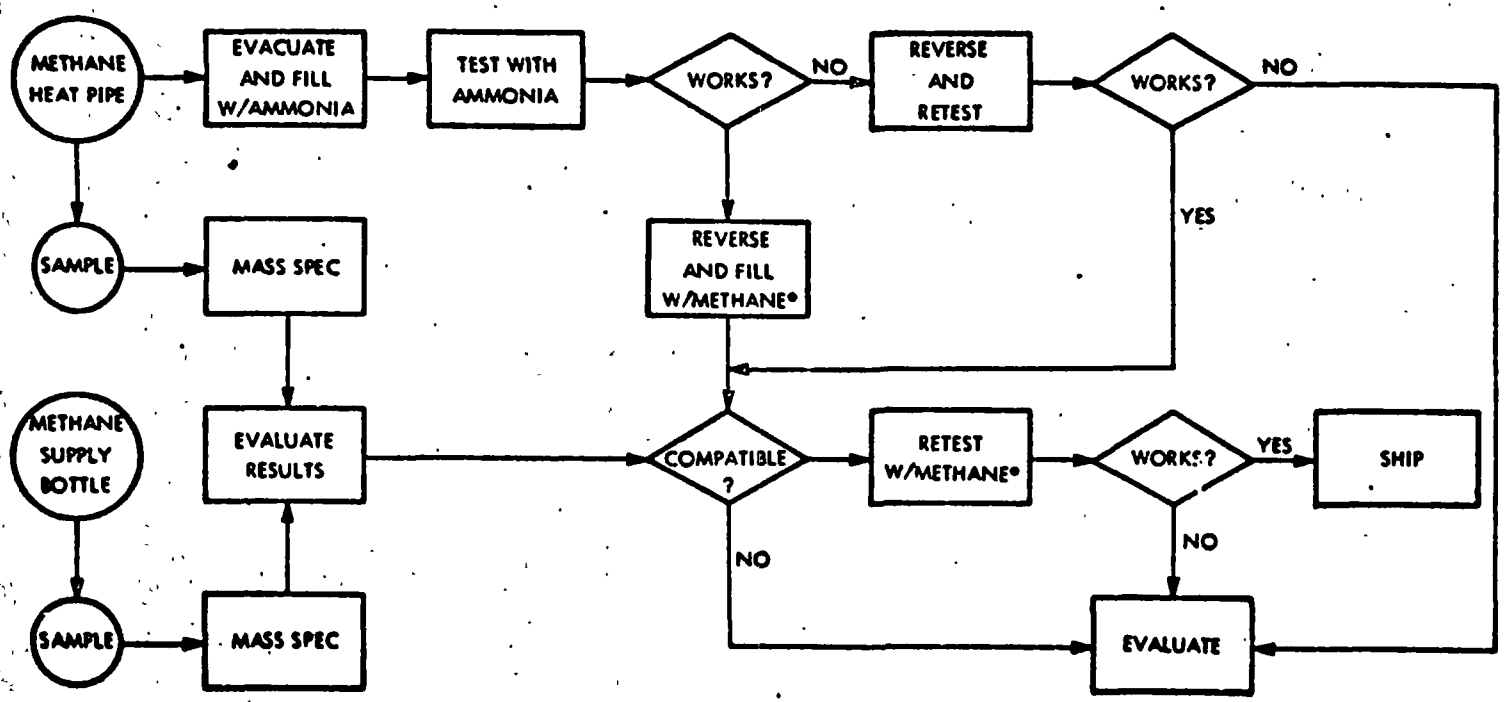

Figure 5-15 Troubleshooting Test Plan for Methane Heat Pipe

concentrations of C_2H_6 can be explained by the refluxing/outgassing operation which would tend to concentrate condensible imputities as the pure methane and the non-condensibles are burped out.

Table 5-2 Gas Chromatography Results

Constituent	Heat Pipe	Supply Bottle	Matheson Spec*
H_2	3 ppm	2 ppm	0
O_2 + Ar	12 ppm	115 ppm	8 - 10 ppm
N_2	40 ppm	165 ppm	40 - 50 ppm
C_2H_6	37 ppm	28 ppm	20 - 30 ppm
C_3H_8	< 2 ppm	< 2 ppm	5 ppm
CO_2	< 2 ppm	< 2 ppm	40 - 50 ppm

A mass spectrographic analysis was also performed to determine water content and to corroborate the gas chromatogrph data. The constituents identified by the gas chromatography were confirmed by the mass spectrographic analysis. The conclusion from these tests was that the research purity methane had significantly higher impurity levels than the supplier specification. Refluxing and venting of the heat pipe appears to have been successful in reducing the non-condensible impurities (which can be seen by comparing the heat pipe sample with the supply bottle sample). The mass spectrographic analysis also indicated the presence of about 7 ppm of water which is nearly within the supplier specifications.

The relatively high concentration of nitrogen was felt to be a potential cause for the apparent lack of priming of the wick. It was discovered that nitrogen is extremely soluble in methane, and has a very steep slope of solubility as a function of temperature (solubility decreases with increasing temperature). From Reference 11, the solubility coefficient was given as

$$\alpha_{N_2 - CH_4} = 0.0821\, e^{\frac{549}{T}}$$

where O is the Ostwald coefficient which is equal to the weight ratio of the dissolved gas to that in the vapor, and T is the temperature in degrees kelvin. At 130°K, the Ostwald coefficient is 5.6 which means that 85 percent of the nitrogen is dissolved in the methane. Thus, for a single venting, a maximum of about 15 percent of the nitrogen would be vented. At 77°K, the Ostwald coefficient is 103. This explains why attempts to remove the nitrogen by freezing the methane in LN_2 failed - over 99 percent of the nitrogen had gone into solution.

Ammonia Tests

The heat pipe was thoroughly evacuated and charged with 22.4g of ammonia, which corresponded to the 14.3g methane charge (107%). The pipe was tested with a 1 cm adverse tilt and burned out at 40 watts. With a 1 cm reflux tilt, the pipe burned out at 55 watts. At that point, it was hypothesized that there was an insufficient fluid charge in the pipe. The pipe was then filled to a charge of 24.7 g of ammonia and was retested in the same configuration. This time, the pipe burned out at 70 watts with a 1 cm adverse tilt and at 100 w with a 1 cm reflux tilt. The cooling system was then modified so that the pipe could run below ambient temperature. The water was run through a bath circulator which provided a water inlet temperature of ~ 2°C. It was felt that this would preclude condensation of the working fluid in the bellows by exposing the bellows to ambient air temperature and running the heat pipe below 20°C. Upon retesting, a substantial improvement in the performance of the pipe was noticed. At a 1 cm adverse tilt, the pipe burned out at 120 w. The burnout data are shown in Figure 5-16 for the various test cases. Theoretical predictions are also shown for comparison. The burnout data indicate a static height of approximately 7 to 8 cm, compared to a theoretical static height of 10 cm. The reduced static height is probably due to the screw threads rather than the axial wick. The axial wick was definitely primed during these tests.

Although the burnout data was substantially higher, the theoretical maximum heat transport capacity with ammonia is over 400 watts. In accordance with the troubleshooting plan, the pipe was reversed and tested with the heaters on the 15 cm (condenser) and removed at the 20 cm (evaporator) end. For this test, the pipe was installed in the straight condition for subsequent

testing with methane. Although higher performance was expected, the burnout values were actually lower (see Figure 5-16). As a matter of fact, they were lower almost exactly by the ratio of the heater surface area for the two cases (the heater area in the forwared test was ~ 77 cm^2 vs. 52 cm^2 in the reverse test). At zero tilt, the pipe burned out at 110 watts compared to 160 watts in the forward mode. This points to a limit in the secondary rather than the axial wicking system. A subsequent test showed that this was indeed the case. In this test, the pipe was taken to burnout at a 3 cm adverse tilt (~ 30 Watts). After temperatures in the evaporator were substantially elevated, the power was reduced by 5 Watts and the system was allowed to stabilize. When the power was reduced, the evaporator temperature dropped and stabilized, indicating recovery. The test was repeated at a 5 cm adverse tilt with similar results. If the burnout were in the primary wick, the axial wick would have deprired. Since the wick can only prime against a 0.2 cm adverse tilt, the pipe could not possibly recover with a 3 cm or 5 cm adverse tilt.

The low burnout limit in the secondary wicking system was somewhat surprising since both the standoffs and the screw threads were sized to carry considerably greater heat loads. One explanation which was hypothesized is that a capillary limit is reached at the interface between the wick standoffs and the screw thread grooves. This effect is illustrated in Figure 5-17 which shows a magnified physical model of the intersection of the 200 mesh screen standoff with the V-grooves.

When the axial wick is stressed (note meniscus depression between screen wires), the meniscus in the V-grooves recedes down the wall to a stress level consistent with capillary and hydrodynamic flow requirements. In this model, both the screen and the V-grooves may be capable of handling the liquid flow, but the connecting flow area may be insufficient. When this occurs, the meniscus in the V-grooves will recede more, further reducing the interconnecting flow area until dryout eventually occurs. Loose contact between the standoffs and the V-grooves would produce the same effect.

Further support of this conclusion can be drawn from the data in Figure 5-16. The burnout points for the 20 cm evaporator case with a 24.7 g charge indicate a static height of only 7 cm compared to a theoretical static height

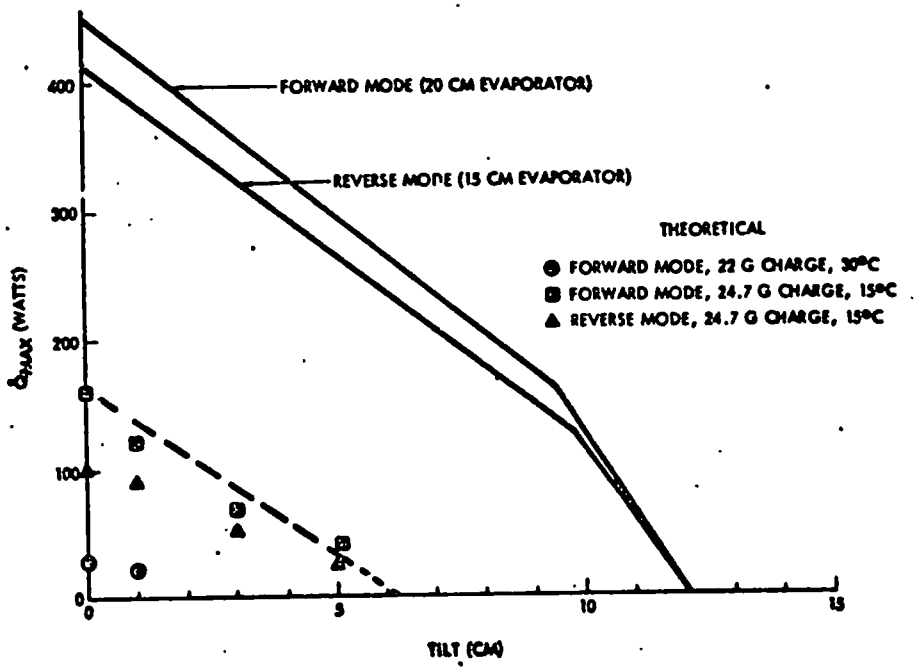

Figure 5-16 Test Results with Ammonia at 280°K

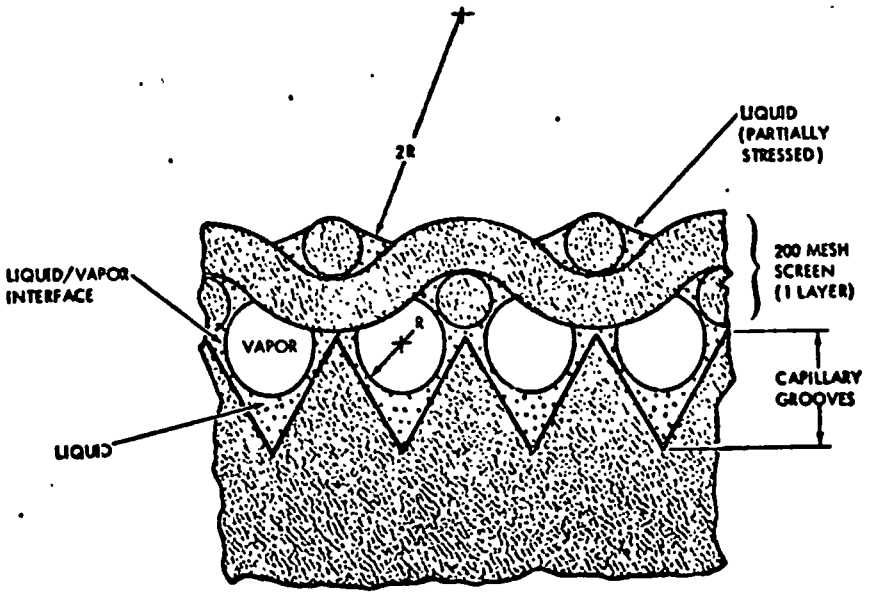

Figure 5-17 Schematic of Capillary Interface Between Screen Wick and V-Grooves

installed in the test fixture. Burnout tests were run at 140°K and at 120°K. At zero tilt (level), the pipe carried 20 watts but burned out at 30 watts at both 120°K and 140°K. An attempt was made to prime the wick by tilting the pipe to a 1 cm reflux with 5 watts of power applied. The pipe was held in this condition for approxiamtely one hour. The tilt was then changed to 3 cm adverse to check if the wick was primed. The pipe burned out at the 5 watt load. Successive attempts to prime the wick were equally unsuccessful. Burnout tests were repeated with reflux tilts of 2 cm and 4 cm. Results of the tests are summarized in Table 5-3.

Table 5-3 Burnout Test Results

Temp. (°K)	Tilt* (cm)	Max. Power Before Burnout (Watts)
120	0	20
	-2	30
	-4	110
140	0	20
	-2	40
	-4	130

* Negative sign indicates reflux tilt

Results in Table 5-3 indicate that the wick was not primed. During one test the pipe carried 70 watts at a 2 cm reflux, but this could not be repeated during subsequent attempts. The test results were reviewed with the Technical Monitor at which time it was agreed that the flexural tests should be suspended and the heat pipe opened and inspected.

Visual Examination

The end caps were machined off and the ends were inspected - no corrosion was evident. The wick was static pressure tested before it was removed by replacing the wick closeout plug and inserting the gas pressurization tube. The pipe was submersed in methanol and the wick was pressurized with nitrogen. The wick held ~ 5-3 cm of water pressure without leaking (at higher pressures the pressurization tube leaked due to the difficulty of installing it in situ). The wick was then removed and the test was

of 12 cm. The static height is a measure of the pumping ability of the wick and affects both the slope and the zero tilt intercept of the performance curve. If a line drawn through these data points were shifted to a 12 cm static height, the zero tilt intercept would be ~ 300 W, or about 64 percent of theoretical. The slope of the curve is approximately 90 percent of that of the predicted curve, indicating that the wick permeability is nearly as predicted.

Other tests were performed tc determine the sensitivity of performance to fluid change. Figure 5-18 shows the maximum horizontal heat transport as a function of the fluid change. Based on these data, the optimum charge appears to be between 24 and 25 g (this would correspond to a methane charge of 16.1 to 16.8 g).

Based on the above results, it was decided to retest the pipe with an increased methane charge. The pipe was charged with 18 g of methane and was installed in the chamber in the straight configuration. Tests were run at 140K and at several elevations to determine the burnout capacity. At 2 cm reflux, the pipe carried 90 W and burned out at 100 W. However, at positive elevations of 1 cm and 2 cm, it burned out at 20 W and 15 W respectively. The thermal conductance of the pipe was also appreciably lower at positive elevation compared to the reflux test. A plot of the calculated thermal conductance as a function of tilt is shown in Figure 5-19. The thermal conductance was calculated at a maximum power input before burnout in each case. The condenser was evidently blocked by excess liquid at positive elevations. (The 18 g methane charge compares to an ammonia charge of ~ 27 g of ammonia).

Although the positive elevation burnout data were below expectations, the 100 W burnout at a 2 cm reflux tilt was nevertheless encouraging. If the -2 cm burnout point is extrapolated to a 7 cm static height, then the projected burnout at zero elevation would be approximately 80 W. At 0.5 cm tilt, the projected burnout limit would be 72 watts which compares very favorably with the early test data which in our case showed burnout at about 70 W.

The high power heat pipe was charged with 16.9 g of methane and was

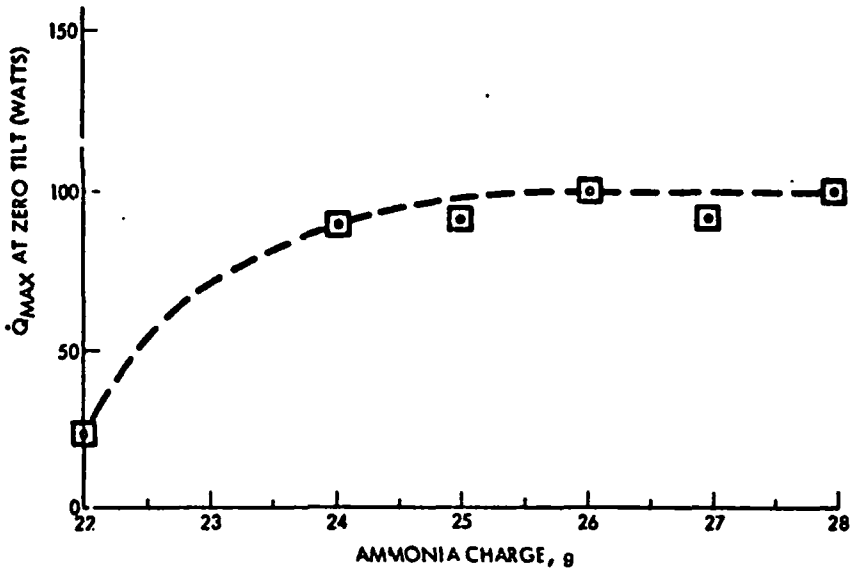

Figure 5-18 Maximum Heat Transport vs. Ammonia Charge

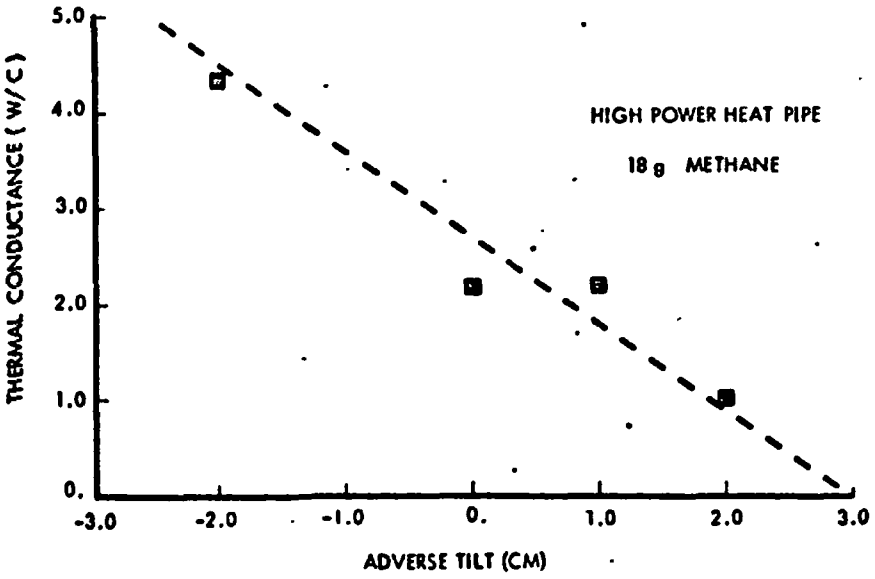

Figure 5-19 Thermal Conductance vs. Tilt

repeated. The wick held a minimum of 5.6 cm (2.2 in) of water. This corresponds to a capillary radius of 8.3×10^{-3} cm which is equivalent to approximately 80 percent of 200 inch pumping. This is approximately the same level to which the wick was qualified before it was installed in the pipe, hence there was no degradation in static capillary pressure.

Inspection of the wick showed no signs of corrosion - the screen was clean and bright except at the very ends of the standoffs where the screen had discolored due to high temperature during welding of the end caps.

EVALUATION

In both the ammonia tests as well as the methane tests, the achieved burnout values were one-third or less of the theoretically predicted values. The single exception to this was the 67 watt burnout point at 140°K and 0.5 cm adverse tilt with methane (approximately 70 percent of theoretical). Ammonia tests results seem to indicate that the wick was at least partially primed, and that the screw thread grooves may have been limiting. In general, the methane test data indicate that the wick was not primed. This was most probably due to the presence of a non-condensible gas such as nitrogen which was a substantial impurity in the methane supply. Pressure depriming has also been considered as a possibility. The open tunnel in the composite wick may be causing the problem if pressure depriming is the answer.

6.0 LOW TEMPERATURE HEAT PIPE FABRICATION AND TEST

The low temperature heat pipe was fabricated in the same manner as the high power heat pipe, except that the design of the wick standoffs in the evaporator was changed based on the test results of the high power pipe. Results of the fabrication and test program are summarized in the following text.

HEAT PIPE FABRICATION

The low temperature heat pipe was fabricated in accordance with the drawing in Figure 6-1. The primary difference between it and the high power heat pipe are (1) the flexible hose diameter is reduced to 0.64 cm (1/4 in) to provide greater flexibility; (2) the diameter of the evaporator and condenser sections are smaller; (3) the wick uses 54 mesh screen internally and 250 mesh externally; and (4) the standoff bridges in the evaporator are changed to a four element web design as shown in Figure 6-1. This design was felt to provide better communication and a greater interconnecting flow area between the standoffs and the screwthread grooves. The fabrication sequence and procedures were identical to those for the high power heat pipe (Figure 5-2).

Flexible Container

The flexible container was purchased as an integral unit with schedule 80 stainless steel tubes welded to the bellows. The geometry of the flexible container is shown in Figure 5-3. One flexible hose assembly was burst tested and failed in the bellows at a pressure of 1.14×10^8 Pa (16,500 psi). This is over four times the estimated containment pressure at 315°K (2.4×10^7 Pa = 3500 psi). However, the yield point of the bellows is 2.76×10^7 Pa (4000 psi), which means that if the pipe were proof tested to 1.5 times the working pressure, permanent yield would occur in the bellows. To avoid this, a 75 cm^3 reservoir was attached to the end of the pipe prior to filling (see BAKEOUT AND FILLING).

The evaporator and condenser sections were drilled and honed to an

DETAIL -005 [5]
SCALE 4/1

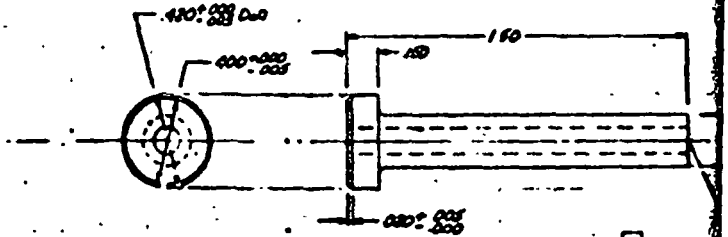

DETAIL -006 [6]
SCALE 4/1

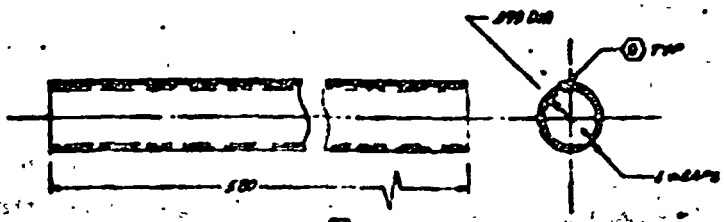

DETAIL -007 [7]
SCALE 10/1

FOLDOUT FRAME 1

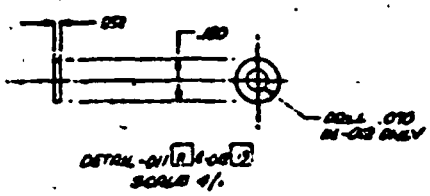

DETAIL -011 & 006
SCALE 4/1

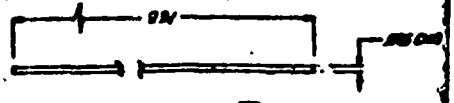

DETAIL -003
SCALE 1/1

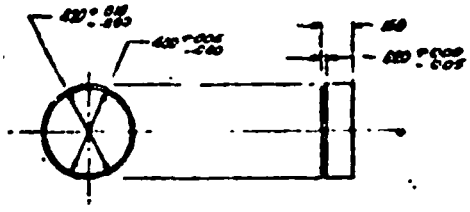

DETAIL -005
SCALE 4/1

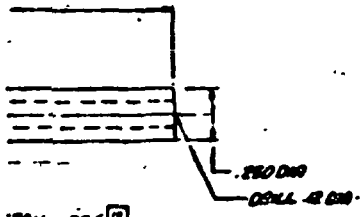

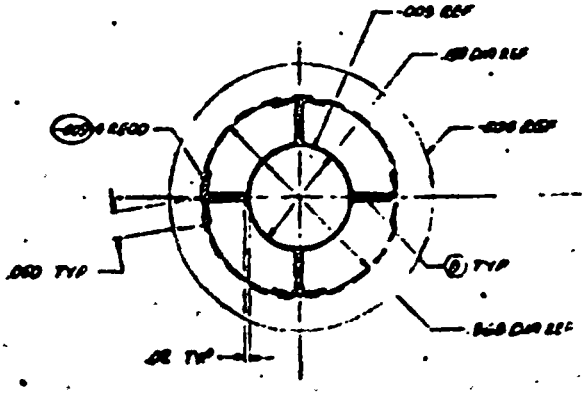

SECTION F-F
SCALE 8/1
EVAPORATOR SECTION

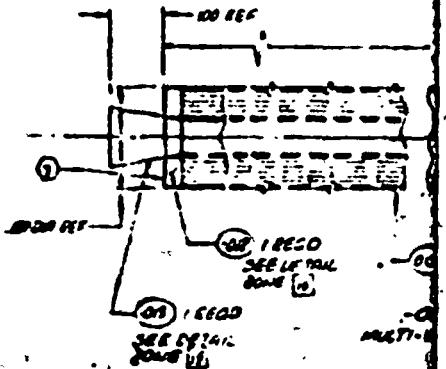

FOLDOUT FRAME 2

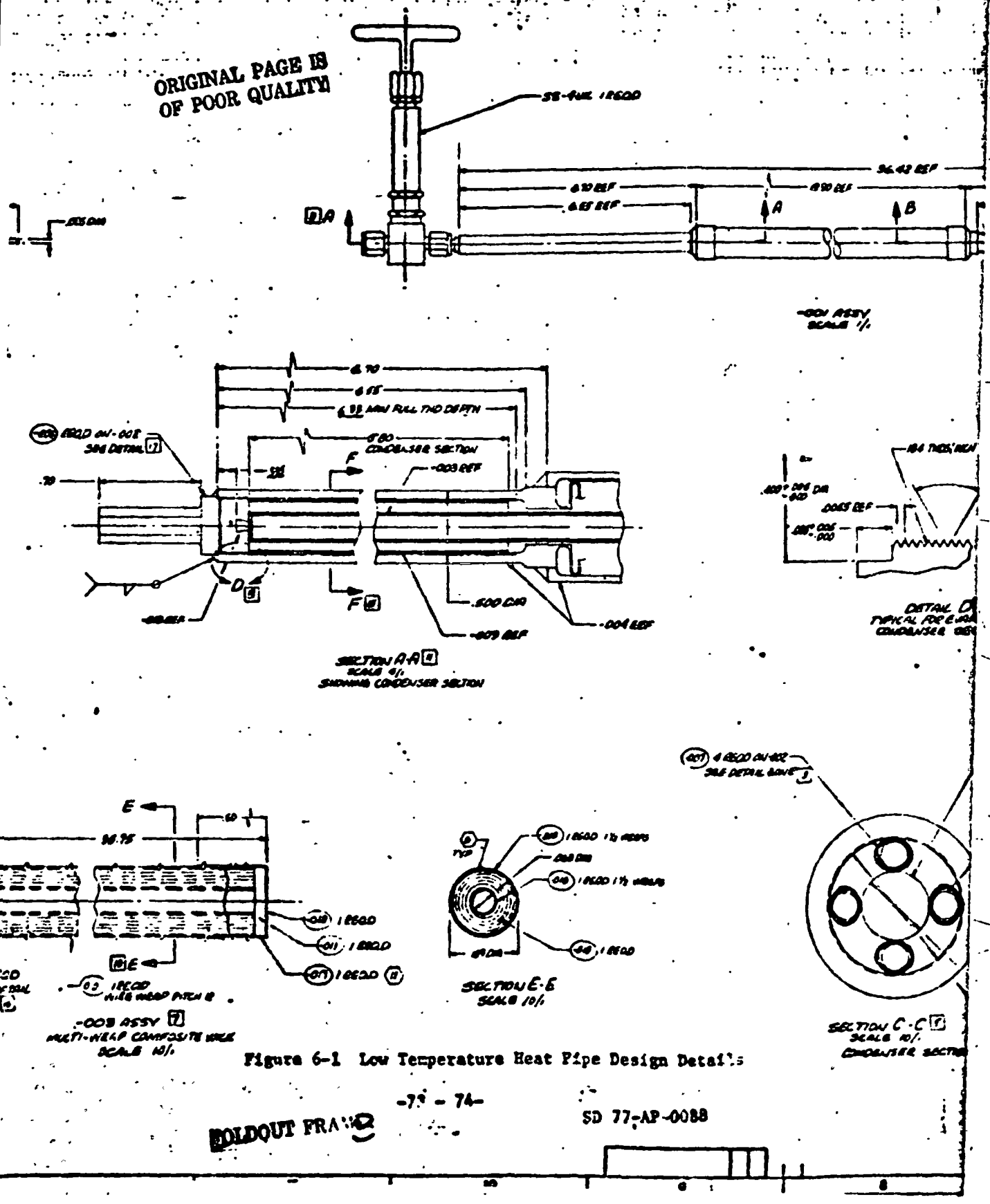

Figure 6-1 Low Temperature Heat Pipe Design Details

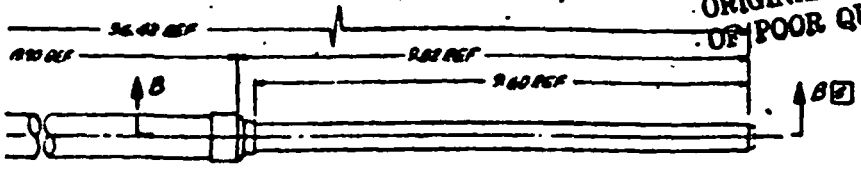

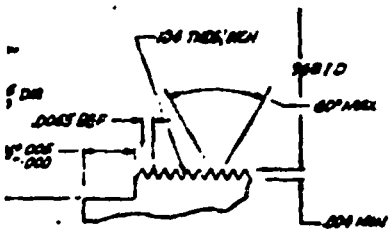

DETAIL D
TYPICAL FOR EVAPORATOR & CONDENSER SECTIONS

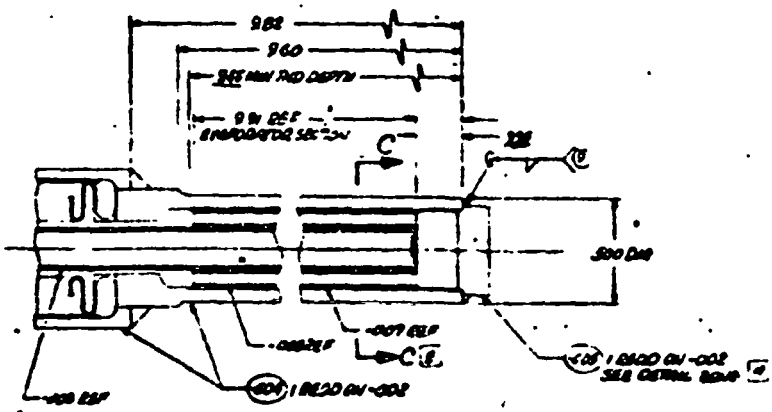

SECTION B-B
SCALE 4/1
EVAPORATOR SECTION

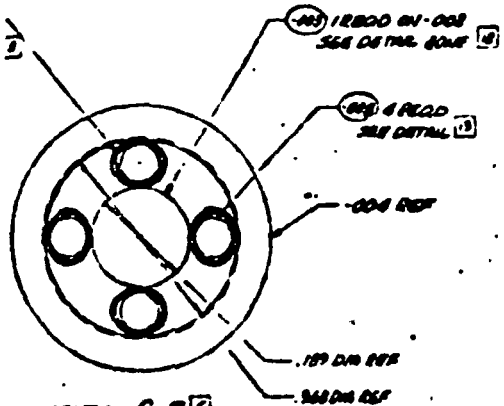

SECTION C-C
SCALE 10/1
CONDENSER SECTION

FOLDOUT FRAME 4

FOLDOU

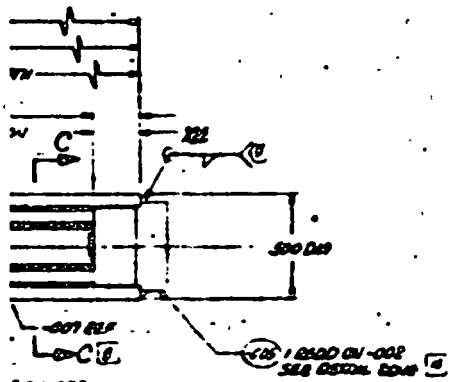

FOLDOUT FRAME

internal diameter of 0.93 cm (.368 in). The long thin tubes proved to be extremely difficult to machine to the tolerances required for threading. In the first attempt, eccentricity, axial alignment, and cylindricity were out of tolerance (a tolerance of .002 to .004 cm TIR is required since the threads are only ~ .013 cm deep). The assembly was then sent out to a gun boring specialist and was subsequently internally honed. The pipe was then successfully threaded. In future applications, it is recommended that high tolerance standard tubing be used such that no internal drilling is required. This approach was employed on a subsequent program to fabricate a flexible variable conductance heat pipe, and the threading operation was very successful.

Primary Wick Fabrication and Testing

The primary wick was rolled stainless steel (type 316) screen of two different size wire and mesh. The inner layer or tunnel had an I.D. of .16 cm and was 250 x 250 mesh x 0.0041 cm diameter wire screen, while the middle layers were 54 x 54 mesh x .014 cm diameter wire screen. The cover or outer layer was of the same screen as the tunnel. The tunnel was fabricated from a 1.27 cm wide by 1.02 cm long, 250 mesh screen cut on a 45° bias, wrapped tightly on an 0.16 cm diameter mandrel and resistance welded longitudinally for the full length. With only one patch repair, the tunnel, static pressure tested in the methanol bath, achieved a level of 7.4 cm Δ H with no leaks. The minimum required Δ H was 6.55 cm (90% of 200 mesh pumping). After a 4.2 cm wide by 102 cm long section of 54 mesh screen was tack welded to the overlap of the tunnel, and unit was retested in the methanol bath. A leak in the seam of the tunnel at 6.7 c . H was left as is and the 54 mesh screen was tightly rolled on the tunnel to a final O.D. of .44 cm, and then cut to 89.5 cm.

Attempts at wrapping the 54 mesh middle layers with the outer 250 mesh screen and resistance welding longitudinally proved to be unsuccessful. It appears that the thin 250 mesh screen is too sensitive to minor pressure variations to provide consistently acceptable welds. The difference in stiffness between the 30 mesh and the 54 mesh is enough to adversely affect the welding conditions. To overcome this problem, the outer wrap was made separately by welding a tubular sleeve of 250 mesh screen, cut on a 45° bias,

on a special chem milled copper mandrel. The mandrel was a .465 cm diameter rod chem milled to .439 cm diameter except for approximately 1.27 cm (1/2 in) on one end. After testing the welded sleeve in the methanol bath (no "leaks" at 7.4 cm Δ H), the sleeve was slid back on the mandrel and then slid over the larger mandrel end on to the existing wick assembly. To insure tight contact between the outer and middle layers, the O.D. was spirally hand wound with 0.0058 cm diameter 316 stainless steel wire at about a .16 cm pitch. With the wire tied off at both ends, the wick was subjected to a static pressure test. Since the first leak did not occur until a level of 7.1 cm Δ H was reached, the wick was considered acceptable.

To close off the ends of the primary wick, two subassemblies were made as follows:

(a) A tubular section of 250 mesh was welded longitudinally on a .439 cm diameter mandrel.

(b) After being cut into 2.54 cm (1 inch) lengths, a close-off cap - one with a hole and one without a hole (Figure 6-1) was inserted into the end of each piece and resistance welded circumferentially.

(c) Both subassemblies were tested in the methanol bath with results no lower than 8.6 cm Δ H.

(d) The subassemblies were cut to 1.27 cm (1/2) inch long, slipped over the ends of the wick and wrapped in place with the 0.0058 cm diameter stainless steel wire. Figure 6-2 shows an as-fabricated subassembly and a subassembly on the primary wick.

(e) The completed unit was weighed and found to be 23.98 grams. Again tested in the methanol bath, the first "leak" appeared at 6.9 cm Δ H.

A flow permeability test was performed both with and without the inside mandrel. Test results are shown in Figure 6-3. The data indicate a permeability of 3.8×10^{-4} m^4 with the mandrel in (no tunnel), and

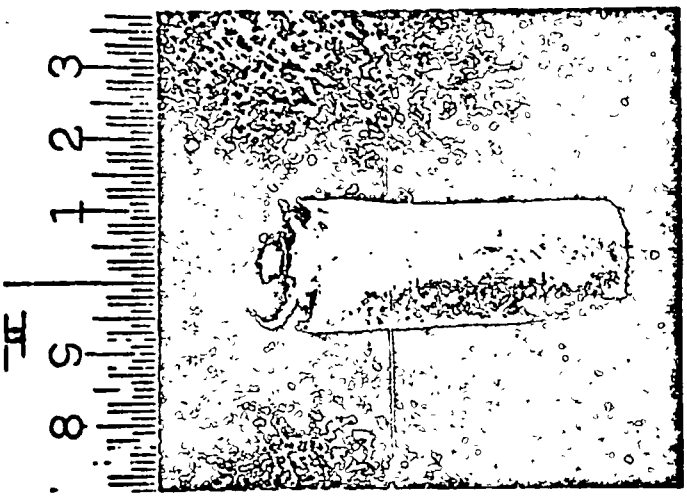

a) End as Fabricated

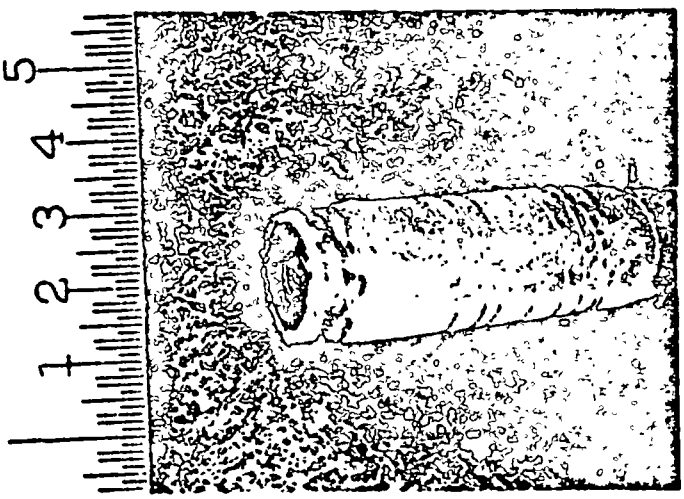

b) End After Installation

Figure 6-2 Wick Closeout End for Low Temperature Heat Pipe

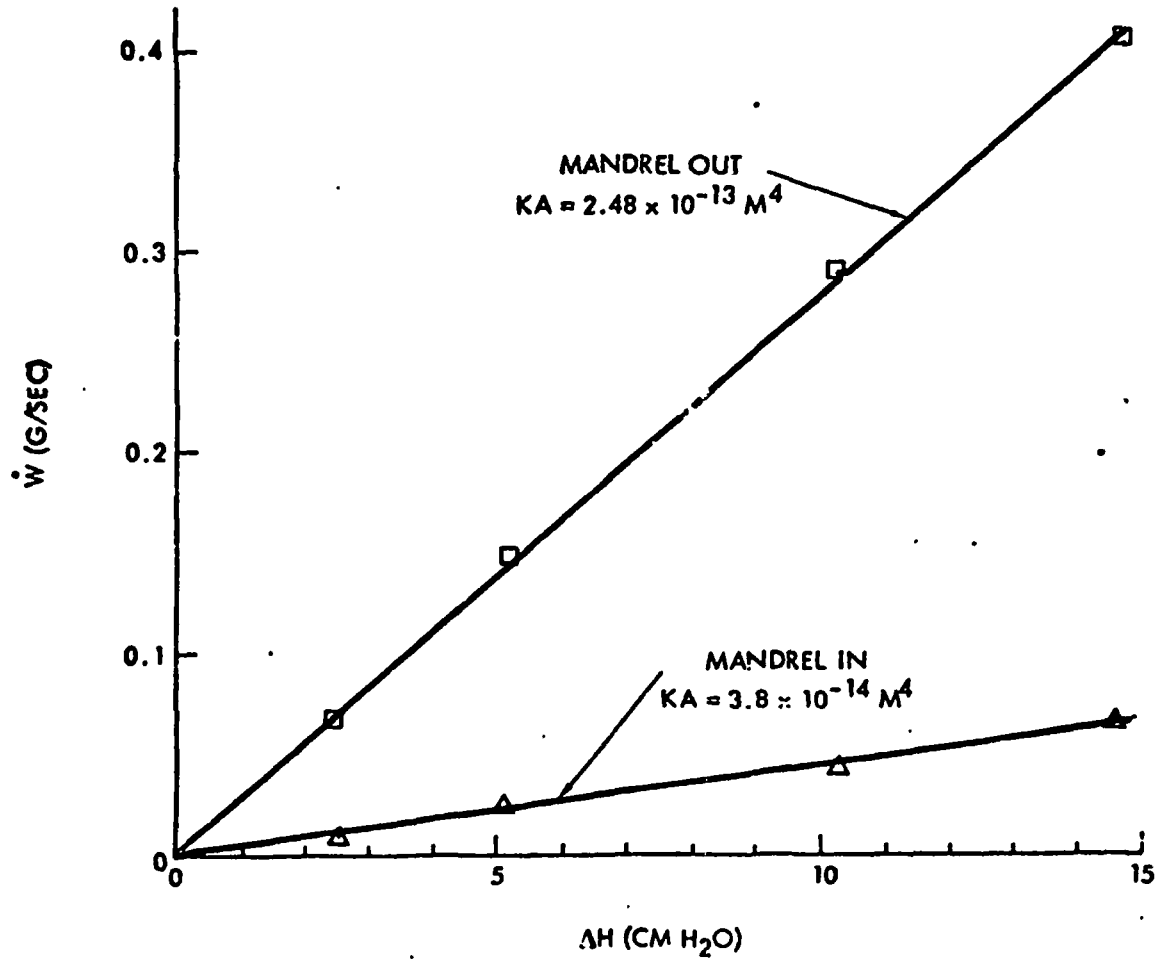

Figure 6-3 Flow Permeability Test Data Low Temperature Heat Pipe Wick

2.48×10^{-13} in^4 with the mandrel out (tunnel primed). The permeability of the wick with the mandrel in was approximately three times theoretical, as the case with the high power wick. It was concluded that this also was due to the gaps between the layers.

Wick Standoffs (Bridges)

To complete the heat pipe wicking system, the standoff wicks and rods for the evaporator and condenser sections were fabricated. For the condenser section, four sections of 250 mesh 316 stainless steel screen were wrapped around a .24 cm diameter mandrel, welded longitudinally, and then cut to 14.7 cm long. Four 316 stainless steel rods, of the same length, were chem milled to a diameter of 0.19 cm.

The evaporator stand-off wick was fabricated from four 23.6 cm long sections of 250 mesh screen formed into "U" sections, welded together longitudinally along 3 seams, wrapped on the primary wick and then welded along the fourth seam. Figure 6-4 shows the configuration of the evaporator standoff.

The four separate wick standoff bridges were used in the condenser section rather than the web type in the evaporator. This was required to permit installation of the wick into the flexible hose assembly without damage to the wick standoffs. (The diameter in the flexible section is only 0.64 cm compared to .93 cm in the evaporator and condenser, hence the webs could not be pulled through the heat pipe).

Fill Tube and End Cap

The fill tube and end cap were machined from 316 stainless steel rod stock in accordance with Figure 6-1. The ends of the evaporator and condenser were counter bored .064 cm deep by 1.02 cm diameter.

Final Assembly

Subsequent to LOX cleaning per Rockwell Specification No. MA0110-018, all the components as shown in Figure 6-5 were assembled to complete the heat pipe fabrication. After the primary wick assembly was installed and located with the condenser stand-off wicks and rods, the end cap was GTA welded to the evaporator end and the fill tube was GTA welded to the

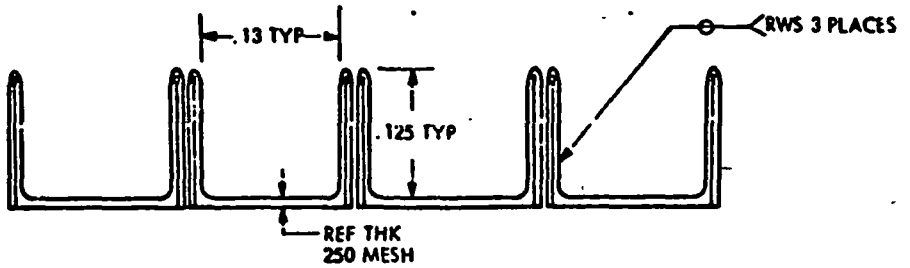

INITIAL LAYUP

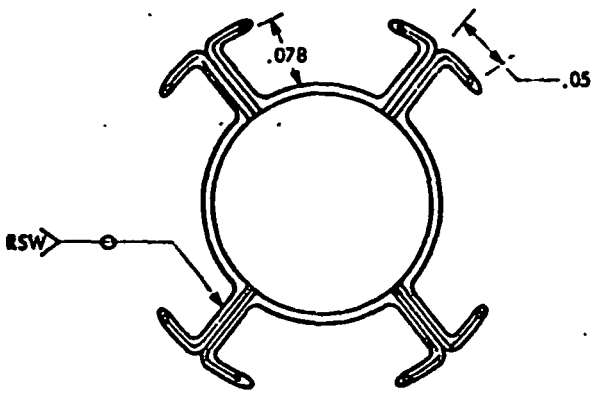

FINAL CONFIGURATION

Figure 6-4 Evaporator Standoffs for Low Temperature Heat Pipe

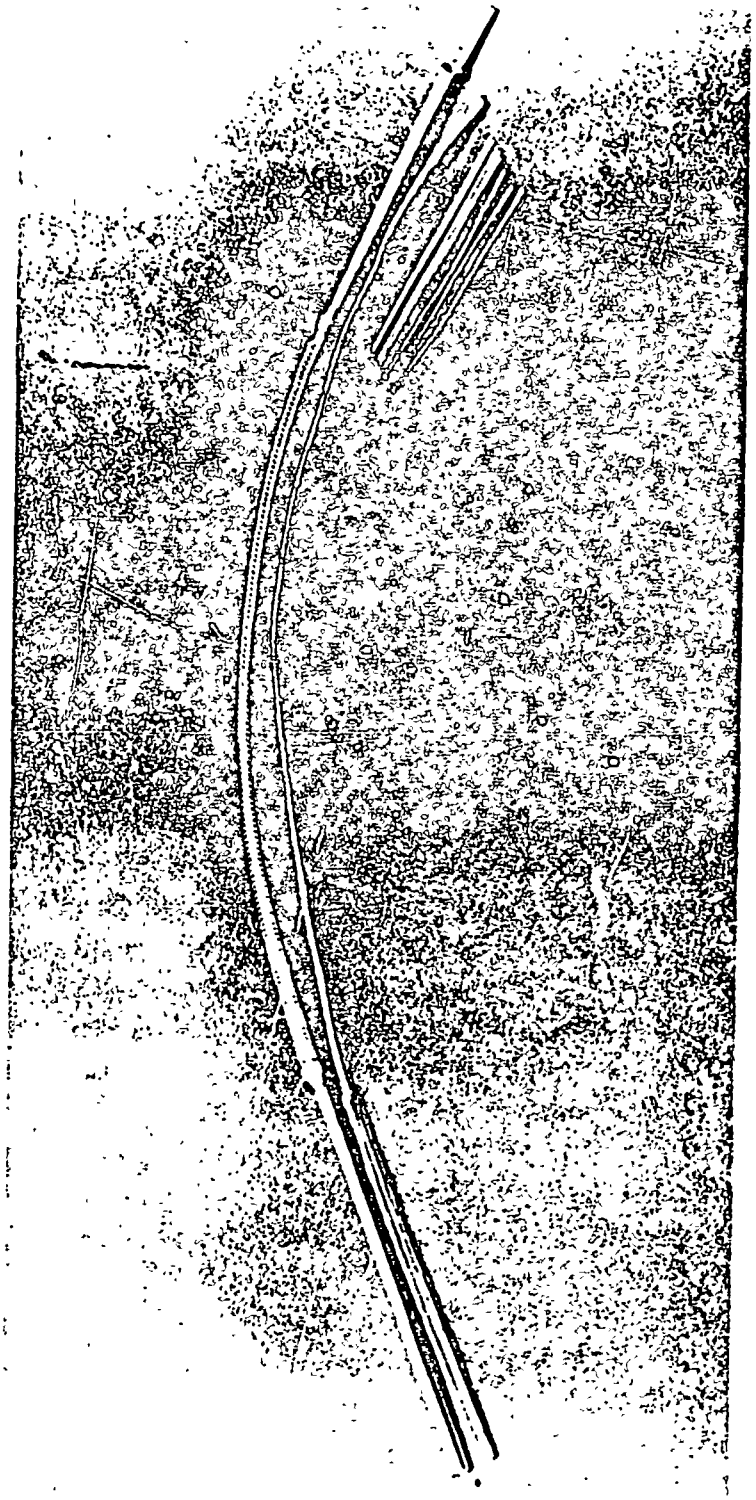

ORIGINAL PAGE IS
OF POOR QUALITY

Figure 6-5 Low Temperature Heat Pipe Components

evaporator end and the fill tube was GTA welded to the condenser end - both with 316 stainless steel filler alloy. The assembly was proof pressure tested at 2.76×10^7 Pa (4000 psig) and helium leak tested at 2.07×10^7 Pa (3000 psig). This was followed by a recleaning to the MA0110-018 specification.

BAKEOUT AND FILLING

The heat pipe was baked out and filled in the same manner as the high power pipe. Based on the final fill calculations, it was determined that the pressure at 315°K could exceed the design value of 2.07×10^7 Pa (3000 psi). Since the pipe was only proof tested to 2.76×10^7 Pa, it was decided to add a 75 cm^3 reservoir onto the condenser end of the pipe. This reduced the expected pressure by about 30 percent and was acceptable. The reservoir was LOX cleaned before installation. The final assembly is shown in Figure 6-6.

Bakeout

The heat pipe assembly was installed in the bakeout fixture and hooked up to the high vacuum system. The pipe temperature was maintained at 250F (121 C) for 18 hours and the vacuum was maintained below 10^{-6} micron after the initial decay.

Filling

The theoretical 100 percent fill charge for the oxygen based on an 80°K minimum operating temperature is 16.1 g including the vapor space in the pressure reservoir. The pipe was initially charged with 21.6 g of oxygen to provide excess for venting. The vent line was installed through the vacuum chamber with a 1/8 in ss line to allow the heat pipe to be vented during operation in the vacuum chamber.

TEST PROGRAM

Heater and thermocouple locations for the low temperature heat pipe are shown in Figure 6-7. The pipe was installed in the test fixture shown in Figure 6-8, leveled, and installed in the vacuum chamber.

Tests were conducted with oxygen inventories ranging from 17-20 g to provide sufficient charge for priming of the tunnel. The nominal operating temperature was 90 $\pm$ 5°K. The heat pipe system was wrapped with multi-layer

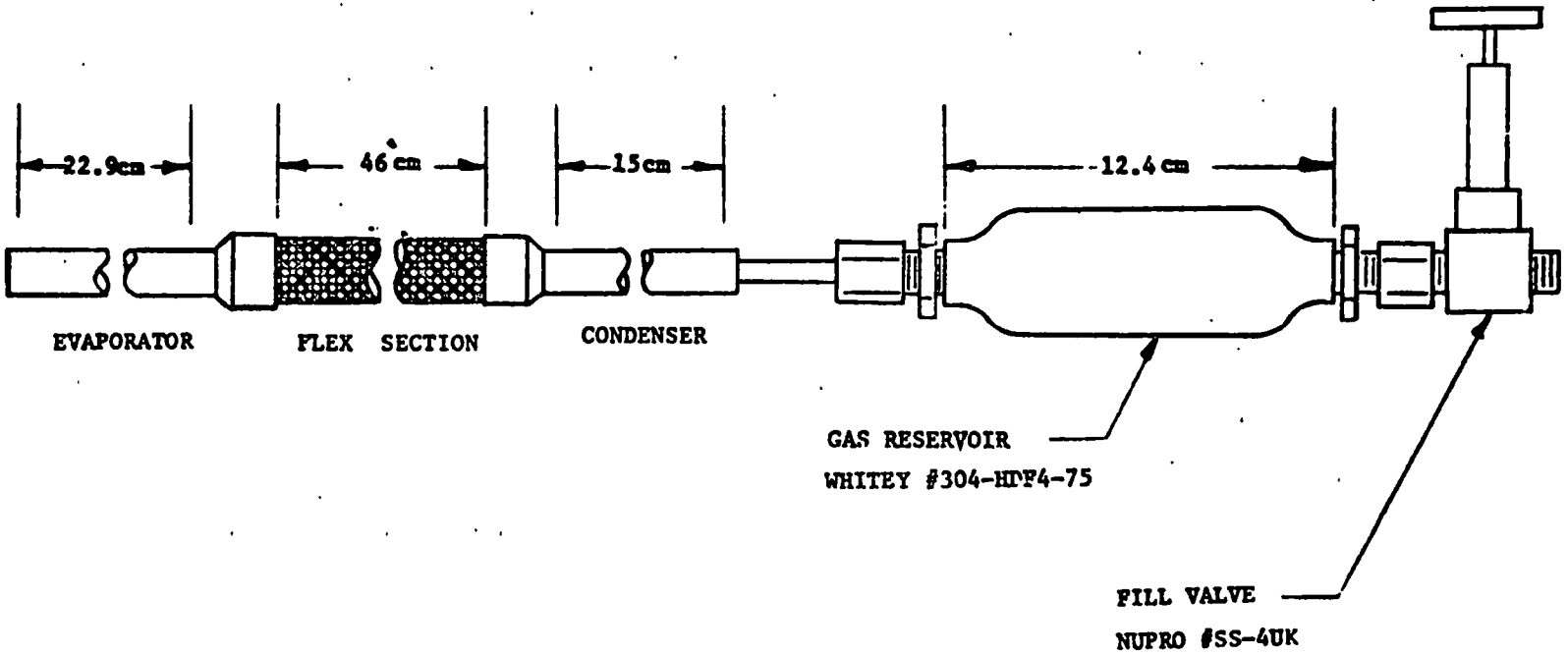

Figure 6-6 Low Temperature Heat Pipe and Pressure Reservoir Assembly

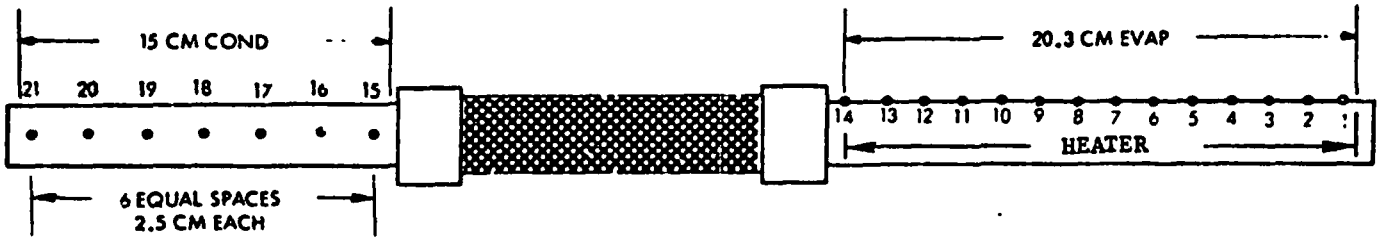

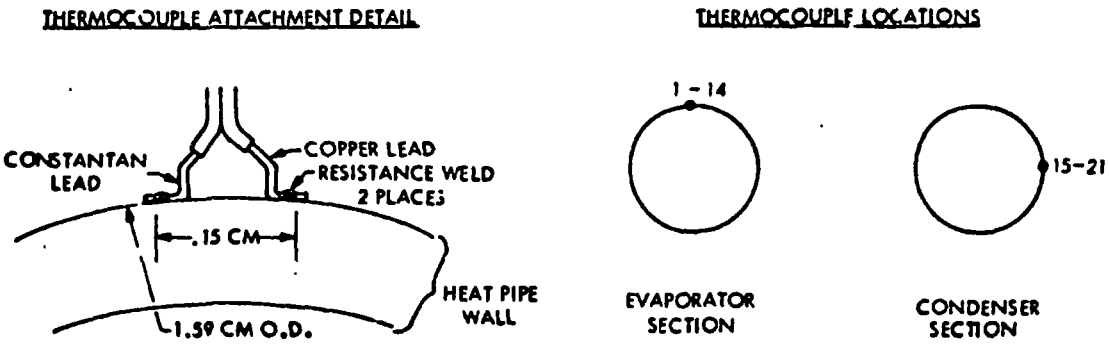

Figure 6-7 Heater and Thermocouple Locations for Low Temperature Heat Pipe

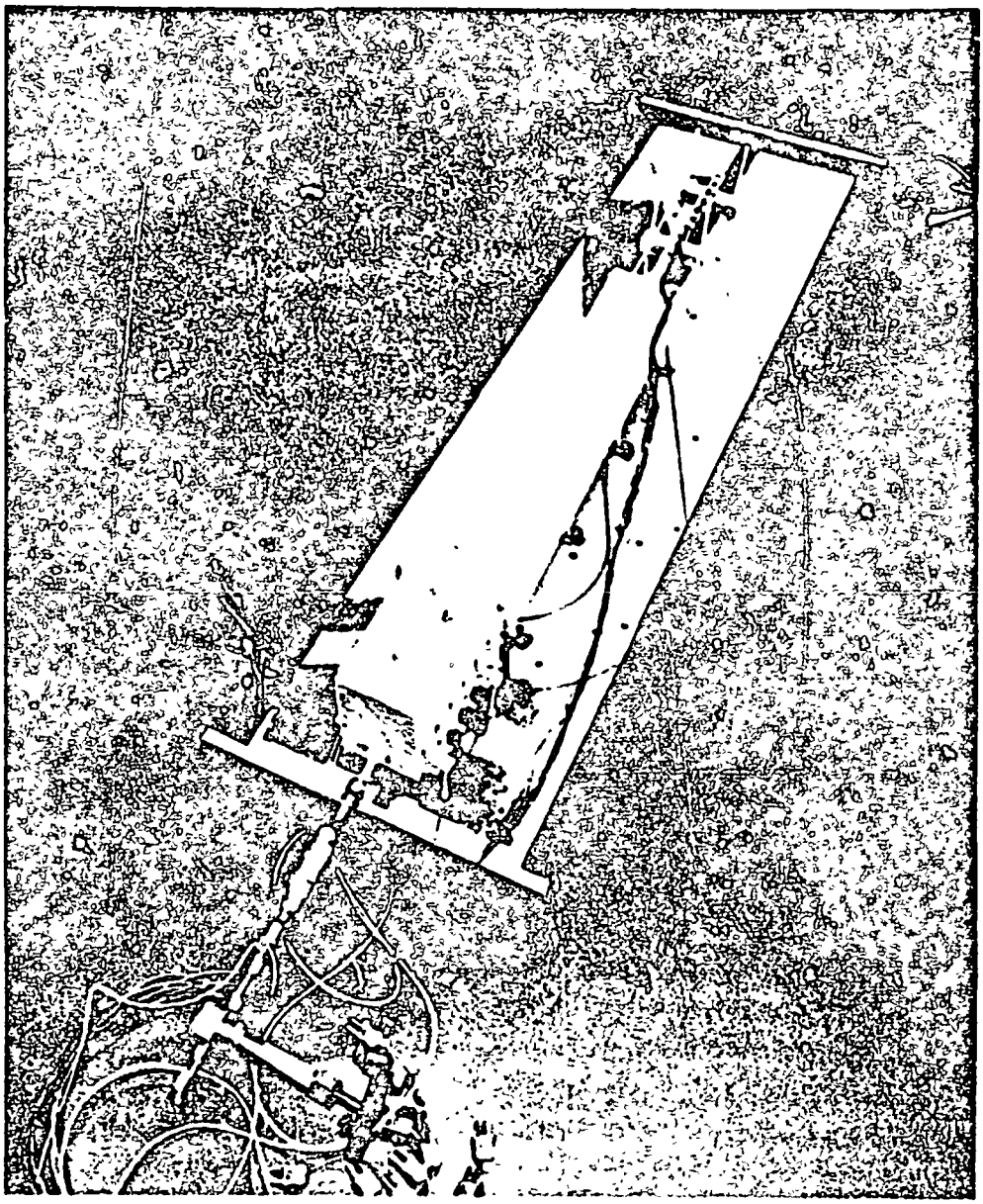

Figure 6-8 Low Temperature Heat Pipe Test Fixture

insulation and tested in an ambient temperature vacuum chamber. A liquid nitrogen bath was attached to the condenser to provide cooling.

The first tests were conducted with a 17.6g charge and with the heat pipe in a straight configuration. Results showed that the heat pipe was burning out at 6 W to 8 W horizontally. Although the burnout values were higher than the 4.5 W specification, there was some concern since the theoretical transport capability was over 20 watts. The pipe was recharged with 21.5 g of oxygen, was refluxed for 4 hours, and then vented to a final charge of 17.9 g. Burnout values were unchanged and indicated that the wick was only partially primed.

The test fixture was modified to allow venting of the heat pipe through the vacuum chamber wall during testing. The pipe was charged with 20 g oxygen and installed in the chamber and test fixture. The pipe was this time installed in an 80 degree bend configuration to provide comparative test data with the straight configuration (a 90° bend would not fit in the chamber).

Results obtained during cooldown from room temperature conditions with the heat pipe horizontal shown in Figure 6-9 (the fluid inventory was still 20 grams which represented approximately a 20% excess without tunnel priming). The results in Figure 6-9 show the condenser having been cooled to below the critical point of oxygen (155°K) in less than 20 minutes after liquid nitrogen cooling was started. Approximately two (2) hours are required for the liquid to advance through the flexible section. Cooldown proceeds much slower through the evaporator because its relatively high thermal mass is directly coupled via the wick bridges to the main wick. There are no bridges in the flexible bellows portion and hence the liquid advances more rapidly through this section since the heat load is smaller being due only to radiation between the bellows and the liquid. Also, as the liquid front progresses toward the evaporator the rate of cooling decreases due to the increasing transport length. The evaporator becomes isothermal after about three (3) hours after the liquid has advanced through the flexible section. The slight gradient (<2°C) in the condenser end is probably due to excess fluid since transport tests indicated that the tunnel never primed.

The maximum transport capability that was measured for the pipe is shown

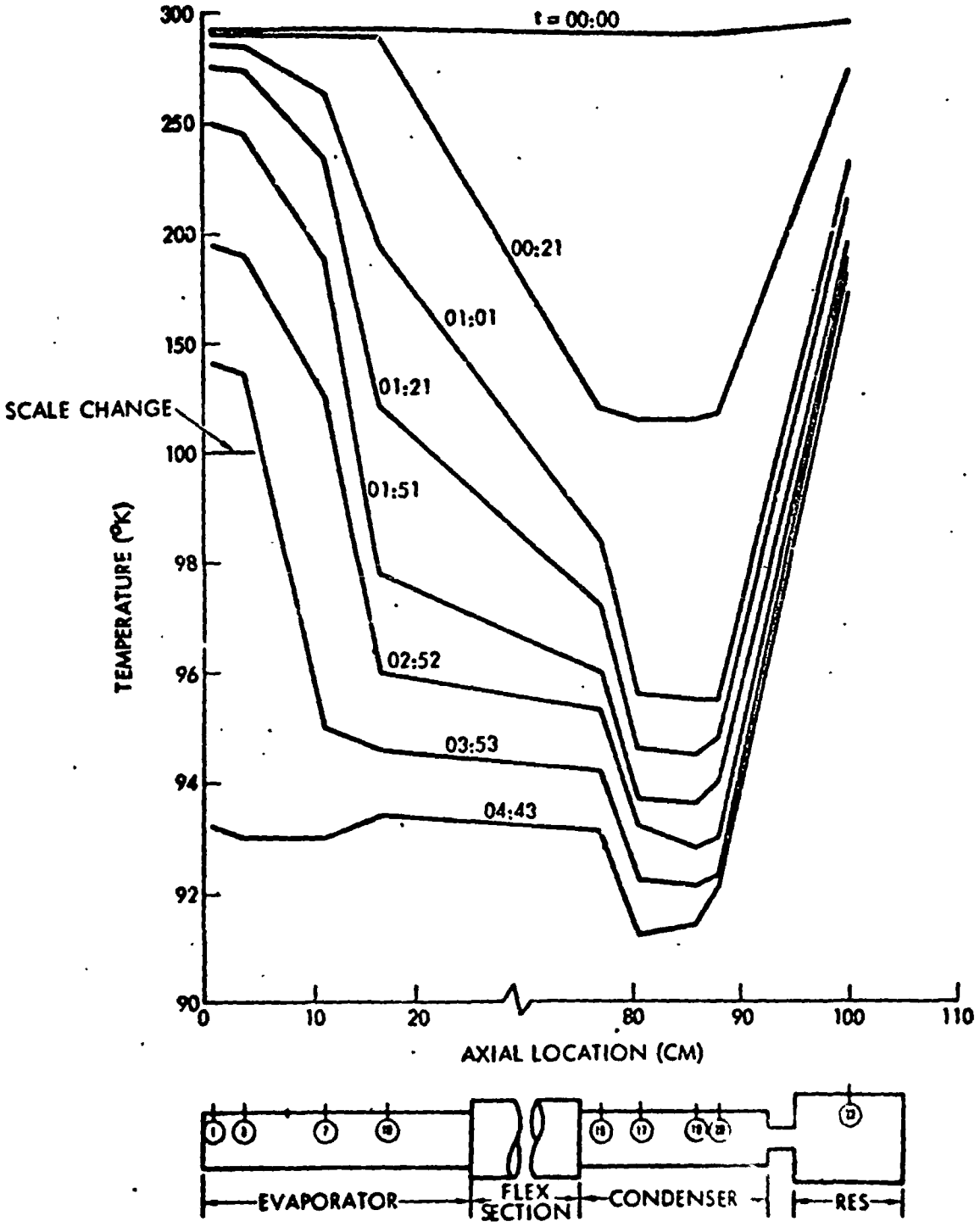

Figure 6-9 Transient Cooldown Data

in Figure 6-10 versus heat pipe elevation. Also shown is the theoretical performance for an open artery and for a closed artery without a primed tunnel. Nominal operating conditions are 90°K. It should be noted that "0-g" equivalent performance corresponds to operation at an elevation which is equal to half the diameter of the main wick (in this case, 0.5 D_w = 0.23 cm). At a horizontal elevation the wick must pump against gravity across its diameter and the transport capability will be less than what would be obtained in "0-g".

The extrapolated "0-g" transport for the straight configuration is 7.8 watts which is 42% better than predicted for the open artery but only 30% of the closed artery's capability. The transport with the 80° bend appears to be slightly below that of the straight configuration.

The static height for a concentric wick is given by

$$h_s = h_o + t_b$$

where

h_o = Heat pipe elevation where the heat load is zero

t_b = Thickness of the wick bridge between the tube wall and the main wick

An examination of the data shows that the static height extrapolated from the measured data is twice that which can be obtained with the coarse mesh screen, but only 44% of the theoretical for the 250 mesh outer layer. Since the static height is equal to the maximum capillary pumping head, these results would indicate that composite pumping which is twice that of the open artery and about half the theoretical maximum has been achieved. This in turn implies that the "0-g" extrapolation should also be a factor of two better than that of the open artery. The fact that the equivalent "0-g" performance is only 42% better means that the flow losses are greater than predicted. The higher losses could be attributed to lower liquid flow conductance (KA), higher vapor losses which are perhaps due to perturbations in the flexible section, or inadequate flow within the circumferential screw thread grooves. Performance at higher evaporator heat fluxes is essentially the same which would eliminate the grooves as a performance limit. The increased performance

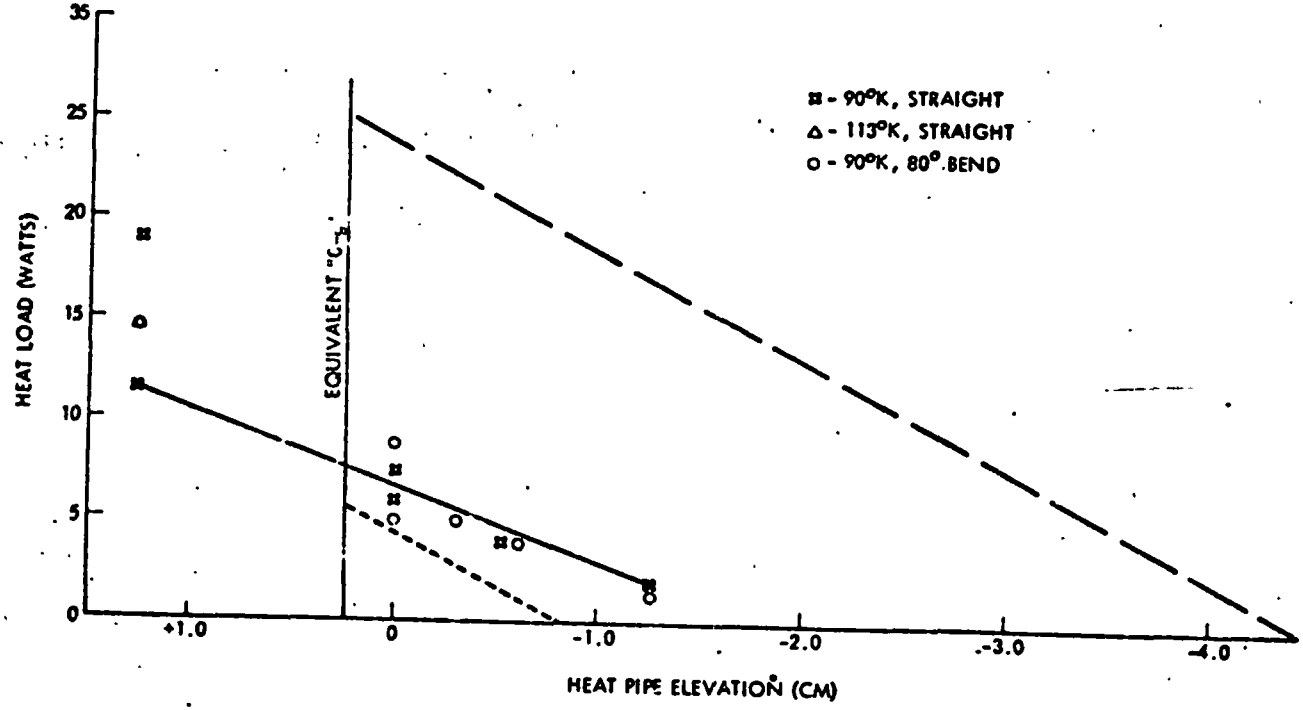

Figure 6-10 Test Data with Oxygen Vs. Theoretical Performance

(14.5 W) obtained at a 1.27 cm positive orientation and at an operating temperature of 113°K would indicate that vapor losses may be causing the reduction. However, the same performance was also obtained at 90°K with the 80° bend. In addition, 19 W transport was also measured at this elevation at 90°K with the straight pipe which would indicate that the degree of arterial priming could be a variable. Hence it would seem that the reduced performance can be attributed to incomplete priming of the arterial wick and to a reduction of the liquid flow conductance over what was measured for the wick when it was tested before insertion into the pipe.

The lower-than-theoretical burnout data may be due to pressure depriming of the composite, or to a non-condensible gas bubble in the wick which limits the realizable capillary head to less than 200 or 250 mesh pumping. In hopes of determining which of these two it might be, two additional tests were performed. First, the pipe was tested with methanol which has a low vapor pressure, and then with a special ultra-high purity grade of oxygen to minimize any trace contaminants of non-condensible gases. No improvement was observed in either test, but the gas bubble hypothesis does appear to be the most reasonable explanation. The high solubility of cryogenic fluids to other non-condensible gases (e.g., methane/nitrogen) makes purification and outgassing very difficult.

7.0 FLEXURAL CYCLE TESTS

One of the original contract objectives was to subject both the high power and low temperature heat pipes to a series of flexural cycle tests to determine the bending force required and the effect of repeated cycling on their performance as heat pipes. However, when it became clear that additional investigative thermal tests would be required, it was decided to eliminate the flexural cycle tests on the high power and low temperature heat pipes to provide additional time for parametric testing as well as testing with other fluids. A limited amount of flexural testing was completed on a high power heat pipe burst specimen (the burst specimen was identical to the high power heat pipe except that it had no wick inside - all other details were the same). Results of that testing are summarized below.

TEST SET-UP

A flex cycle test fixture was designed which would allow the heat pipe to be flexed through a 180 degree arc at a controlled bend radius at ambient and at cryogenic temperature. A schematic of the test setup is shown in Figure 7-1. The pipe is supported in the flexible bellows section by clamp on pivot blocks. One pivot block is attached to an overhead swing arm which is used to move the heat pipe through a prescribed bend pattern. The other pivot block is attached to a stationary support structure. The swing arm is moved by a hydraulic cylinder (Figure 7-1). A load cell is placed in line with the hydraulic cylinder to measure the bending force. A linear motion transducer is also used to accurately measure the deplacement. The heat pipe and pivot structure are lowered into an insulated tank which is filled with LN_2 during cryogenic tests.

During initial checkout of the system, it became apparent that the flexible bellows would not bend at a constant radius because of the greater stiffness where the braid attaches to the evaporator or condenser end. This results in the pipe tending to bend to tighter radius in some areas and a more gentle radius in others. The manufacturer's specification specifies a minimum bend radius of 15.2 cm (6 in) below which permanent (plastic) yield

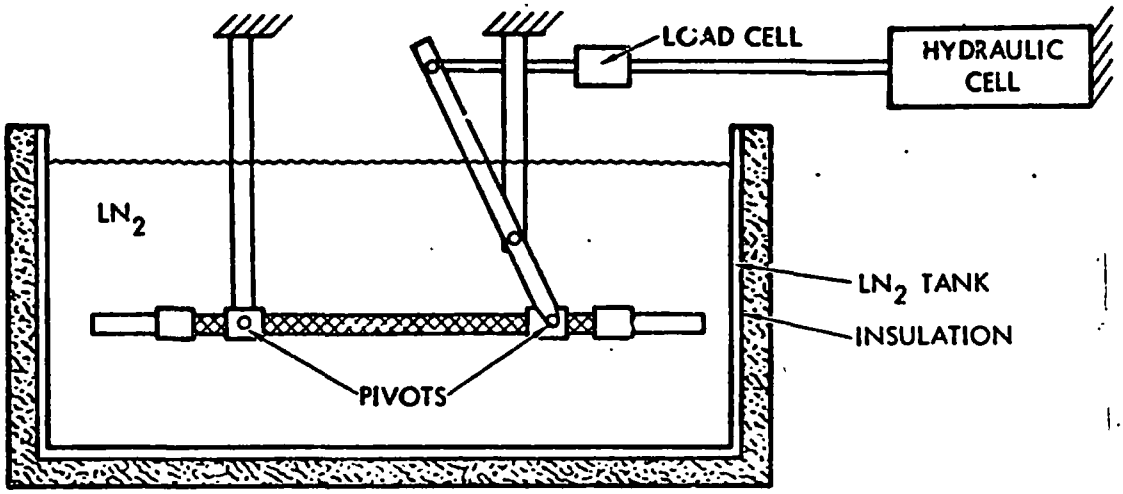

a) EXTENDED

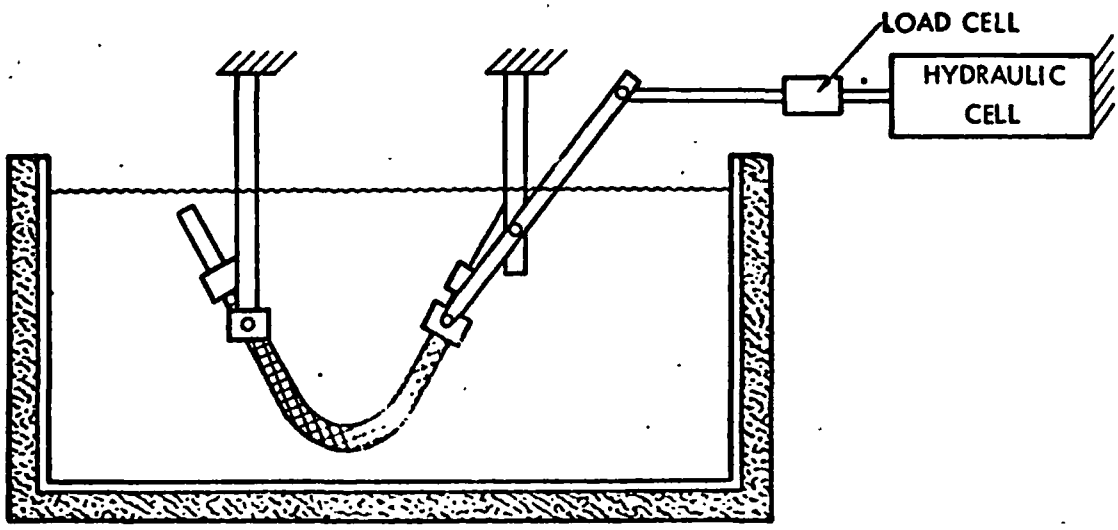

b) PARTIALLY BENT

Figure 7-1 Flex Cycle Test Set-up

could occur in the bellows. To prevent this, a contour plate was made up as shown in Figure 7-2. The contour plate forced the heat pipe to follow a constant bend radius of 15.2 cm. The heat pipe was attached to the contour plate at the top by a hold down wire as indicated in Figure 7-2. As it turned out, this increased the required bending force substantially because of the stiffness in the bellows near the evaporator and condenser ends.

TARE TESTS

A series of tare tests were run to determine the added load due to friction in the test fixture as well as gravity forces on the heat pipe and test fixture. First, the system was set in motion without the heat pipe installed, the measured tare load was 18.5 Nt. This value was used for all subsequent calculations.

Next, two tests were run at ambient temperature with the heat pipe specimen installed. In the first test, the pipe was bent such that the two ends pointed upward when the pipe was bent to 180° (upright). Then, the test was repeated with the two ends pointing downward where the pipe was bent to 180° (inverted). The difference between these two gives an indication of the effect of the weight of the heat pipe on the bend force measurement. As it turned out, the difference was negligible (69.6 Nt vs. 68.7 Nt). Subsequent tests were fun in the upright configuration.

FLEX TESTS

A flex test measurement was made at ambient temperature. The tank was then filled with LN_2 and the system was allowed to stabilize in temperature. The pipe was then run for ~ 1000 cycles at approximately 10 cycles per minute. Strip chart measurements were made at cycle numbers 1, 150, 290, 515, 745, and 995. Figure 7-3 shows the bend/load profile at cycles # 1, 515 and 995. An ambient test was also run after the cryogenic tests. A summary of the peak loads for these tests is shown in Table 7-1.

EVALUATION

The bending loads were considerably higher than the initial design objective (~ 13 Nt) for two reasons. First, a double braided rather than an unbraided or a single braided bellows had to be used to provide a burst

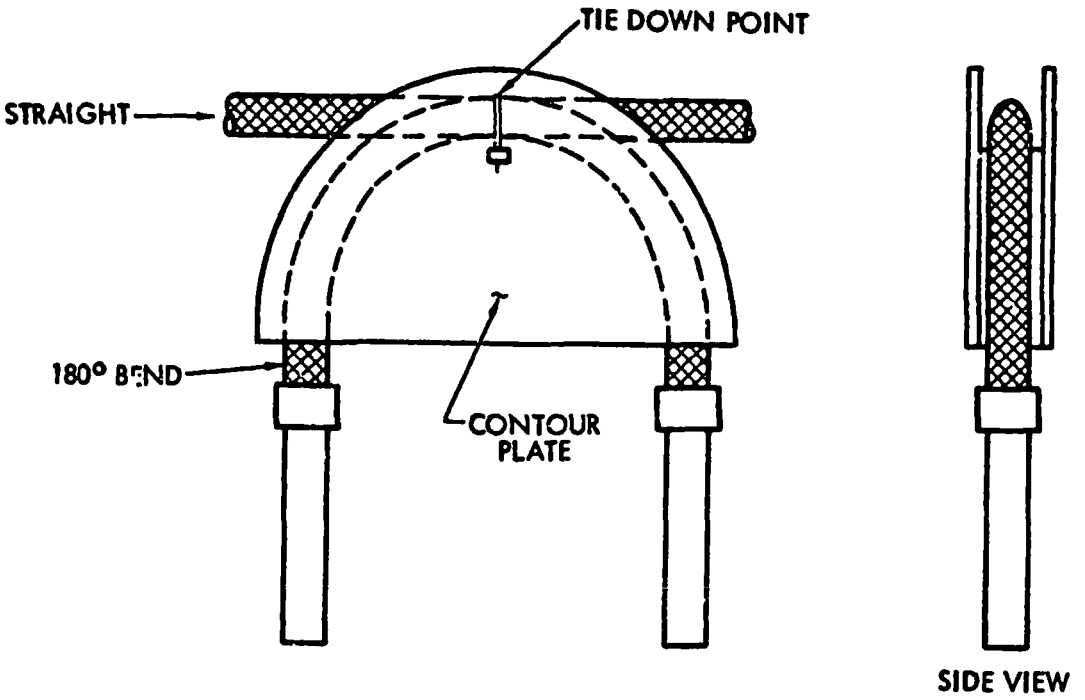

Figure 7-2 180 Degree Contour Plate

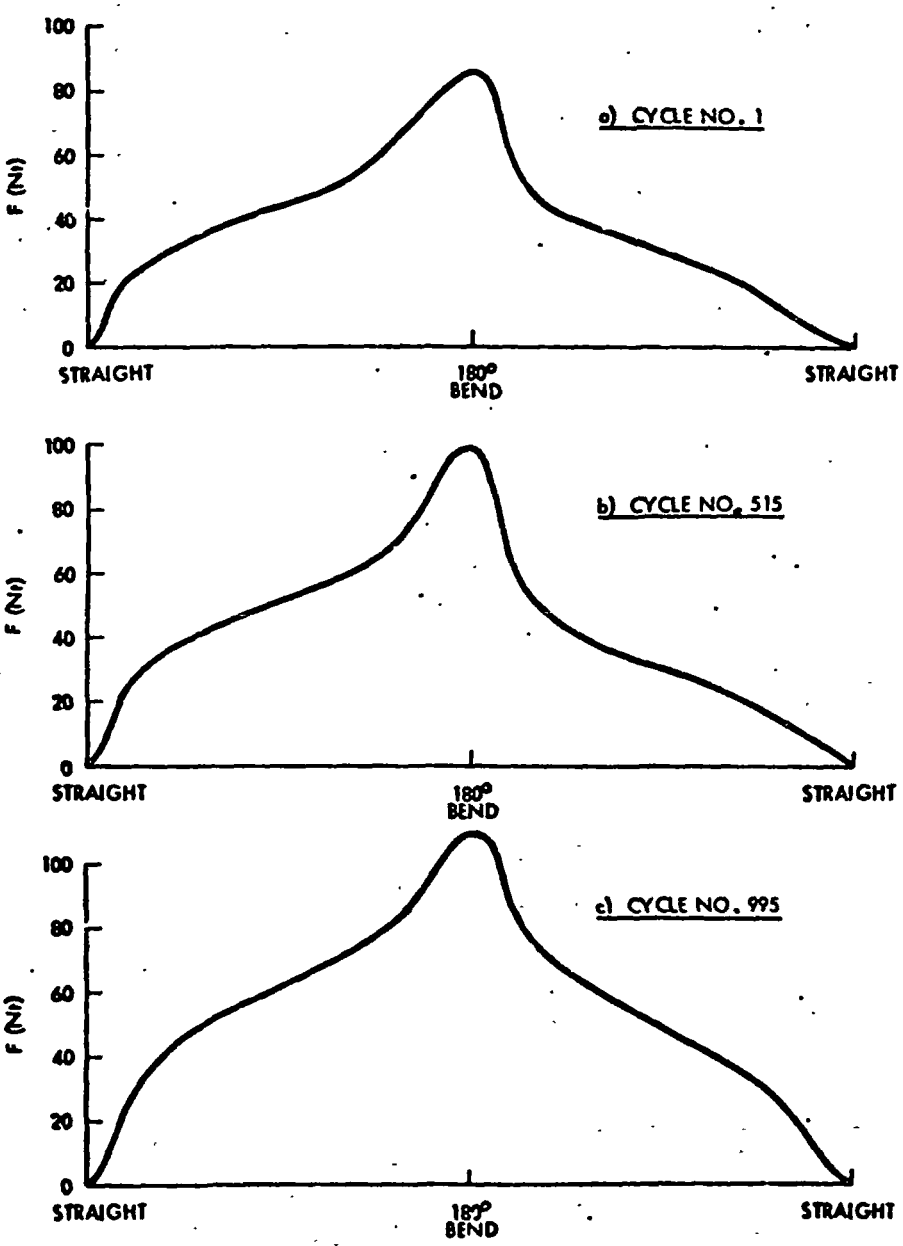

Figure 7-3 Flexural Bending Force Profiles

Table 7-1 Results of Cryogenic Heat Pipe Cyclic Testing

Cycle	Test Temp.	Peak Force (Nt)
Pre-LN_2 test	room	69.6
1	LN_2	83.6
150	LN_2	89.8
290	LN_2	95.9
515	LN_2	99.0
745	LN_2	105.2
995	LN_2	108.3
Post-LN_2 test	room	108.3

safety factor of 4.0. The double braid significantly increases the overall stiffness of the assembly. Second, the pipe had to be controlled to a constant bend radius to prevent possible damage to the bellows. In an application, this could easily be precluded by making the bellows a little longer such that the minimum bend radius would always be greater than the specified minimum.

Another notable conclusion from the tests is that the peak load continual increased during the 1000 cycle test from an initial value of 69.6 Nt at room temperature to a final value of 108.3 Nt in the post LN_2 test run (cycle No. 1001). This is most likely due to work hardening of stainless steel bellows or the braid. It could also be caused in part by movement of the braid wires during motion so as to increase the system stiffness. Figure 7-4 shows the peak force as a function of the test cycle number. As indicated in Figure 7-4, the slope is tapering aft but the peak force was still increasing even at 1000 cycles. Further testing is recommended to determine the long term effect of cycling on bending force.

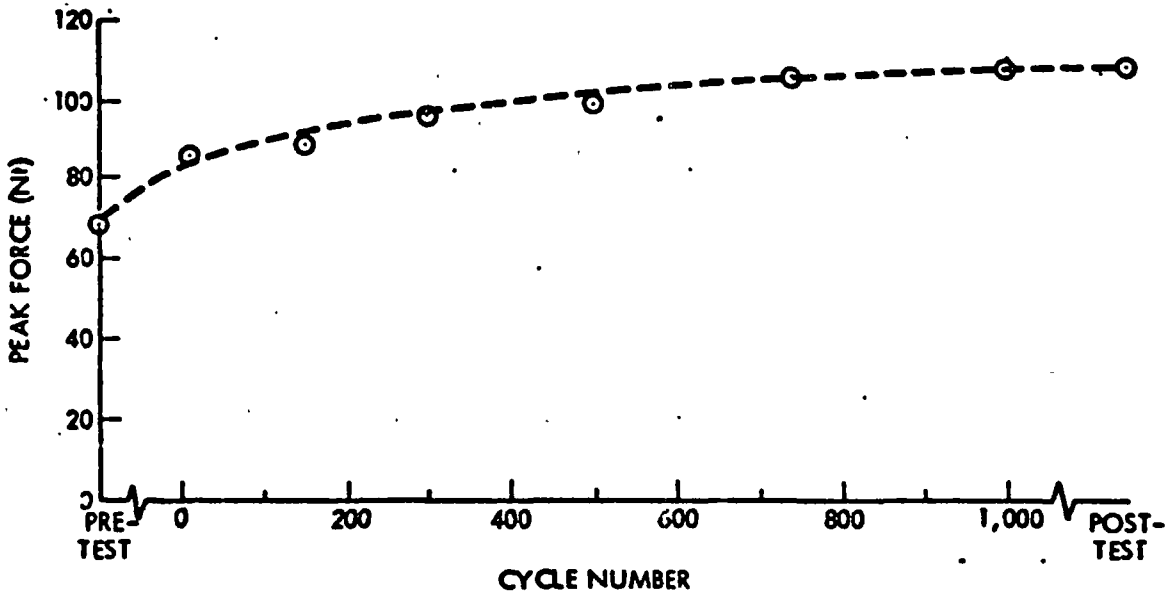

Figure 7-4 Peak Binding Force Vs. Flex Cycle

8.0 CONCLUSIONS AND RECOMMENDATIONS

GENERAL

The concept of a flexible cryogenic heat pipe has been demonstrated successfully, although the ultimate performance capability of the spiral multiwrap composite wicking system was never realized in either the high power (methane) or the low temperature (oxygen) heat pipe. The wicks were very flexible but the flexibility of the container was severely restricted by the double braided stainless steel bellows which was required for pressure safety. Notwithstanding the difficulties which were encountered, the pipes successfully demonstrated the concept of flexible cryogenic heat pipes over a range of temperature, and the demonstrated performance levels are sufficient for many potential space applications. Additional research in the area of composite and artery wicks with cryogenic (as well as ambient) temperature fluids is strongly recommended since it affects not only flexible heat pipes, but also rigid heat pipes and especially gas controlled heat pipes.

FLEXIBILITY

The bias-wrapped spiral screen wick design provided excellent flexibility. The wick can be bent to a very small bend radius (1 or 2 cm) and flexed repeatedly without damage. The flexibility of the system was limited by the flexible bellows container. Because of the high contaminent pressure associated with cryogenic fluids, and the requirement for a pressure safety factor of at least 4.0, the bellows had to be double braided which significantly increased the bending stress. The flexural cycling test program was not performed, however, because it was felt that the thermal test program was more demanding.

The high temperature heat pipe used nominal 3/8 in (.95 cm) flexible hose and had a minimum bend radius of 15.2 cm compared to a specification of 20 cm. The bending force was measured on a burst test facsimile of the high power heat pipe. The bending force at a 180 degree bend angle was initially ~ 70 Nt and increased to 108 Nt after 1000 cycles. Although

the low temperature pipe was not tested for flexibility, it was considerably more flexible than the high power pipe, and may have met the 13.3 Nt bending force requirement. No degradation in performance was observed during tests in which the heat pipe was bent 80 degrees (a 90 degree bend could not be accommodated due to limitation of the vacuum chamber).

PERFORMANCE

Compared to the original specifications, the thermal performance results were mixed. The low temperature heat pipe exceeded the specification by more than 30 percent (>6 w versus 4.5 w). The high power heat pipe exceeded the 40 W transport requirement in only one test (67 W at 140°K and 0.5 cm adverse tilt). In other tests, the pipe carried approximately 35 W at the upper end of the 110 to 140°K temperature range, and only 15 W at the low end.

In terms of the theoretical performance, the results were more disappointing. The theoretical heat transport of the high power heat pipe was over 100 W at 130°K, and that of the low temperature pipe was over 24 W at 90°K. It should be noted that these values are based on the measured permeability of the wick which was approximately three times theoretical. In both cases, the wick appeared to be only partially primed, and the 200 mesh capillary pumping was not achieved.

The most probable explanation for the reduced capillary performance is that a non-condensible gas bubble was present in the wick. When the wick is stressed, the bubble grows in size and length as the surrounding liquid pressure drops, until it eventually blocks the entire evaporator. This conclusion is based on the following rationale:

(1) The slope of the burnout versus tilt data was in accordance with the theory and the measured permeability, hence the transport conductance was not the cause.

(2) The wick in the high power heat pipe was removed after the methane and ammonia tests, and there was no degradation in bubble pressure.

(3) Mass spectrometry tests on the methane indicated relatively high concentration levels of methane and other non-condensible trace contaminants (40 ppm of nitrogen in the heat pipe after outgassing). The impurites were due to trace contaminants in the supply bottle and not due to corrosion as evidenced by the fact that the impurity levels in the heat pipe were generally lower than in the supply bottle, and hydrogen levels were insignificant.

(4) Test data with both the high power and the low temperature heat pipe indicate that the wick was pumping at levels which exceeded the open composite pumping capability, so the wick must have been primed at least to some degree.

The problem of composite and artery wicks in the presence of non-condensible gas is not new. With cryogenic fluids, the problem is even more acute because of the high solubility of non-condensible gases. In addition, the solubility decreases with increasing temperature for most gases, the dissolved gas in the condenser section would tend to come out of solution at the slightly warmer evaporator.

RECOMMENDATIONS

It is strongly recommended that further research and testing be conducted to determine the mechanisms of permature burnout in composite wicks with cryogenic fluids, and to develop systems or processing procedures to overcome this problem in fixed conductance heat pipes. Methods of reducing the room temperature contaminent pressure should also be investigated. These may include solid or liquid absorbant materials, or techniques such as on-orbit charging from a pressure bottle. Applications for flexible heat pipe technology are many, and further research should be continued.

REFERENCES

1. Wright, J. P. and W. R. Pence. Development of a Cryogenic Heat Pipe Radiator for a Detector Cooling System. ASME Paper No. 73-ENAs-47, July 1973.

2. Saaski, E. and J. P. Wright. A Flexible Cryogenic Heat Pipe. AIAA Paper No. 75-658, May 1975.

3. Technical Proposal for a Flexible Cryogenic Heat Pipe Development Program. Rockwell Space Division, SD 74-SA-0188-1 (January 29, 1975).

4. Schlitt, R., et al. Parametric Performance of Extruded Axial Grooved Heat Pipes from 100 to 500°K. AIAA Paper No. 74-724, July 1974.

5. Harwell, W., et al. Cryogenic Heat Pipe Experiment. AIAA Paper No. 75-729, May 1975.

6. Quadrini, J. and R. Kosson. Design, Fabrication, and Testing of a Cryogenic Thermal Diode. Interim Report, NASA CR-137616, December 1974.

7. Kirkpatrick, J. P. and P. J. Brennan. Performance Analysis of the Advanced Thermal Control Flight Experiment. AIAA Paper No. 75-727, May 1975.

8. Marcus, B. D. Theory and Design of Variable Conductance Heat Pipes. NASA CR-2018, April 1, 1972.

9. Wright, J. P. et al. Development and Test of Two Flexible Cryogenic Heat Pipes. AIAA Paper No. 76-478, July 1976.

10. Heat Pipe Technology - Final IR&D Report for CFY 1975. Rockwell Space Division, SD 75-SA-0200, December 1975.

11. Saaski, E. W. Heat Pipe Temperature Control Utilizing a Soluble Gas Absorption Reservoir. NASA CR-137792, February 1976.

APPENDIX A

WICKPER PROGRAM UTILIZATION MANUAL

CONTENTS

WICKPER PROGRAM UTLIZATION MANUAL

1.0 INTRODUCTION

This is a utilization manual for the digital computer code WICKPER. The WICKPER program predicts the performance characteristics of the multi-wrap and spiral-artery wick configurations. Input variables allow the user to select various working fluids, operating temperature ranges, wick component characteristics and heat pipe geometries. The code determines the wick cross-sectional area and the corresponding fluid inventory which provide the maximum transport capability for a specified configuration and set of operating conditions. Performance characteristics for this design are then generated over a specified temperature range. Three possible operating modes, the open artery, and a closed artery with and without a primed tunnel, are evaluated for both "0-g" and "1-g" environments.

2.0 ANALYSIS

2.1 Wick System Configuration

Cross sections of the multi-wrap composite and spiral-artery wicks are illustrated in Figures 1 and 2, respectively. Both wick systems have four common elements:

(1) Main wick - This wick runs the lengtn of the heat pipe and provides the flow path and pumping head for condensate return from condenser to evaporator. Two types of wicks are considered.

(a) Multi-wrap - This consists of alternating layers of coarse and fine mesh screen. A homogeneous core consisting of continuous wraps of coarse mesh screen can

also be handled by setting the fine mesh wire diameter equal to zero. This core is completely enclosed by a fine mesh screen which develops the composite pumping.

(b) Spiral artery - In this configuration spacer wires are placed between successive wraps of fine mesh screen. The periphery is again enclosed with fine mesh screen to establish the composite effect.

(2) Tunnel - This is centrally located in the main wick. In the primed mode, the tunnel significantly increases the liquid flow conductance (KA), therein increasing the transport capability of the system. The tunnel is assumed to be primed via the Clapyeron mechanism.

(3) Interconnecting bridges - The bridges, each formed by circular wraps of fine mesh screen, link the main wick to the secondary wick in the evaporator and condenser zones.

(4) Secondary Wick - These are screw thread grooves which provide circumferential distribution of the working fluid in the evaporator and condenser sections.

2.2 Wick Properties

Each component of the wick system has a characteristic permeability and effective pore radius. The WICKPER code has the capability of either calculating these theoretical wick properties or using specified values.

The theoretical permeability of the wire mesh screen is defined by the Kozeny Equation.

$$K = \frac{1}{122} \quad \frac{\varepsilon^3}{(1-\varepsilon)^2} d^2 \tag{1}$$

The smallest effective pumping radius characteristic of a particular mesh size is

$$r_p = \frac{1}{2M} \tag{2}$$

The permeability for the concentric annuli in the spiral artery wick is defined by

$$K = \frac{D_h^2}{48} \tag{3}$$

The tunnel permeability is determined by

$$K = \frac{D_h^2}{32} \tag{4}$$

Equation 4 also defines the permeability for triangular grooves (i.e. the circumferential grooves). The hydraulic diameter in each case is defined as

$$D_h = \frac{4A}{WP} \tag{5}$$

The area (A) and wetted perimter (WP) of the wick elements are further defined in Table 1.

2.3 Heat Transport Capability of Wick Elements

A thermal impedance schematic of the heat pipe's wick system is shown in Figure 3. The heat transport capability of the heat pipe is defined by a system of equations which specifies the hydrodynamic flow through the individual wick elements and also through the vapor core.

TABLE 1. GEOMETRIC EQUATIONS USED IN DETERMINATION OF WICK ELEMENT PERMEABILITIES.

Wick Element	Geometric Equations
Spiral Artery	$A_n = \pi D_s (D_t - D_s + N_{wr}(4D_{fw} + 2D_s)) - A_{s_n}$
	$WP_n = 2\pi (D_w - 4D_{fw}) - 2\pi D_s + \frac{\pi^2}{SP} D_s D_w$
Tunnel	$A = \pi D_t^2 / 4$
	$WP = \pi D_t$
Secondary Wick	$A = \phi_1 r^2$
	$WP = 2(\cot \alpha) r$
	$\phi_1 = \cot \alpha - \frac{\pi}{2} + \alpha$
	$\phi_2 = 2 \phi_1 / \cot \alpha$

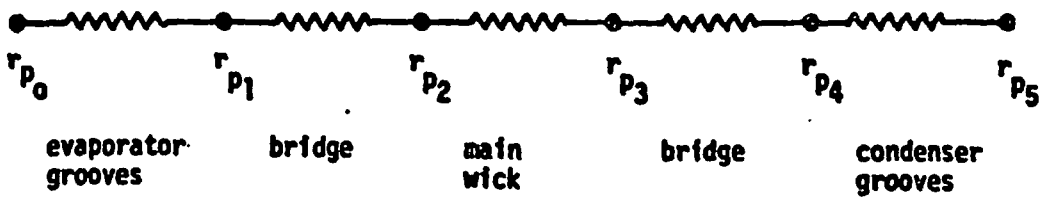

Fig. 3 Schematic of heat pipe wick impedance system.

2.3.1 Main Wick

The closed form solution for the steady-state hydrodynamic heat transport capability of the main wick is:

$$Q = \frac{2(KA)_w F (1 + \eta) \cos \theta}{L_{eff} r_{p_2}} N_\ell \left(1 - \frac{r_{p_2}}{r_{p_3}}\right) \quad (6)$$

The parameter η is defined as the ratio of the sum of all pressure differences due to body forces to the available capillary pressure.

$$\eta = \frac{r_{p_2} (h_w + h)}{2H \cos \theta} \quad (7)$$

where H, the wicking height factor , is a property of the working fluid and is defined as

$$H = \frac{\sigma}{\rho_\ell g} \quad (8)$$

The contact angle of the fluid (θ) is assumed to be zero for this analysis. The height of the main wick in a horizontal position is defined by h_w and the elevation of the heat pipe by h. The friction parameter F represents the ratio of the flow pressure drop of the liquid to the sum of the flow losses for the liquid and vapor.

$$F = \frac{\Delta p_\ell}{\Delta p_\ell + \Delta p_v} = \frac{1}{\phi \frac{\nu_v}{\nu_\ell} \frac{(KA)_w}{(KA)_v} + 1} \quad (9)$$

The permeability of the vapor area in the annulus between the wick and heat pipe wall is defined by Eq. 3. The wick tunnel has a vapor core in the unprimed mode whose permeability is defined by Eq. 4.

The factor ϕ depends on whether the vapor flow is laminar or turbulent.

$$\phi = 1, R_{e_v} \leq 2200 \tag{10}$$

$$\phi = 0.0031 (R_{e_v})^{0.75}, R_{e_v} > 2200 \tag{11}$$

with

$$R_{e_v} = \left(\frac{\rho V D_h}{\mu}\right)_v = \frac{4 Q}{\pi \lambda \mu_v (D_a + D_w)} \tag{12}$$

This analysis assumes that the diameter of the adiabatic region (D_a) is equal to the inner diameter of the bellows. The Liquid Transport Factor N_ℓ is defined as:

$$N_\ell = \frac{\rho_\ell \sigma \lambda}{\mu_\ell} \tag{13}$$

The parameter L_{eff} is the effective transport length. Single evaporator and condenser sections with uniform heat addition/removal are assumed and, therefore,

$$L_{eff} = 0.5(L_e + L_c) + L_a \tag{14}$$

2.3.2 Bridges

Closed form solutions similar to Equation 6 exist for the interconnecting bridges. In the evaporator,

$$Q = 2 N_b \frac{(KA)_b}{L_b} N_\ell \left(\frac{1}{r_{p_1}} - \frac{1}{r_{p_2}}\right) \tag{15}$$

and in the condenser

$$Q = 2 N_b \frac{(KA)_b}{L_b} N_\ell \left(\frac{1}{r_{p_3}} - \frac{1}{r_{p_4}} \right) \quad (16)$$

These equations neglect the small elevation head associated with pumping across the bridge. The parameter L_b is the distance across the bridge and N_b the number of bridges. The meniscus recession in the grooves in the condenser section is small and therefore they approach a completely filled condition (i.e. $r_{p_5} = \infty$). Consequently, the hydrodynamic losses in the condenser grooves are small and have negligible effect on system performance. These small losses result in a pumping radius at the groove-bridge interface (r_{p_4}) that is large in comparison to the pumping radius at the bridge-wick interface (r_{p_3}). Consequently, $(1/r_{p_4})$ can be neglected when determining the heat transport capability of the wick system.

2.3.3 Secondary Wick

The heat transport capability of the circumferential grooves is defined as

$$Q = \frac{N_g \pi L_e \phi_1 \phi_2}{192 R \psi^2} N_\ell \left(r_{p_1}^3 - r_{p_0}^3 \right) \quad (A-17)$$

where the parameter N_g is the number of grooves per unit length, L_e is the length of the heat pipe wall in contact with this bridge in the evaporator and ϕ_1 and ϕ_2 are dimensionless factors determined by groove geometry.

The parameter R is the inner radius of the heat pipe and ψ is the distribution angle or half the angle between a bridge pair. A uniform distribution of bridges is assumed and hydrostatic losses associated with pumping the liquid around the grooves are neglected. It is further assumed that the grooves are sharp and therefore the pumping radius of the evaporator grooves at the maximum distance from the bridges (r_{p_o}) approaches zero at maximum stress.

2.4 Heat Transport Capability of the Heat Pipe

The heat transport capability of the heat pipe is defined by the simultaneous solution of the system of individual transport equations. As illustrated in the wick system schematic in Fig. 3, the pumping radii of the various wick elements are equal at common interfaces. Additionally, these radii adjust to provide uniform heat transport across each element within the system.

The maximum transport capability of a heat pipe will be limited generally by either the main wick or the grooves. If the maximum heat transport of the wick system requires a pumping radius at the groove-bridge interface (r_{p_1}) which is greater than the pore radius of the fine mesh screen used for the bridges and the main wick envelope, the grooves are limiting. If the grooves are capable of providing the maximum heat pipe transport with a value of(r_{p_1}) which is less than the fine mesh pore radius, the main wick is limiting.

The system of individual transport equations is highly non-linear in a "1-g" environment. The WICKPER code uses an incremental type procedure to converge on the system solution. For the "0-g" environment, the transport equation for the main wick (Eq. 6) is simplified and explicit solutions for the effective pumping radii and corresponding heat transport are used.

2.5 Fluid Inventory

The mass of the working fluid required for heat pipe operation is determined for the optimum wick design. The mass of fluid required to satisfy each individual wick element is calculated and then summed to determine the total inventory. For the main wick and interconnecting bridges, the liquid masses are defined by

$$m_{\ell_w} = \rho_\ell (ALc)_w \tag{18}$$

and

$$m_{\ell_b} = \rho_\ell (ALc)_b \tag{19}$$

For the main wick tunnel in the primed mode

$$m_{\ell_t} = \rho_\ell (AL)_t \tag{20}$$

The mass of liquid required for the circumferential grooves is

$$m_{\ell_g} = \rho_\ell (NAC)_g (L_e + L_c) \tag{21}$$

The mass of vapor contained in the annulus between the main wick and the heat pipe envelope is

$$m_v = \rho_v ((AL)_e + (AL)_a + (AL)_c) \tag{22}$$

The mass of vapor present in the wick tunnel in the unprimed mode is

$$m_{v_t} = \rho_v (AL)_t \tag{23}$$

The sum of the liquid and vapor mass charges for the individual elements yields the total fluid requirement.

For the unprimed tunnel mode:

$$m_f = m_{\ell_w} + m_{\ell_b} + m_{\ell_g} + m_v + m_{v_t} \quad (24)$$

and for the primed tunnel mode:

$$m_f = m_{\ell_w} + m_{\ell_b} + m_{\ell_g} + m_{\ell_t} + m_{v} \quad (25)$$

3.0 PROGRAM DESCRIPTION

3.1 General

The WICKPER program and the supplemental subroutines were written in FORTRAN EXTENDED and designed to operate on the CDC 6600 system. The program listing and flow charts are contained in Appendix A. All of the constants and variables utilized within the program are identified at the beginning of the program listing. The program deck consists of job control cards, a program source deck, input data cards and program termination cards. The heat pipe geometries, wick properties, fluid properties and program options are defined by the input data.

WICKPER is structured in two stages. The program initially determines the wick cross-sectional area which provides optimum performance for the closed artery/unprimed tunnel operating mode in a "1-g" environment. The performance characteristics of this wick configuration are then generated either for a "0-g" or "1-g" environment in three operating modes:

(1) Open Artery - The main wick's pumping head is limited to the maximum head developed by the coarse mesh or spiral annulus.

(2) Closed Artery/Unprimed Tunnel - The main wick's capability is limited by the maximum pumping head developed by the fine mesh screen envelope.

(3) Closed Artery/Primed Tunnel - The pumping head developed by the fine mesh screen is limiting and the flow conductance of the tunnel $(KA)_t$ is added to the liquid's flow conductance in the main wick.

Several subroutines supplement WICKPER. Their names and functions are listed below:

- FLUPRT - Inputs and outputs fluid properties.
- MULWRAP - Calculates wick and vapor core geometry and flow conductance for the multi-wrap wick configuration.
- SPIRART - Calculates wick and vapor core geometry and flow conductance for the spiral artery wick configuration.
- BRIDGE - Calculates and outputs geometry and flow conductance of interconnecting bridges.
- MFMWP - Calculates and outputs the fluid mass charge for the multi-wrap wick configuration.

Sample inputs and outputs are presented in the following section and in Appendix A to illustrate WICKPER program operation.

3.2 Input Description

A listing of the input deck is shown in Table 2. The FORTRAN variables and constants are identified at the start of the program listing in Appendix A. The input cards allow the user to select heat pipe geometries, wick element characteristics, fluids, operating temperatures, environments ("o-g" or "1-g") and overall wick configuration (multi-wrap or spiral artery).

A sample input sequence is presented in Table 3. The program options, specified by the input on card No. 3, are detailed below:

TABLE 2. INPUT DATA CARD LIST

Input Card No.	Format	Fortran Names	Description
1	4E20.5	DIE, DI, DOB, DIC	Heat pipe geometry
2	4E20.5	XLE, XLA, XLC	" "
3	8I5	KCAL, IWICTYP, ITEMP, IEL	Program Options
4	8I5	MF, MC, MBR, NGV, MBR, NVBR	Wick element characteristics
5	4E20.5	DT, DFW, DCW, DBRW	" "
6	4E20.5	S, DS, SP, ALPHA	" "
7	4E20.5	THD, THW	" "
8	A10	WICK	" "
* 9	4E20.5	RPF, XKB, POROB	" "
* 10	4E20.5	XKW, POROW	" "
+ 11	A10	FLUID	Fluid properties
+ 12	FIG.3	TEMP	" "
+ 13	7E10.4	RHOL, RHOV, SIGMA, XLAMDA, XMUL, XMUV, H	" "
14	4E10.4	RHOL, RHOV, TEMP	" "

* Input cards used only if KCAL ≠ 1

\+ Card set repeated several times for fluid properties at different operating temperatures.

TABLE 3. SAMPLE INPUT

```
              .12319E-01              .56520E-02              .1N2AHE-01              .12319E-01
              .20300E+00              .65660E+00              .15000E+00
    1     1     6     0
  200    30   200 72H3     4     2
              .24130E-02              .58420E-04              .33020E-03              .58420E-04
              .10500E+01              .3H10UE-03              .25400E-02              .39270E+00
              .13335E-03              .541U2E-04
MIILTI-HPAH
   METHANE
   110.000
 .42671+03 .1557E+01 .1424E-01 .51HH+04 .1217E-03 .4145E-05 .3414E-05
   METHANE
   100.000
 .4407F+03 .7447E+00 .1652F-01 .5311E+04 .1592F-03 .3777E-05 .3821E-05
   METHANE
   110.000
 .42671+03 .1557E+01 .1424E-01 .5164E+04 .1217F-03 .4165E-05 .3416E-05
   METHANE
   120.000
 .4124E+03 .3246E+01 .1219E-01 .4457E+04 .9504E-04 .4665E-05 .3015E-05
   METHANE
   130.000
 .3977F+03 .6134E+01 .1016E-01 .4716E+04 .7710F-04 .5123E-05 .2606E-05
   METHANE
   140.000
 .3814F+03 .1024E+02 .8140F-02 .4462F+04 .6494E-04 .5518E-05 .2185E-05
   METHANE
   150.000
 .3435E+03 .1604E+02 .6250E-02 .4171E+04 .5614E-04 .5966E-05 .1754E-05
 .4407E+03 .7447E+00 .1000E+03
```

(1) KCAL = 1. This specifies that the pore radius and permeability of the fine mesh screen are calculated rather than specified.

(2) IWICTYP = 1. The overall wick configuration in this analysis is the multi-wrap composite wick.

(3) ITEMP = 6. This is the number of discreet operating temperacures at which the optimized wick is evaluated.

(4) IEL = 0. This indicates that the heat pipe is evaluated in a "0-g" environment.

Note that since KCAL = 1, the input cards identified as Nos. 9 and 10 in Table 2 are omitted. A total of seven sets of fluid property data cards (Nos. 11, 12, and 13 in Table 2) appear, one for wick optimization and six for different operating temperatures (ITEMP = 6). The final card specifies the liquid and vapor densities at the temperature at which the mass charge is determined.

3.3 Output Description

A listing of a typical output, corresponding to the sample input data listed in Table 3, follows the program listing in Appendix A. The program output is presented in two stages: data relating to the wick optimization and performance data in either "0-g" or "1-g".

3.3.1 Wick Optimization

The geometry of the heat pipe, basic wick characteristics, and the fluid properties at the optimization temperature are tabulated initially. This is followed by main wick and bridge geometry and corresponding heat pipe performance characteristics for successive concentric wraps of the main wick. The optimum number of wraps is the final output of this stage.

3.3.2 Performance of Optimized Wick

The fluid properties at the operating temperature are listed first, followed by the heat pipe performance characteristics for the three possible operating modes: open artery and closed artery, with and without a primed tunnel. This includes heat transport capability, flow pressure drop ratio, Reynold's number of the vapor flow and the effective pumping radii at the wick element interfaces. If the heat pipe is evaluated in an "1-g" environment, the heat pipe performance characteristics are output at several heat pipe elevations ranging from a horizontal orientation to the static wicking height.

This entire output is repeated for each operating temperature.

NOMENCLATURE

Symbol	Description	Unit
A	area	m^2
C	circumference	m
D	diameter	m
D_h	hydraulic diameter	m
d	wire diameter	m
F	pressure drop ratio	
H	wicking height factor	m^2
h_w	wick height	m
h	elevation of heat pipe	m
K	permeability	m^2
L	length	m
M	mesh size	m^{-1}
m	mass	kg
N	number of . . .	
N_ℓ	liquid transport factor	W/m^2
p	pressure	N/m^2
Q	axial heat flow rate	W
R	heat pipe inner radius	m
r	groove meniscus radius	m
R_e	Reynolds number	
r_p	pumping radius	m
SP	distance between spacer wires	m

NOMENCLATURE (Continued)

Symbol	Description	Unit
V	velocity	m/s
WP	wetted peremeter	m
α	groove half angle	rad
β	heat pipe orientation with respect to gravity	rad
ε	porosity	
η	gravity factor	
θ	contact angle (fluid and wick)	rad
λ	heat of vaporization	J/kg
μ	dynamic viscosity	N-s /m^2
ν	kinematic viscosity	m^2/s
ρ	density	kg/m^3
σ	surface tension	N/m
ϕ	groove geometry factor	
ψ	fluid distribution angle	rad

Subscript	
a	adiabatic
b	bridge
c	condenser
e	evaporator
eff	effective
fw	fine wire
g	groove
ℓ	liquid

NOMENCLATURE (Continued)

Subscript	Description
n	nth wrap of wick
s	spacer wire
t	tunnel
v	vapor
w	wick
wr	wraps

WICKPER FLOWCHARTS

PROGRAM WICKPER

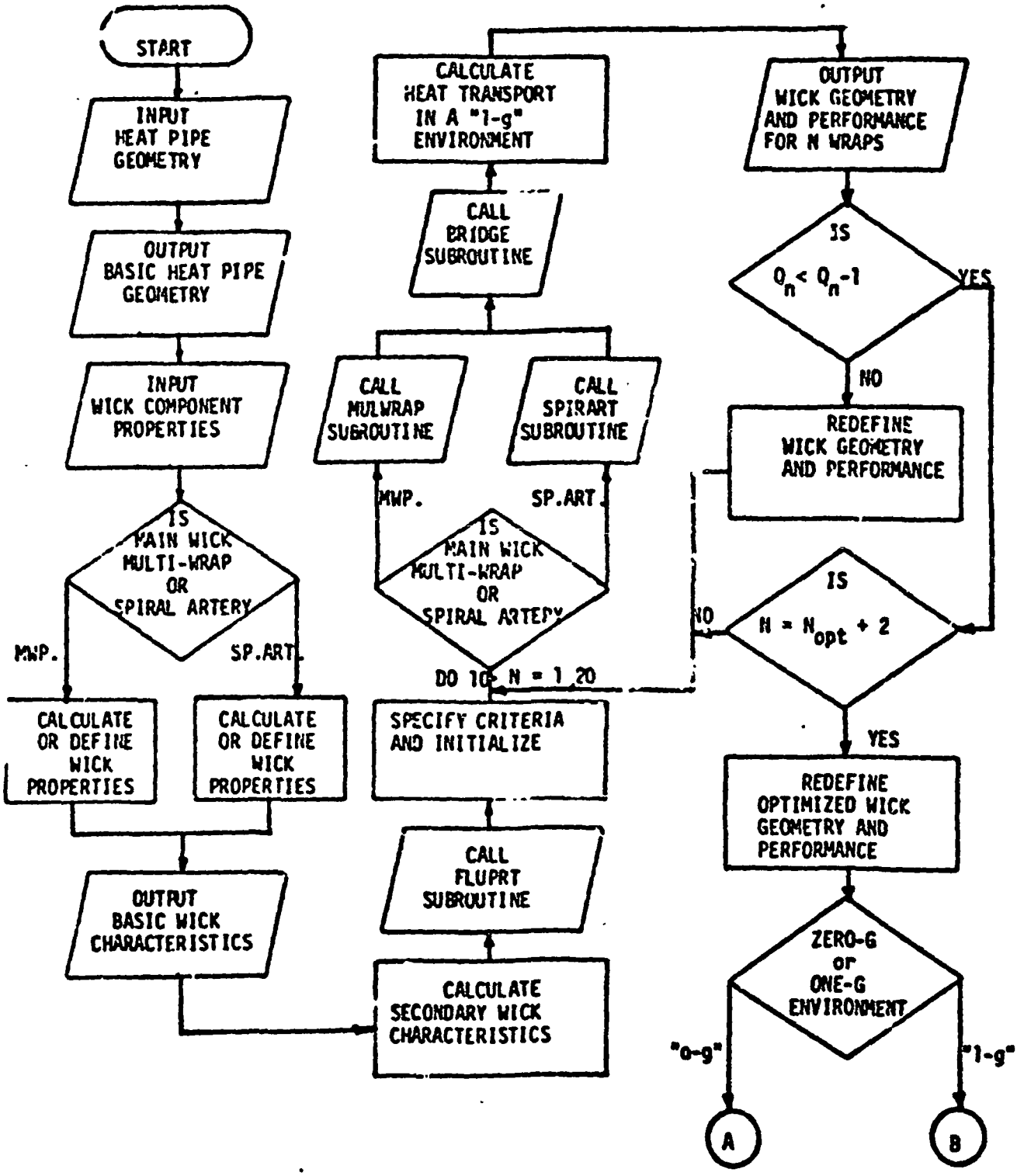

Fig. A-1 WICKPER flowchart - wick optimization section.

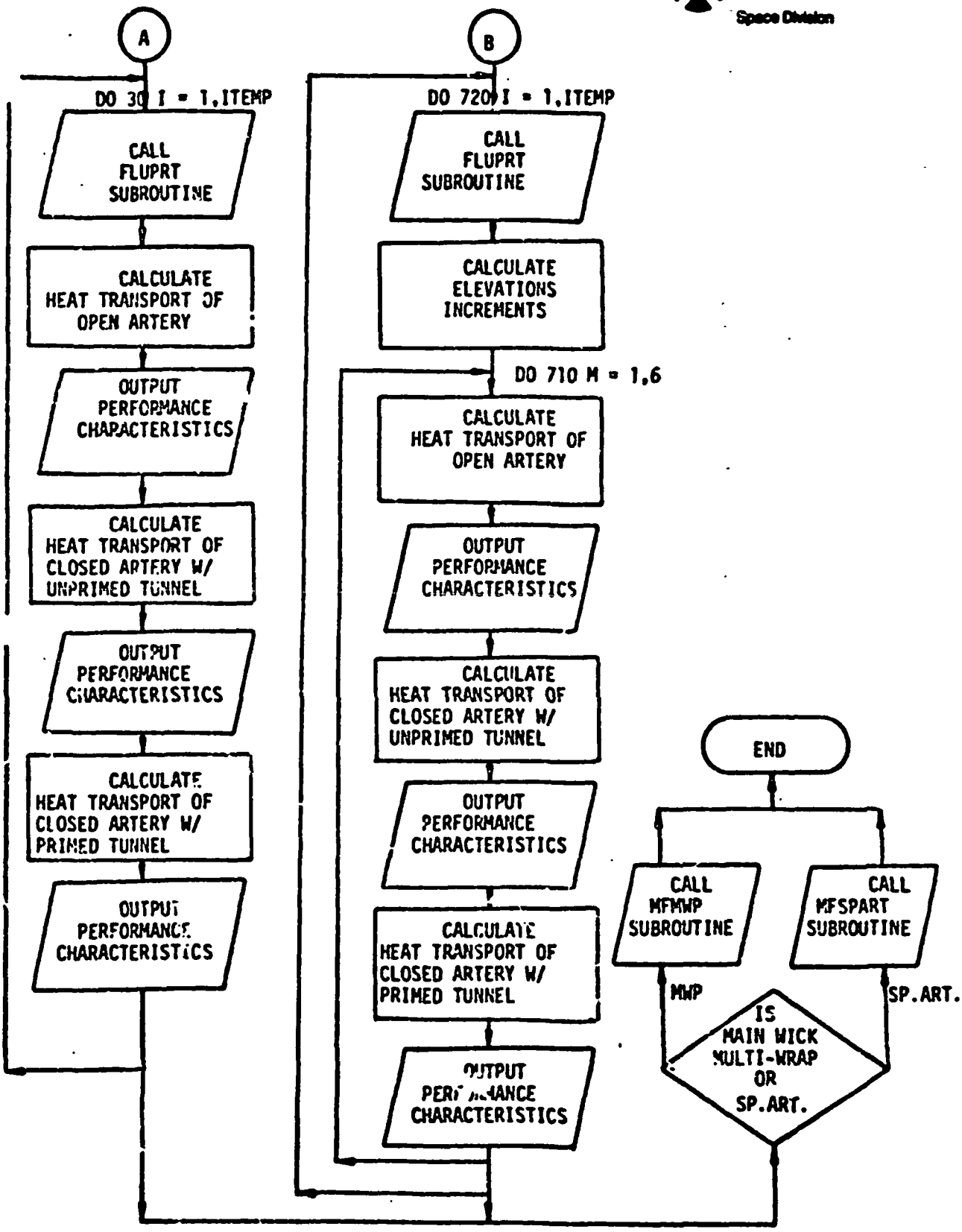
A
DO 30 I = 1,ITEMP
CALL FLUPRT SUBROUTINE
CALCULATE HEAT TRANSPORT OF OPEN ARTERY
OUTPUT PERFORMANCE CHARACTERISTICS
CALCULATE HEAT TRANSPORT OF CLOSED ARTERY W/ UNPRIMED TUNNEL
OUTPUT PERFORMANCE CHARACTERISTICS
CALCULATE HEAT TRANSPORT OF CLOSED ARTERY W/ PRIMED TUNNEL
OUTPUT PERFORMANCE CHARACTERISTICS
B
DO 720 I = 1,ITEMP
CALL FLUPRT SUBROUTINE
CALCULATE ELEVATIONS INCREMENTS
DO 710 M = 1,6
CALCULATE HEAT TRANSPORT OF OPEN ARTERY
OUTPUT PERFORMANCE CHARACTERISTICS
CALCULATE HEAT TRANSPORT OF CLOSED ARTERY W/ UNPRIMED TUNNEL
OUTPUT PERFORMANCE CHARACTERISTICS
CALCULATE HEAT TRANSPORT OF CLOSED ARTERY W/ PRIMED TUNNEL
OUTPUT PERFORMANCE CHARACTERISTICS
END
CALL MFMWP SUBROUTINE
CALL MFSPART SUBROUTINE
MWP
SP.ART.
IS MAIN WICK MULTI-WRAP OR SP.ART.

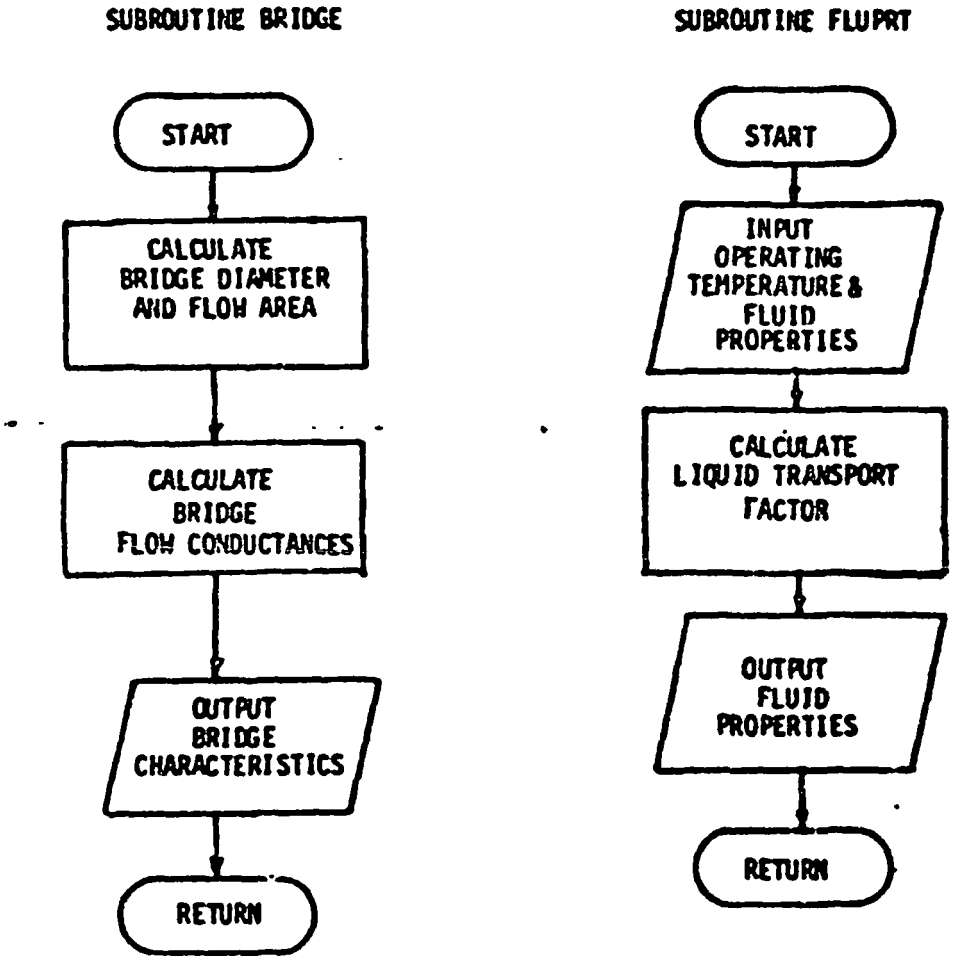

Fig. A-3. WICKPER subroutine flowcharts.

SUBROUTINE MULWRAP/SPIRART

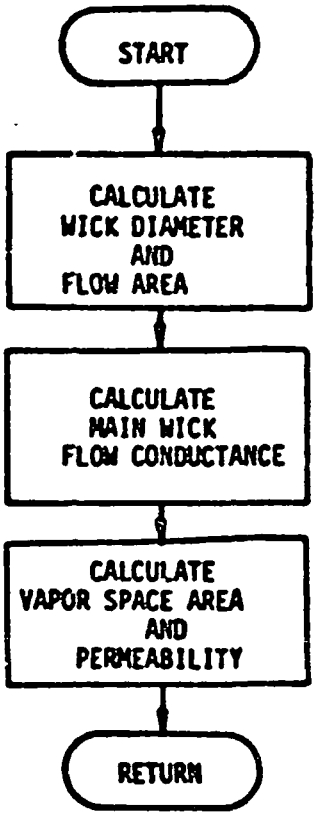

SUBROUTINE MFMAP/MFSPART

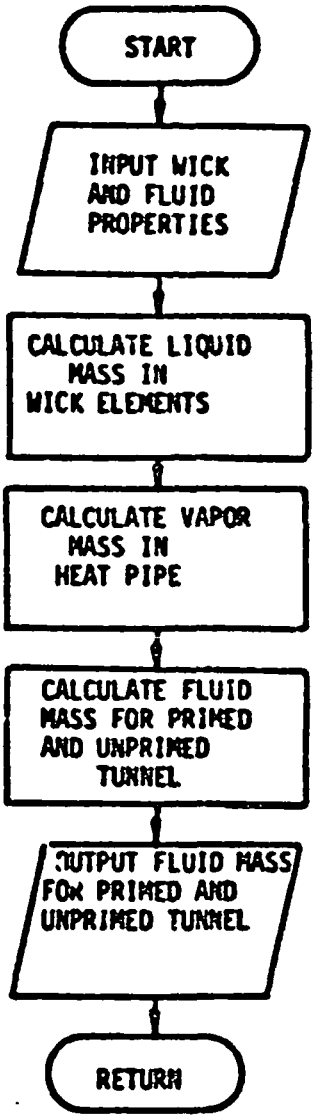

Fig. A-4. WICKPER subroutine flowcharts.

SAMPLE OUTPUT

WICK OPTIMIZATION

APPENDIX B

PARAMETRIC PERFORMANCE PREDICTIONS

(Theoretical Wick Properties)

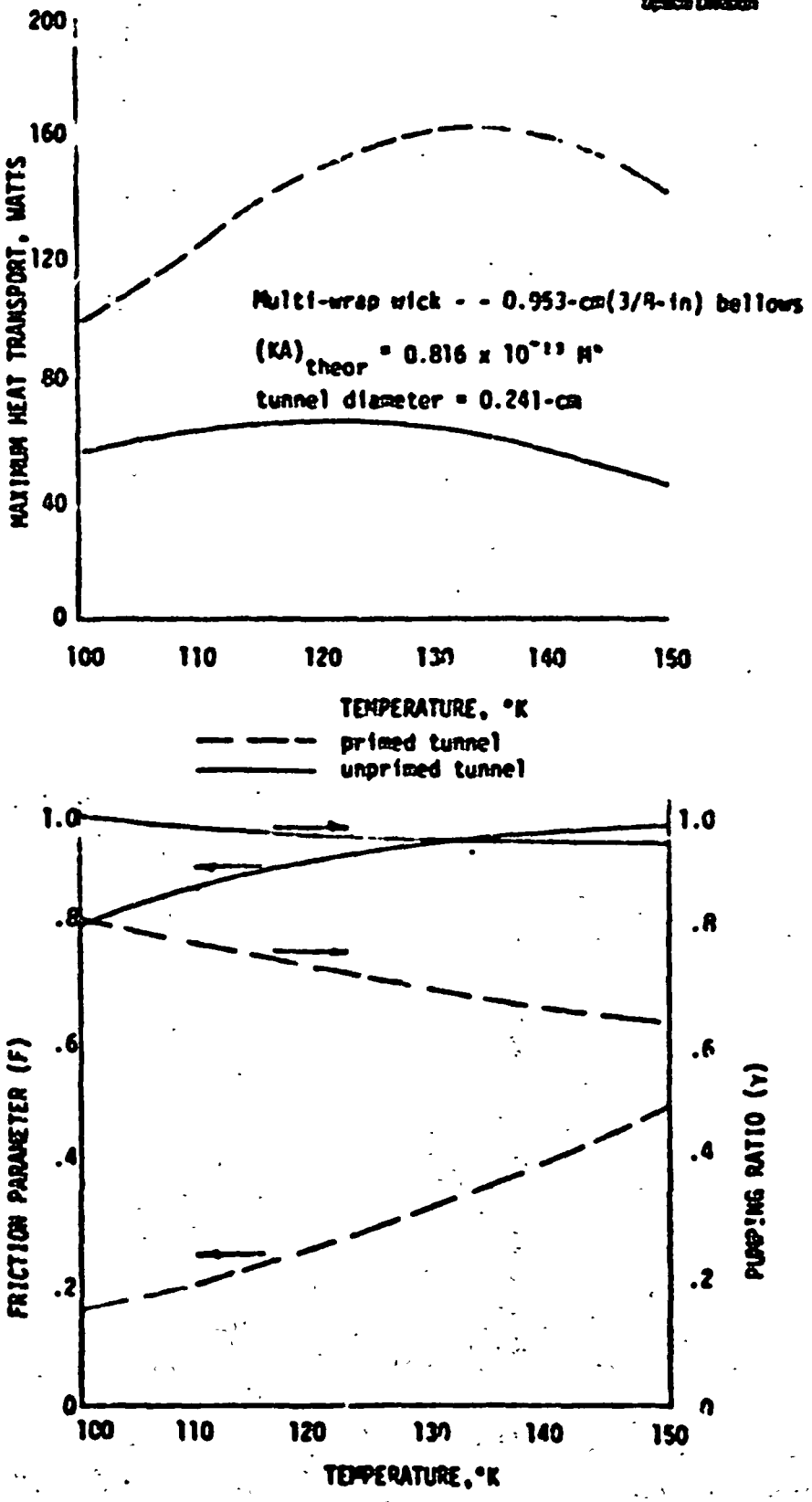

Fig. B-1. Performance characteristics of high power

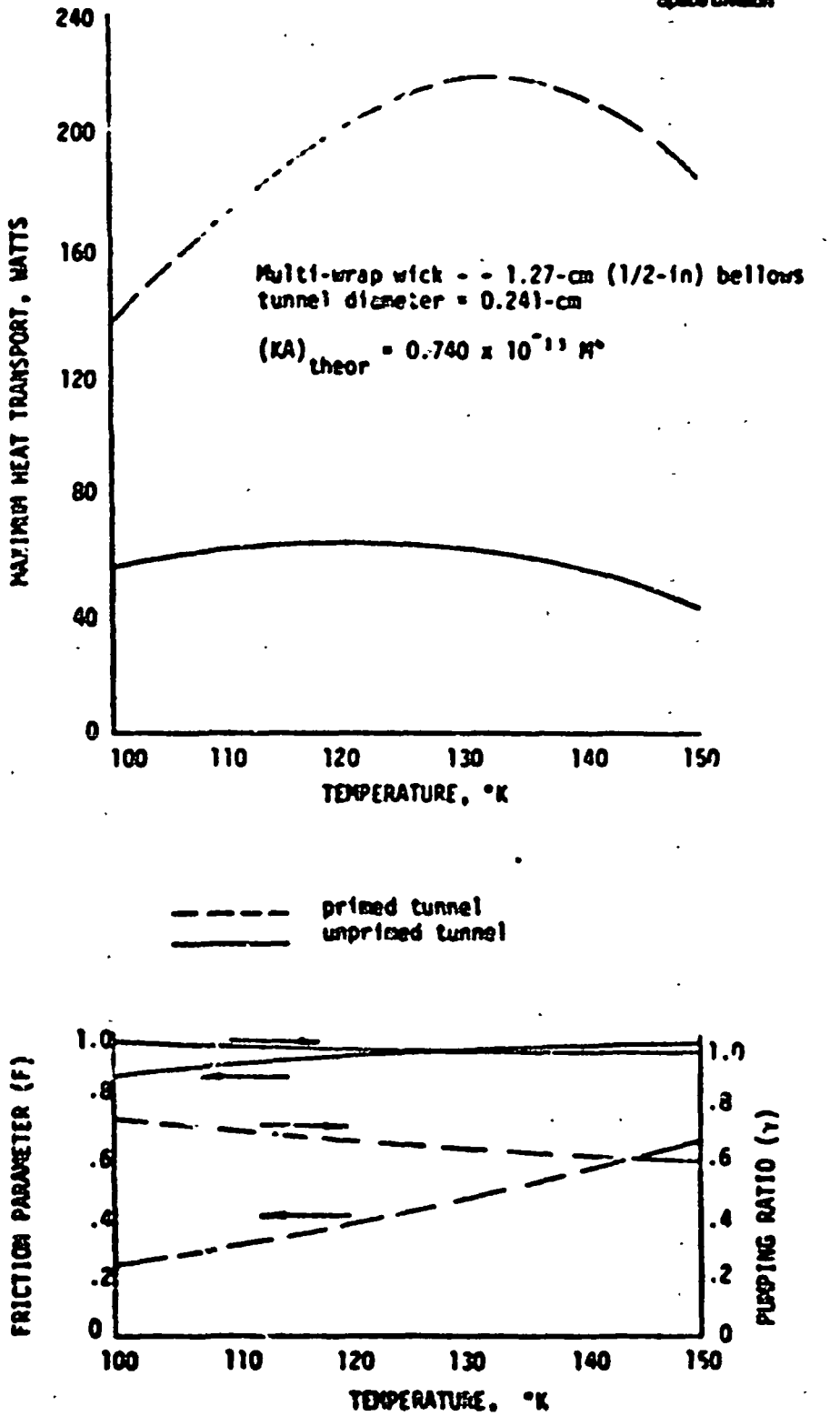

FIG. B-2. Performance characteristics of high power flexible heat pipe in "o-g" (methane)

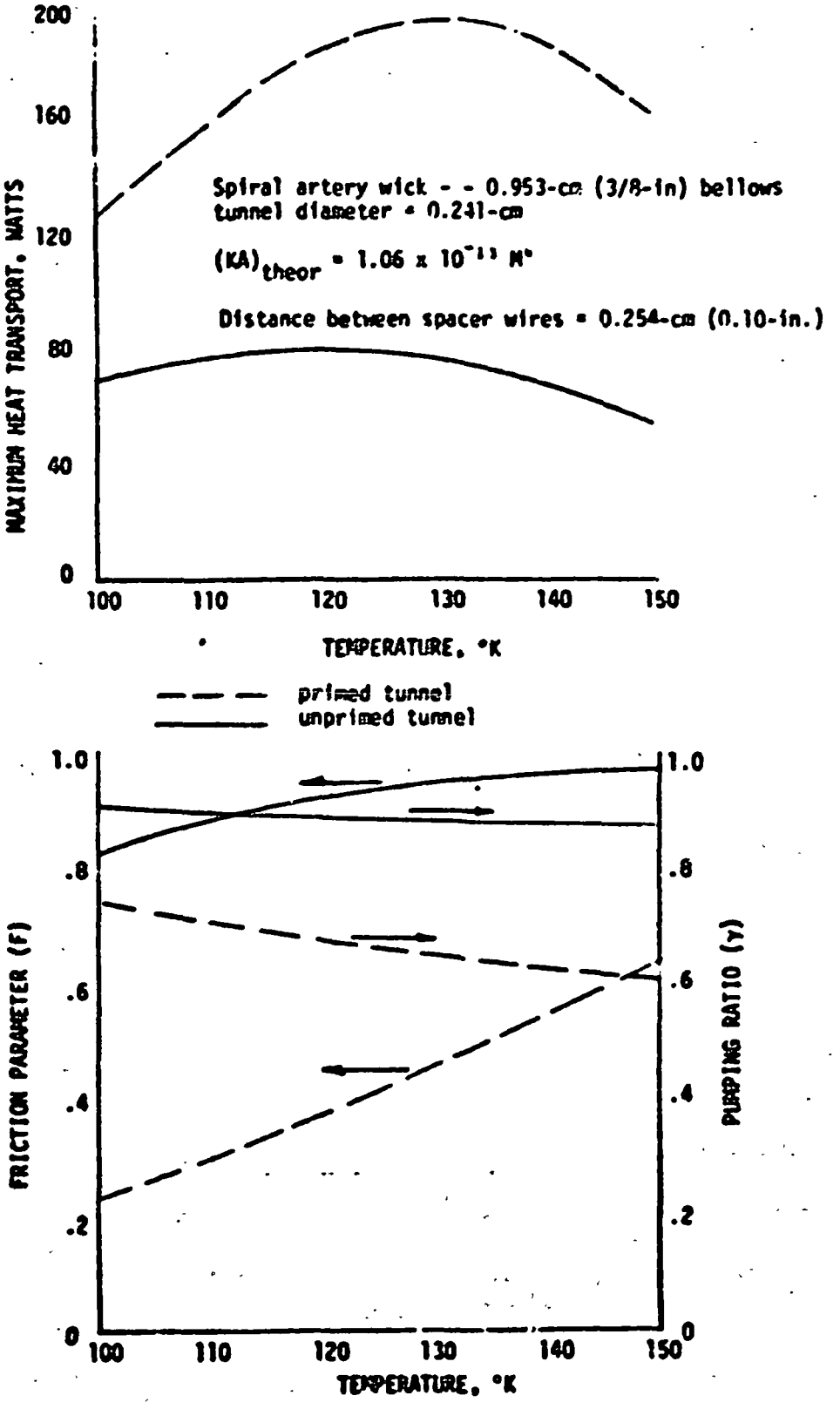

Fig. 3. Performance characteristics of high power flexible heat pipe in "o-g" (methane) sn 77-AP-0088

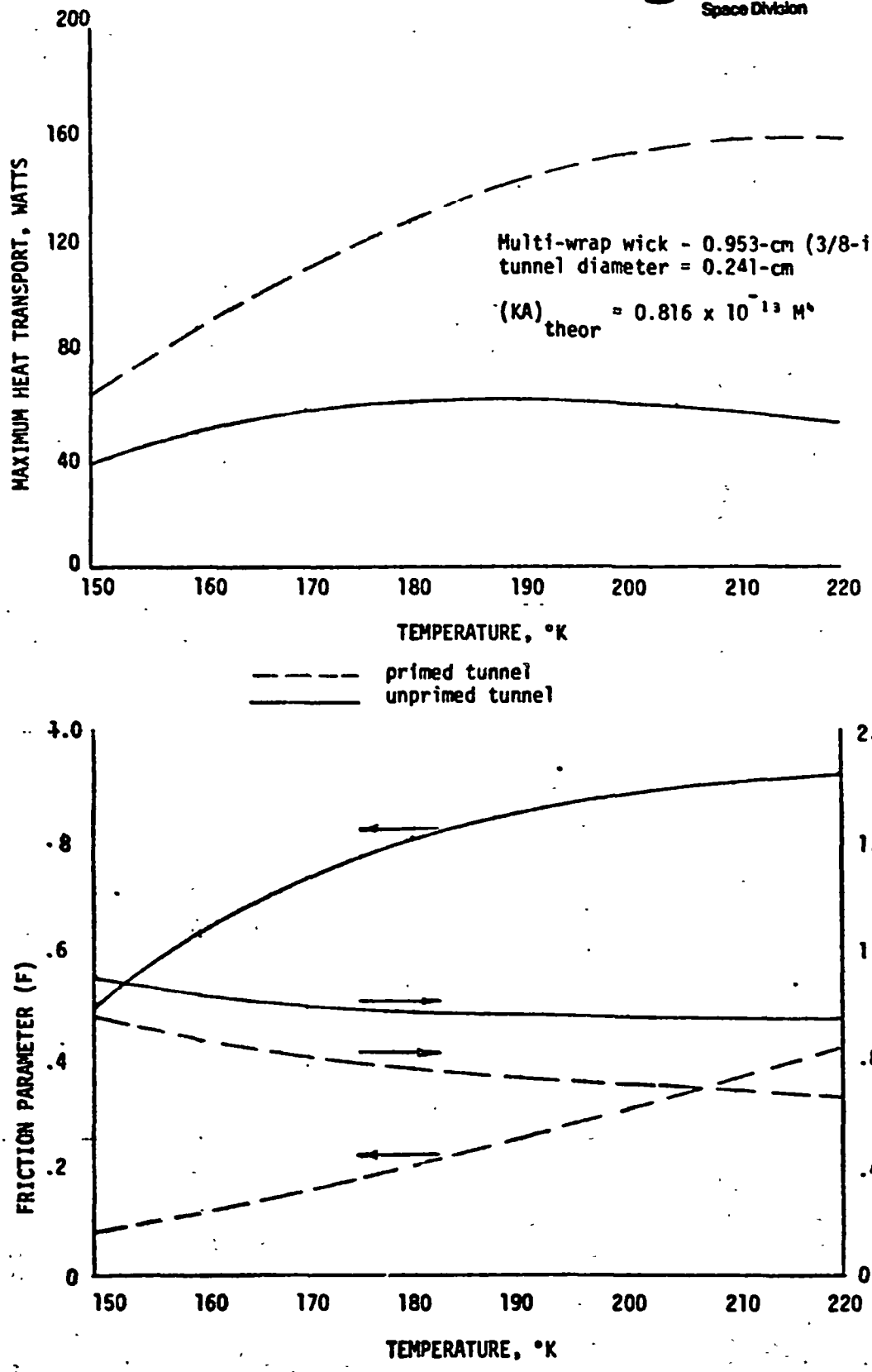

Fig. B-4. Performance characteristics of high power flexible

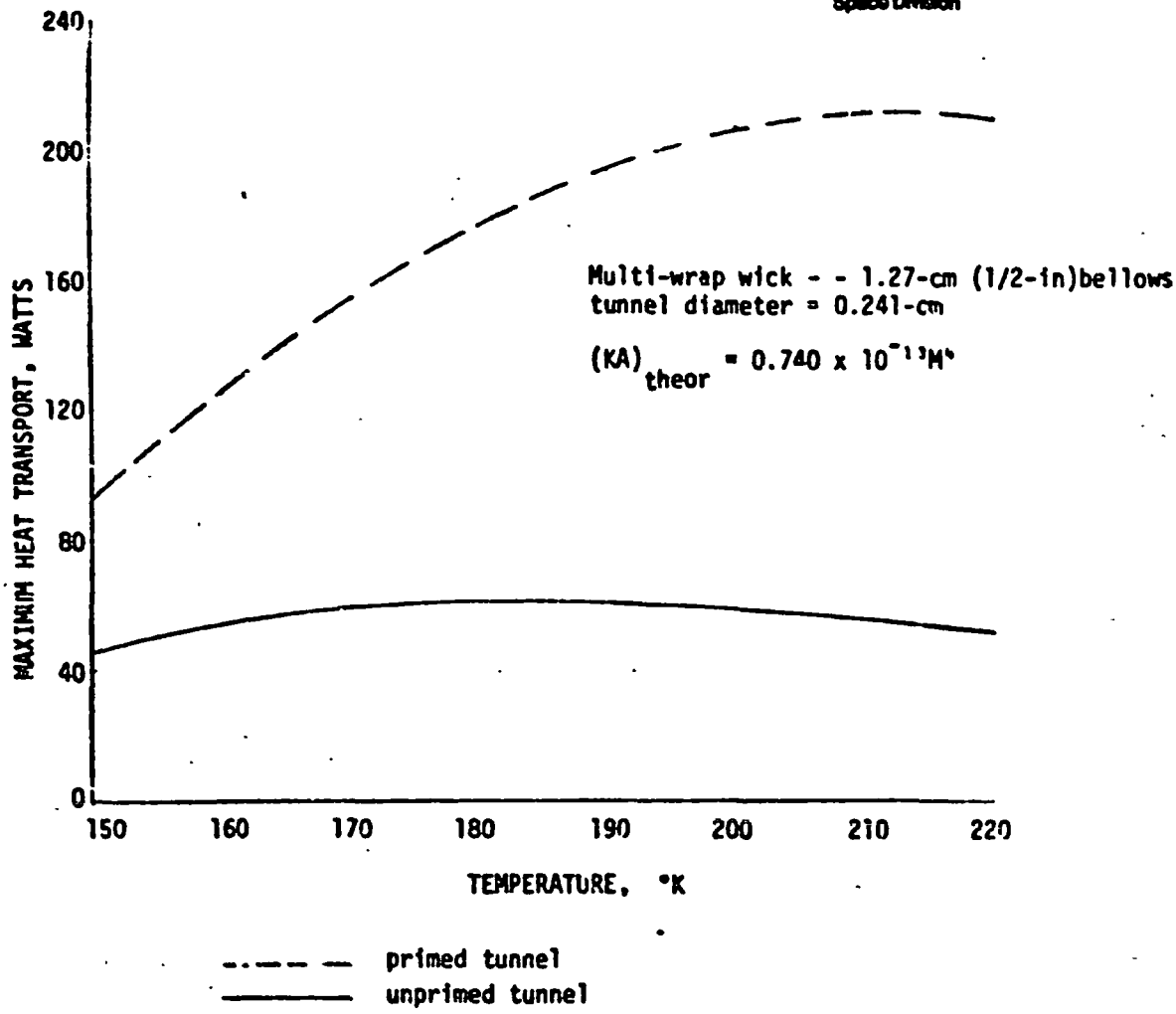

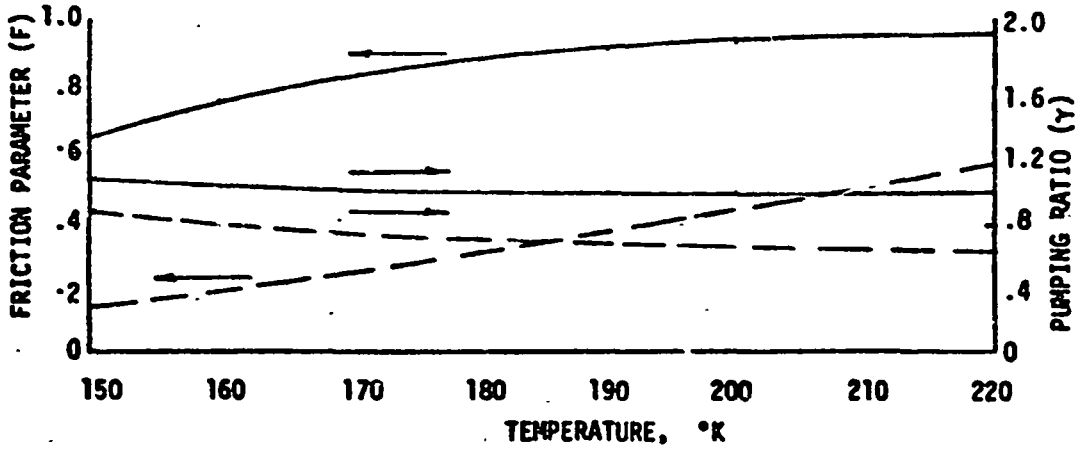

Fig. B-5. Performance characteristics of high power flexible heat pipe in "o-g" (ethane)

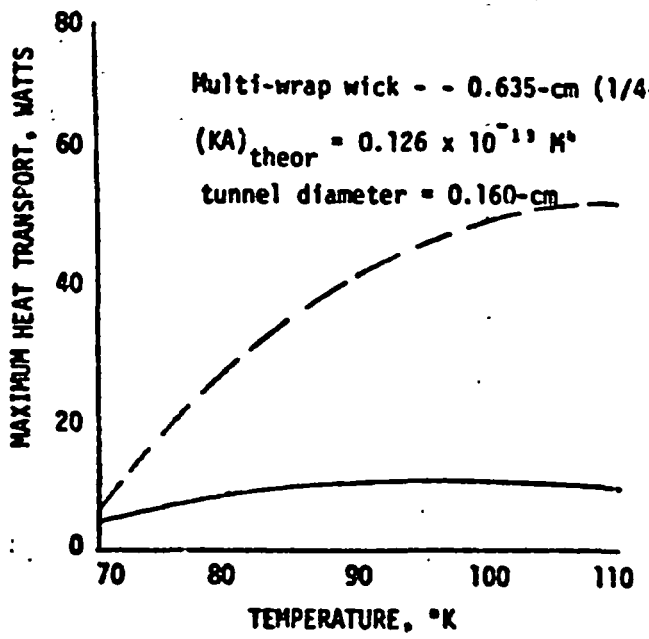

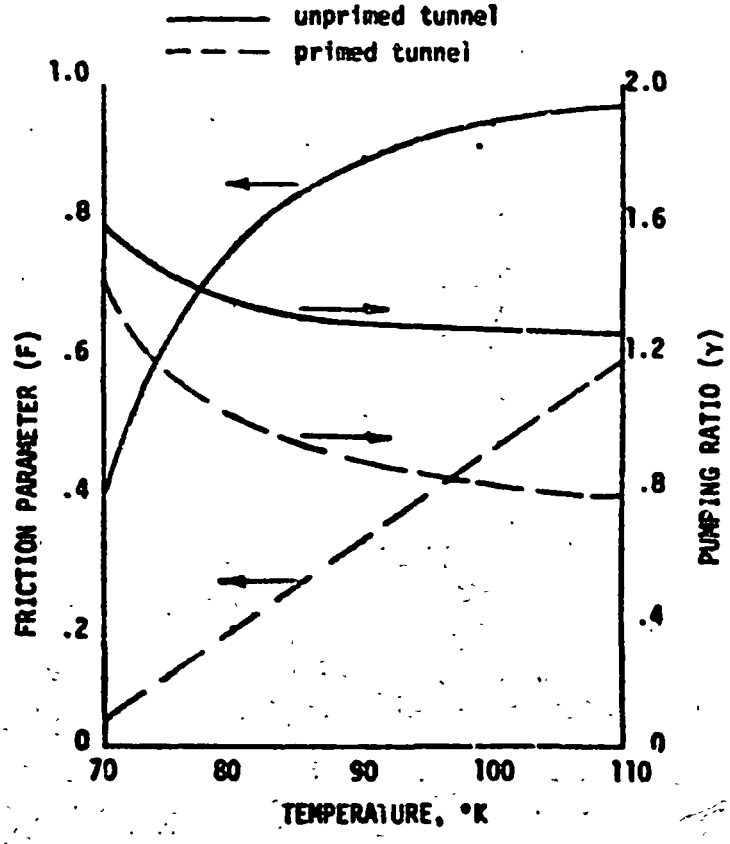

Figure B-6. Performance characteristics of low temperature flexible heat pipe in "0-g" (oxygen)

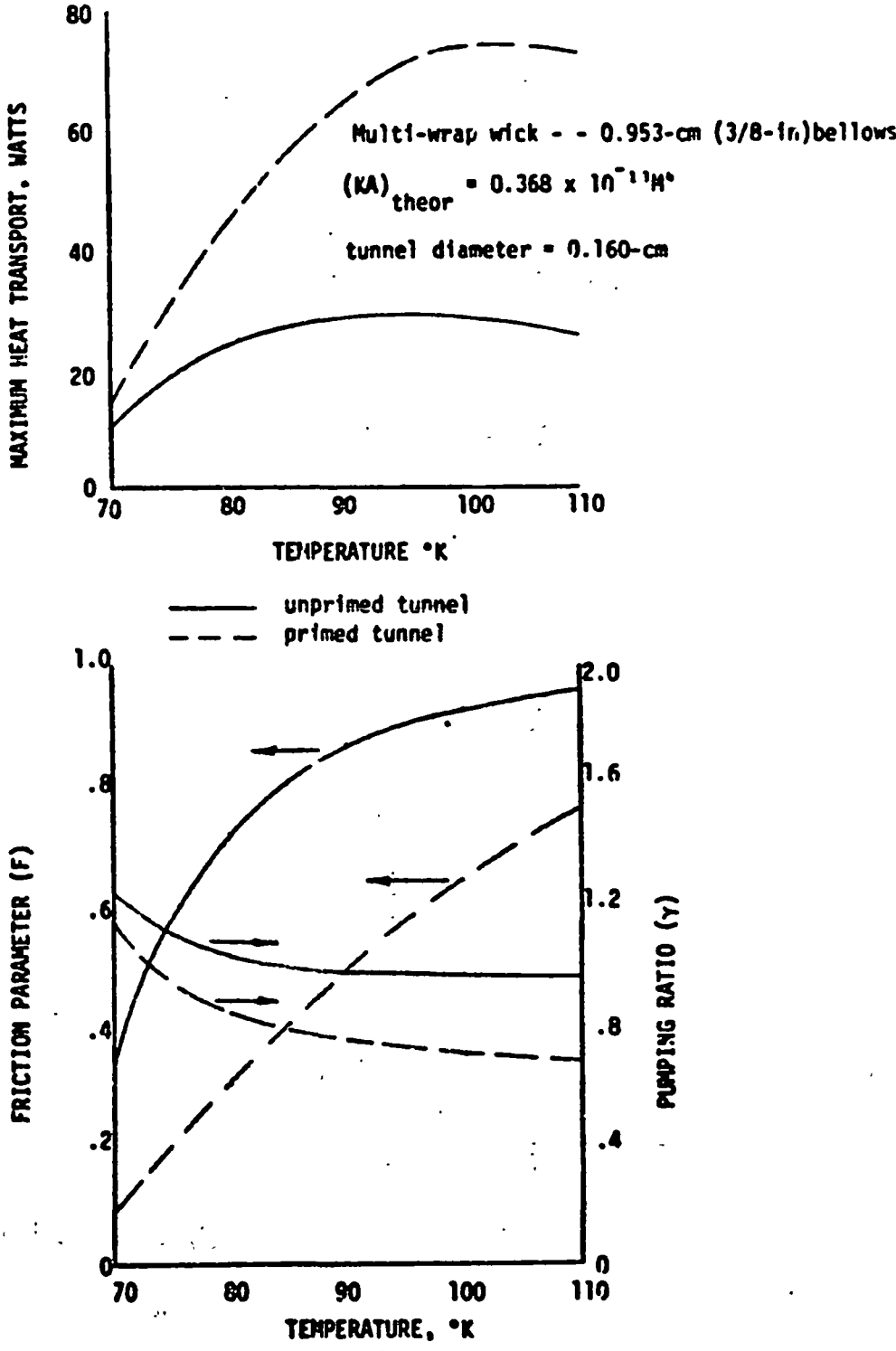

Fig. B-7. Performance characteristics of low temperature flexible heat pipe in "n-a" (oxygen)

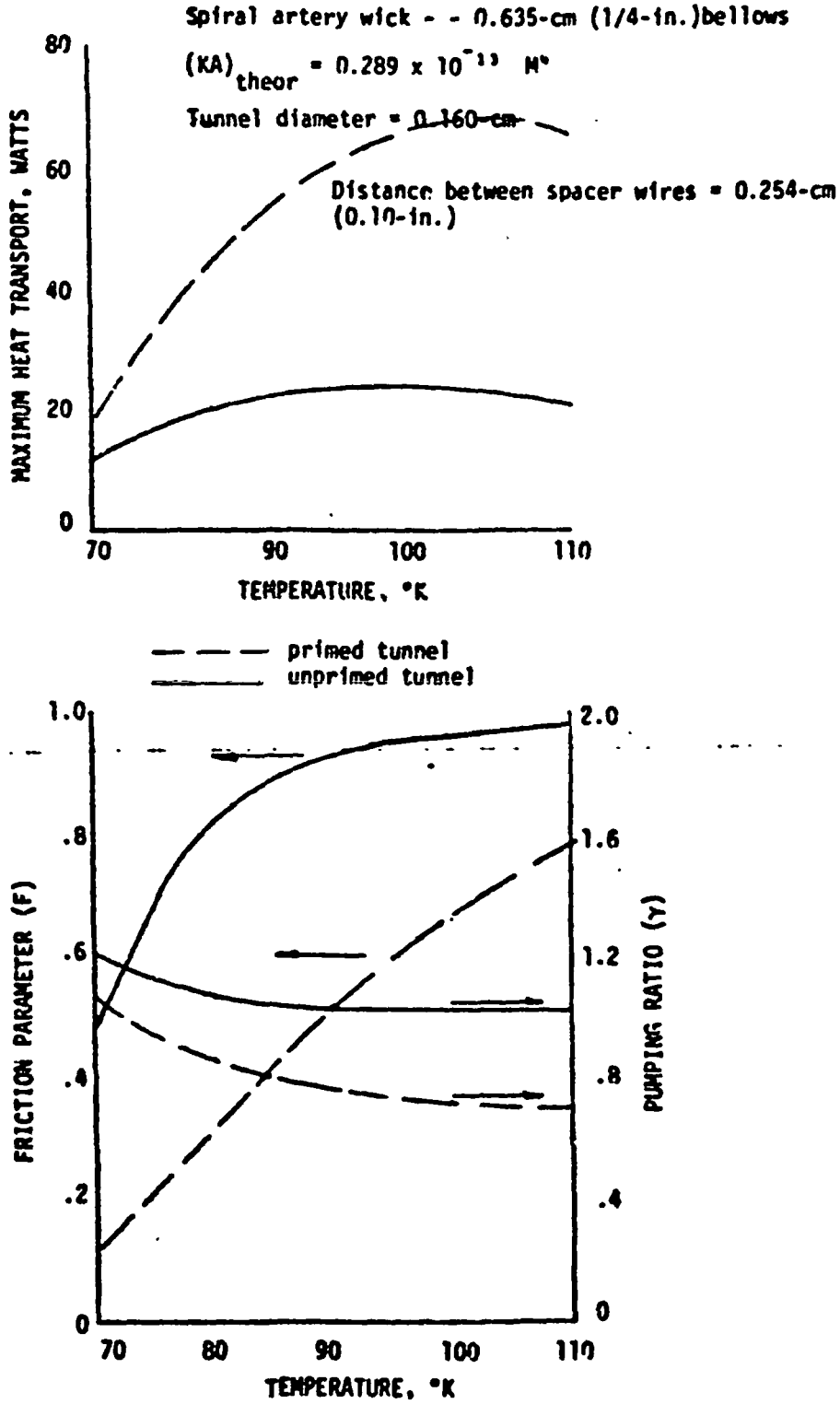

Fig. B-8. Performance characteristics of low temperature flexible heat pipe in "o-g" (oxygen)

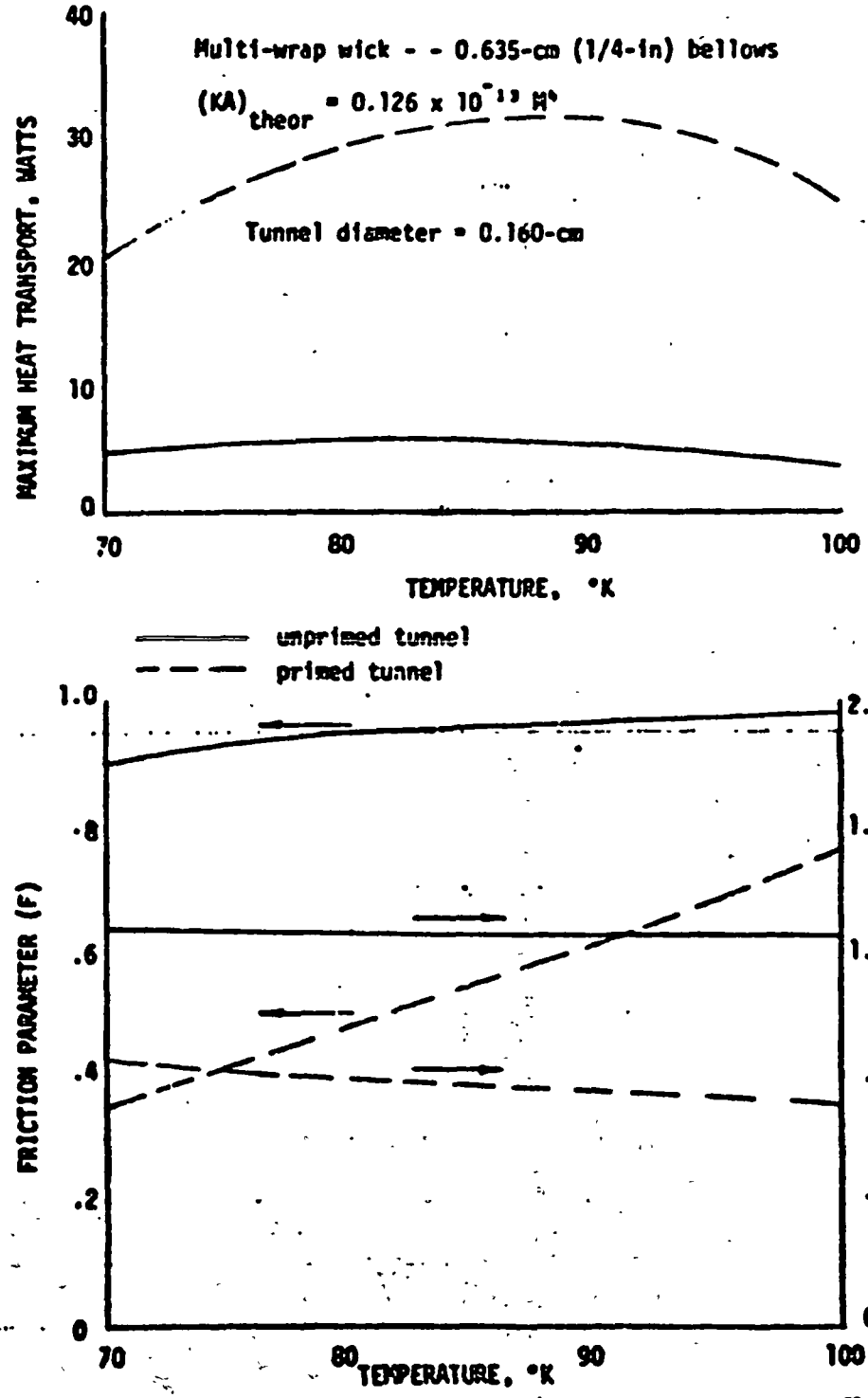

Fig. B-9. Performance characteristics of low temperature flexible heat pipe in "o-g" (nitrogen)

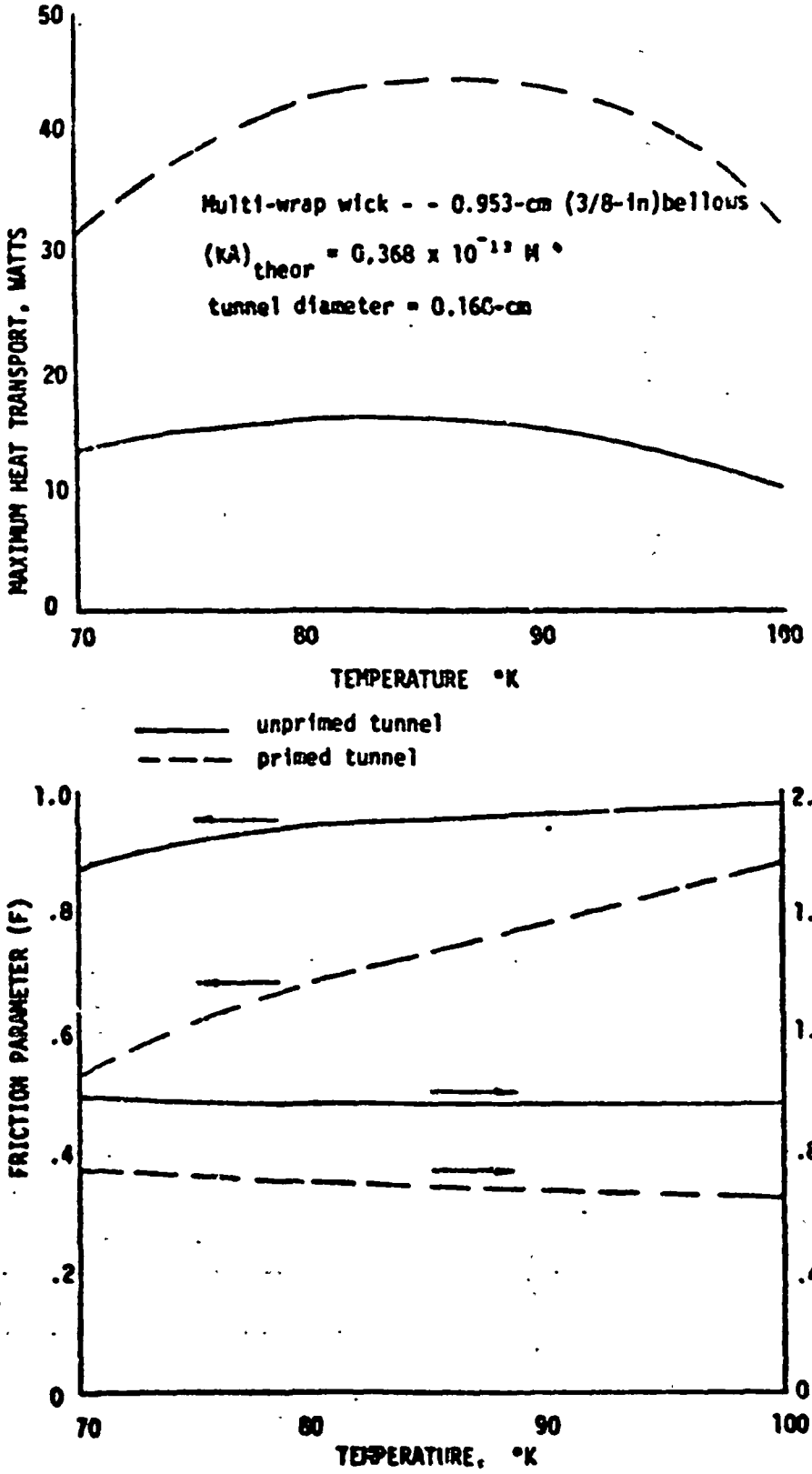

Fig. 8-10. Performance characteristics of low temperature flexible heat pipe [illegible] (reference)